



Ana Luísa Domingues de Almeida Oliveira

DESIGN OF CONNECTIONS IN TUBULAR STEEL TOWERS FOR WEC

DIMENSIONAMENTO DE LIGAÇÕES EM TORRES EÓLICAS DE
AÇO TUBULARES

Dissertação de Mestrado Integrado em Engenharia Civil, na área de Especialização em Mecânica Estrutural,
orientada pelo Professor Doutor Carlos Rebelo

Coimbra, 27 de setembro de 2017



UNIVERSIDADE DE COIMBRA



FCTUC DEPARTAMENTO DE ENGENHARIA CIVIL
FACULDADE DE CIÊNCIAS E TECNOLOGIA
UNIVERSIDADE DE COIMBRA

Ana Luísa Domingues de Almeida Oliveira

DESIGN OF CONNECTIONS IN TUBULAR STEEL TOWERS FOR WEC

DIMENSIONAMENTO DE LIGAÇÕES EM TORRES EÓLICAS DE
AÇO TUBULARES

Dissertação de Mestrado Integrado em Engenharia Civil, na área de Especialização em Mecânica Estrutural,
orientada pelo Professor Doutor Carlos Rebelo

Esta Dissertação é da exclusiva responsabilidade do seu autor.
O Departamento de Engenharia Civil da FCTUC declina qualquer
responsabilidade, legal ou outra, em relação a erros ou omissões
que possa conter.

Coimbra, 27 de setembro de 2017

AGRADECIMENTOS

Com a presente dissertação concluo uma etapa muito importante. Apesar de ser um trabalho individual, muitos nele estiveram envolvidos e ao longo de todo o meu percurso académico, aos quais quero aqui deixar um especial agradecimento:

Ao Professor Doutor Carlos Rebelo, orientador desta dissertação, pela oportunidade, acompanhamento e disponibilidade que sempre demonstrou na elaboração deste documento mas também pelos ensinamentos, conhecimentos partilhados e incentivo. A sua colaboração foi fundamental para a conclusão desta etapa.

Aos professores do Departamento de Engenharia Civil da Universidade de Coimbra pelos conhecimentos e apoio prestados durante todos estes anos, com especial atenção ao Professor Doutor Rui Simões, pelos conhecimentos partilhados, pelas horas disponibilizadas e pela confiança transmitida a todos os alunos da especialidade de Mecânica Estrutural.

A todos os funcionários do Departamento de Engenharia Civil que de alguma forma contribuíram, com especial atenção à Dona Lucinda, que sempre disponibilizou um bocadinho do seu tempo para as nossas conversas sobre o Porto e para me fazer sentir em casa. A todos os colegas e amigos que fiz ao longo do percurso académico, pela força dada nas longas horas de trabalho, por me fazerem sempre acreditar que este dia chegaria. Ao BEST Coimbra por toda a formação, amizade e vivências partilhadas. Um especial agradecimento à Marisa por toda a motivação e apoio.

Por último, um profundo e sentido agradecimento às pessoas que tornaram tudo isto possível, Mãe e Pai, obrigada pela confiança e esforço feito para que eu aqui chegasse. Ao meu Pai um especial agradecimento pelo gosto que me inculuiu nesta área desde criança e à minha Mãe por toda a paciência e por sempre ter acreditado. Aos meus irmãos, obrigada por TUDO, em especial ao José Luís que tantas horas perdeu a ajudar-me a escrever esta dissertação em inglês. Ao meu *special one*, Sandro, por toda a confiança, motivação, amizade e amor.

ABSTRACT

As the demand for renewable energy sources is constantly growing due to the global climate change and the wind power generation has achieved competitive prices, obtaining electric power from the wind became even more appealing. During the last decades, wind farms have been built all over the world, mainly in Europe. Tubular towers are now the most common solution for onshore wind farms.

The wind tower itself accounts for about 15-20% of the total installation cost and its optimization may lead to significant savings regarding costs and material usage. Building higher towers in order to reach zones of higher and more uniform wind speeds is a possible solution as they significantly increase the amount of energy yield of a wind turbine generator. However, they represent higher costs and challenges in terms of transportation and installations. They also lead to another important technical aspect of the design: the connection between tower's segments.

The currently used solution with bolted ring flanges imposes limitations that affect the overall efficiency. To overcome the disadvantages of flange connections such as the complex design, the laborious and cost intensive fabrication process and low fatigue resistance, an innovative solution for assembling segments of tubular steel towers for wind turbines has been recently studied in the framework of European research projects – slip resistant connections with long open slotted holes.

This thesis will compare these two types of connections. The main purpose is to assess the potential benefits from implementing them in tubular steel wind towers. Three different computer programmes were created with *MS Excel* for ring flange connection design verifications (resistance at Ultimate Limit State and fatigue design) and for fatigue design verification of friction connections. The Ultimate Limit State resistance of friction connections was computed using the *Excel-Tool* created during the development of HISTWIN projects.

One example of an 80m-high tower is presented, which enhances the potential benefits of using friction connections as the design is simpler and material costs savings of approximately 80% could be achieved.

RESUMO

Devido às alterações climáticas (aquecimento global) a procura por fontes de energia renovável e limpa tem vindo a aumentar. Como a energia eólica alcançou preços competitivos, a obtenção de energia elétrica através do vento tornou-se ainda mais apelativa. Tal facto levou a que, nas últimas décadas, fossem construídos parques eólicos por todo o mundo, principalmente na Europa, sendo as torres tubulares a principal solução escolhida para parques eólicos em terra (*onshore*).

A torre eólica representa cerca de 15 a 20% do custo total da instalação e a sua otimização poderá levar a uma redução significativa do material usado e, conseqüentemente, do preço. A construção de torres mais altas, com o objetivo de chegar a zonas mais altas onde a velocidade do vento é mais alta e uniforme, é uma possível solução, já que leva a um aumento da energia produzida pela turbina eólica. Contudo, isso representa custos mais elevados e desafios no transporte e instalação da mesma. Outro aspeto técnico importante a ter em conta aquando do dimensionamento são as ligações entre os segmentos da torre.

A solução usada atualmente, com ligações de flange aparafusadas, apresenta certas limitações que condicionam a eficiência global. Para ultrapassar essas desvantagens, nomeadamente o complexo dimensionamento, a trabalhosa e cara fabricação e a baixa resistência à fadiga, uma nova solução tem sido recentemente estudada no âmbito de projetos de investigação Europeus – ligações de atrito de ranhuras alongadas (*long open slotted holes*).

A presente dissertação irá comparar esses dois tipos de ligações, tendo como principal objetivo a avaliação de potenciais vantagens com o uso das ligações de atrito nas torres eólicas de aço tubulares. Foram criados três diferentes programas no *MS Excel* para as verificações no dimensionamento das ligações de flange (resistência ao Estado Limite Último e fadiga) e para a verificação de fadiga das ligações de atrito. A verificação ao Estado Limite Último da ligação de atrito foi feita recorrendo a uma ferramenta *Excel* criada no desenvolvimento dos projetos HISWTIN.

Será apresentado um exemplo de uma torre existente com 80m de altura, o qual reforça os potenciais benefícios no uso de ligações de atrito já que o dimensionamento é mais simples e pode levar a uma redução de cerca de 80% do preço.

TABLE OF CONTENTS

Agradecimentos	1
Abstract	1
Resumo.....	1
Symbols	1
1 Introduction	1
1.1 General Framework.....	1
1.1.1 Wind Energy	1
1.1.1.1 Worldwide energy consumption and sources	2
1.1.1.2 Renewable energies in Europe (Portugal).....	4
1.2 Objectives.....	6
1.3 Outline of the thesis.....	6
2 Background Theory	7
2.1 Historical development	7
2.1.1 The Origins of Windmill.....	7
2.1.2 The tower	8
2.1.2.1 Lattice towers.....	9
2.1.2.2 Concrete towers	9
2.1.2.3 Tubular steel towers.....	10
2.2 Physics concepts of wind energy conversion.....	10
2.2.1 Betz's Elementary Momentum Theory	11
2.2.2 Wind energy converters.....	11
3 State of art.....	13
3.1 Fatigue.....	14
3.1.1 S-N curves.....	14
3.1.2 Fatigue safety assessment.....	15
3.2 Bolted ring flange connections.....	16
3.2.1 Fabrication.....	17

3.2.2	Theoretical background	17
3.2.2.1	Load carrying behaviour of the segment – Fatigue resistance	17
3.2.2.2	Influence of flange imperfections	18
3.2.2.3	Ultimate Limit State	19
3.3	A new type of connections.....	19
3.3.1	Fabrication.....	21
3.3.2	Theoretical background	21
3.3.2.1	Fatigue resistance.....	22
3.3.2.2	Ultimate Limit State	23
3.4	Bolts.....	24
3.4.1	Self-loosening effect.....	25
3.4.2	Loss of pretension	26
3.4.3	Tension Control Bolts	27
3.4.4	Huck BobTail Lockbolts.....	29
3.4.5	Standard Bolts with Nord-Lock washers	30
3.4.6	Friedberg HV Rändel.....	32
4	Connections.....	33
4.1	Design Loads.....	33
4.1.1	Wind Loads.....	33
4.1.1.1	Extreme loads.....	34
4.1.1.2	Fatigue Loads.....	35
4.2	Design of bolted ring flange connections.....	37
4.2.1	Static resistance at ULS	37
4.2.2	Fatigue resistance.....	39
4.2.2.1	Elastic structural behaviour of L-flange connections	40
4.2.2.2	Bolt-load function acc. to Schmidt/Neuper	40
4.3	Design of friction connections.....	41
4.3.1	Static Resistance at ULS.....	41
4.3.1.1	Design Verifications.....	43
4.3.2	Fatigue Resistance.....	43
4.3.2.1	– Elastic resilience acc. to VDI 2230	44

4.3.2.2	Damage Equivalent Loads	46
5	Case Studies	48
5.1	Tower Geometry	48
5.2	Static design loads.....	48
5.3	Fatigue design loads.....	49
5.4	Flange connection	50
5.4.1	Flange geometry.....	50
5.4.2	ULS.....	51
5.4.3	Fatigue.....	52
5.5	Friction connection	55
5.5.1	Geometry	56
5.5.2	ULS.....	57
5.5.3	Fatigue.....	58
5.6	Comparison	59
5.6.1	Resistance.....	60
5.6.1.1	Ultimate resistance	60
5.6.1.2	Fatigue resistance.....	60
5.6.2	Material.....	60
6	Conclusion and recommendations.....	62
	References.....	63
	Appendix	66
	Appendix A – Static resistance at ULS – Flange connections	
	Appendix B – Fatigue resistance – Flange connections	
	Appendix C – Fatigue resistance – Friction connections.....	
	Appendix D – Design tools already developed.....	

SYMBOLS

A_{d3} – nominal cross section of bolt thread;

A_i – nominal cross section of bolt shank body i ;

A_{nom} – nominal cross section of bolt

A_s – Tensile stress area of the bolt;

c – width of shell segment;

C_S – bolt stiffness;

C_D – clamp solid stiffness;

d – nominal diameter of bolt shank;

d_0 – diameter of bolt hole;

d_3 – minor diameter of bolt thread;

D_d – damage index of entire life time;

d_w – outside diameter of the plane head bearing surface of the bolt;

d_{washer} – outside diameter of washer;

E_{bolt} – Young's-modulus of bolt material;

E_{cp} – Young's modulus of clamping package material (shell, cover-plate, washer);

E_{fl} – Young's modulus of flange material;

E_{nut} – Young's modulus of nut material;

E_{shell} – Young's modulus of tower shell material;

$F_{p,C}$ – characteristic preload force in bolt;

F_t – bolt load;

$F_{t,Rd}$ – design tensile resistance of the bolt;

$F_{t,Ed}$ – design tensile force in bolt;

f_{ub} – ultimate tensile strength of the bolt depending on bolt class;

$f_{y,fl}$ – flange yield strength;

-
- $f_{y,sh}$ – shell yield strength;
 $f_{y,shell}$ – characteristic yield strength of tower shell material;
 k_S – correction factor;
 l_{cp} – length of clamping package;
 $l_{eng,thread}$ – length of engaged loaded thread;
 l_{head} – substitutional extension length of bolt head;
 l_i – length of shank body i ;
 l_{nut} – substitutional extension length of nut;
 l_{thread} – free length of unengaged loaded thread;
 m – slope of fatigue strength curve;
 $M_{N,pl,Rd,sh}$ – design plastic bending resistance of the shell considering M - N -interaction;
 $M_{pl,Rd,fl,net}$ – design plastic bending resistance of net cross-section of flange;
 $M_{pl,Rf,sh}$ – design plastic bending resistance of the shell;
 n – number of friction surfaces;
 N – number of cycles to failure;
 n_{bolts} – number of bolts;
 n_i – number of cycles from load (effect) fatigue spectrum;
 N_i – number of cycles from the design fatigue resistance spectrum;
 $N_{pl,Rd,sh}$ – design plastic resistance of shell;
 N_{ref} – reference number of cycles;
 n_{rows} – number of rows;
 n_s – number of bolts per row;
 s – shell thickness;
 S – stress range;
 s_i – shell thickness of the tower cross section i ;
 s_{mean} – mean shell thickness of both tower cross sections;
 t_{fl} – flange thickness;
 Z – tension force in the shell;
-

$Z_{ed,max}$ – maximum force in longitudinal direction;

Z_{ult} – ultimate tensile resistance force of the segment;

β – empirical determined correction factor, taken as 1.25;

γ_{Ff} – safety factor for loads, taken as 1.10;

γ_{M0} – partial factor for preload of high strength bolts, taken as 1.0;

γ_{M2} – partial safety factor, taken as 1.25;

γ_{M3} – partial safety factor at ultimate limit state (Category C), taken as 1.25;

γ_{M7} – partial factor for preload of high strength bolts, taken as 1.10;

γ_{Mf} – safety factor for materials, taken as 1.15;

$\Delta\sigma_C$ – detail category;

$\Delta\sigma_{DEL}$ – design fatigue stress at the considered number of cycles (for use with DEL);

$\Delta\sigma_{E,2}$ – characteristic fatigue resistance associated with a reference number of cycles, N_{ref} ;

$\Delta\sigma_{E,ref}$ – constant amplitude DEL range;

$\Delta F_{p,C}$ – load variation range;

$\Delta\sigma_R$ – characteristic fatigue resistance associated with a reference number of cycles, N_{ref} ;

$\Delta\sigma_{z,mean}$ – mean stress variation range of the net cross section of both tower cross sections;

δ_{bolt} – elastic resilience of the preloaded bolt;

δ_{cp} – elastic resilience of clamping package (steel shells + cover-plate + washers);

$\delta_{eng,thread}$ – elastic resilience of engaged bolt thread;

$\delta_{freethread}$ – elastic resilience of unengaged loaded part of thread;

δ_{head} – elastic resilience of bolt head;

δ_{joint} – elastic resilience of bolted connection, see next chapter;

δ_{nut} – elastic resilience of shank;

δ_{shank} – elastic resilience of nut;

μ – slip factor;

ν – Poisson ration, taken 0.3;

$\sigma_{ult,Ed}(\sigma_x)$ – axial stresses acting in the tower shell;

φ – angle of deformation cone, taken as 35°.

1 INTRODUCTION

1.1 General Framework

Nowadays, global warming has become the most concerning environmental issue. Governments, corporations and even individuals around the world are constantly debating the reality of global warming and studying possible solutions to revert this trend. Renewable clean energies and efficient energy applications then appear as alternatives to fossil energies and potential solutions to this challenging problem. Renewable clean energy is the energy that comes from sources, which are continually replenished, on a human timescale, and do not cause environmental pollution, such as sunlight, wind, rain, waves and geothermal heat.

1.1.1 Wind Energy

Wind is a widely available, free, clean and renewable source, so no matter how much is used today, there will be still the same supply in the future. Wind energy is also a source of clean, non-polluting, electricity and, unlike conventional power plants, wind farms do not emit air pollutants or greenhouse gases, except for the production and construction of the converters and support structures. Although wind farms had relatively little impact on the environment (when compared, for example, to fossil fuel power plants), noise produced by the rotor blades and aesthetic (visual) impacts are a concern. Nevertheless, most of these problems have been reduced or even solved through technological development and by properly placing wind farms.

Wind turbines, like windmills, are assembled on a tower in order to capture more energy; with high hub height (currently above 80m) wind turbines can take advantage of the faster and less turbulent wind. Nowadays, wind turbines are mainly built with a propeller-type rotor on a horizontal axis. Horizontal-axis wind turbines (HAWT) have the axis of the rotor's generator parallel to the wind stream and to the ground. Turbines catch the wind's energy with their propeller-like blades, usually, two or three blades are mounted on a shaft to form a rotor. The purpose of the rotor is to convert the linear motion of the wind into rotational energy that can be used to drive a generator. The blade acts like an airplane wing, *i.e.*, when the wind passes over both surfaces of the airfoil shaped blade it passes more rapidly over the longer (upper) side of the airfoil, thus creating a lower-pressure area above the airfoil. The pressure differential between top and bottom surfaces results in aerodynamic lift, which causes the rotor to turn. In addition to lift force, the wind's force against the front side of the blade, generates a drag force,

which is perpendicular to the lift force and contributes to the thrust acting on the top of the supporting structure.

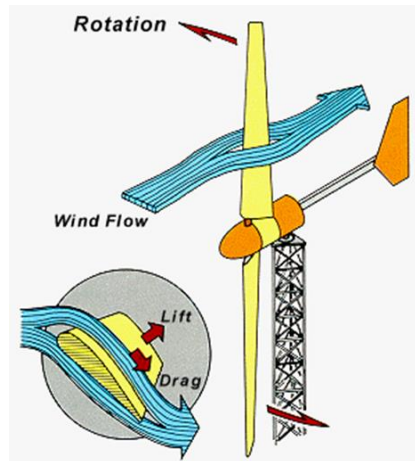


Figure 1.1 – Principles of wind turbine aerodynamic lift (Encyclopedia of Alternative Energy)

The combination of lift and drag makes the rotor spin like a propeller and the turning shaft spins a generator to produce electricity. As one of the primary objective of wind turbine designers is to maximize the aerodynamic efficiency or power extracted from wind, the blade must have a relatively high lift-to-drag ratio. This ratio usually varies along the length of the blade to optimise turbine's energy output at various wind speeds.

1.1.1.1 Worldwide energy consumption and sources

The industrial revolution led to an increase of the production volume which resulted in an exponential economic and population increase, intensifying the need of available resources and energetic consumption. The planet is now hosting about 7.2 billion of people and, with every person born, more resources and energy are needed. However, the problem with most of used sources is that they are finite and responsible for a large percentage of greenhouse gases emissions. The alternative presents itself in the form of renewable energies, with particular relevance to wind energy.

The wind energy is now facing an enormous development, not only the technology is improving but also the amount of annual installed wind capacity is increasing. All over the world, many countries are now installing a wide amount of wind turbines, aiming to achieve a higher percentage of electricity generated by this kind of source. According to Global Wind Energy council (GWEC, 2015), in the last 15 years, the global wind capacity installed is rising almost every year. That shows how important wind energy is becoming all around the world. Figure 1.2 shows that Popular Republic of China, USA and Germany are the leaders of installed capacity in the year of 2015. They are also the ones with higher cumulative capacity at the end of 2015 and everything points out to stay this way.

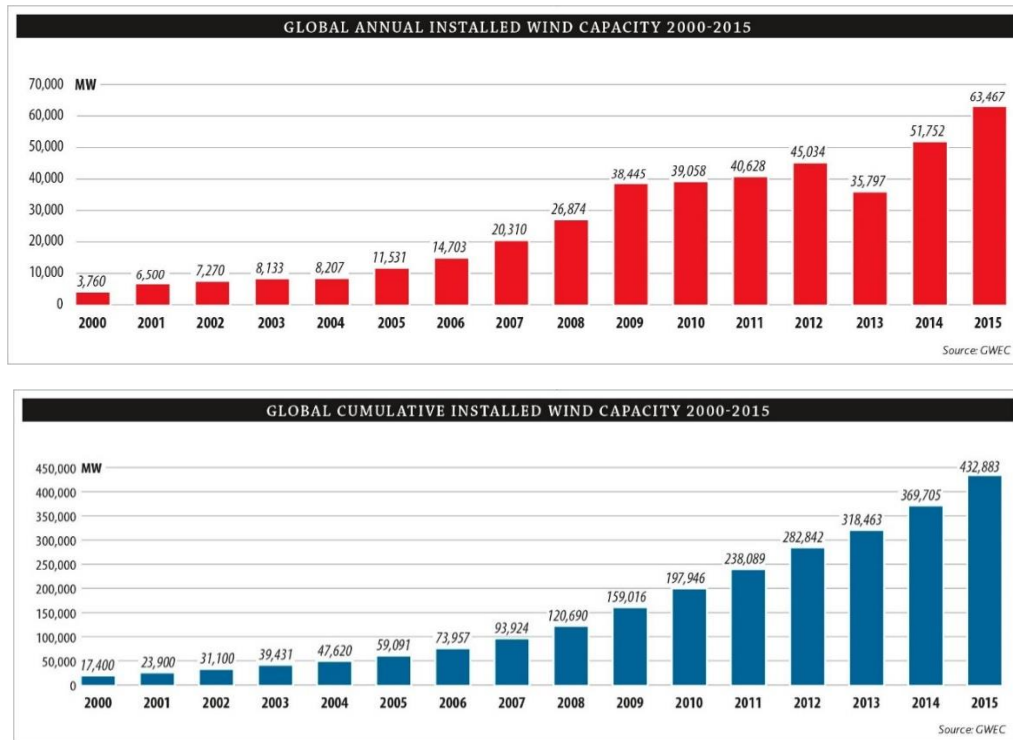


Figure 1.2 – Global annual installed and cumulative installed wind capacity (2000-2015), (GWEC, 2015)

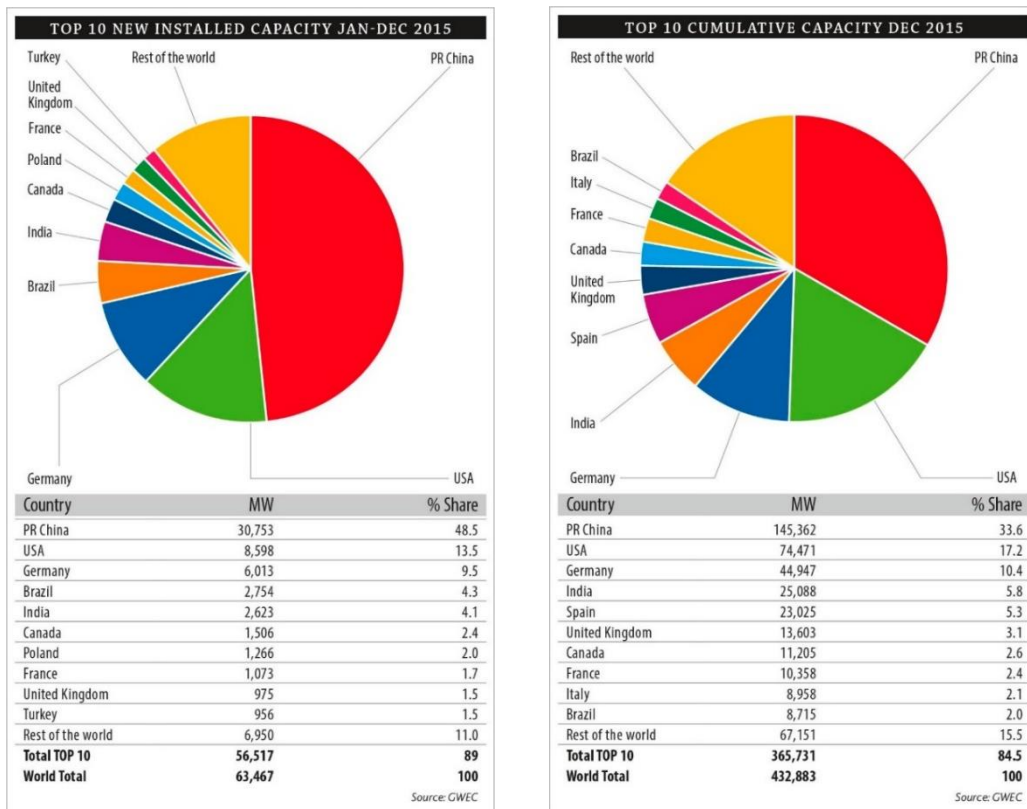


Figure 1.3 – Global TOP 10 new installed and cumulative capacity in 2015 (GWEC, 2015)

1.1.1.2 Renewable energies in Europe (Portugal)

Since 1997 the European Union (EU) has adopted policies to increase the generation and usage of energy from renewable resources. As a result, the wind energy is considerably growing. Over the past 15 years, annual wind power installations in the EU have increased from 3.2 GW in 2000 to 12.8 GW in 2015.

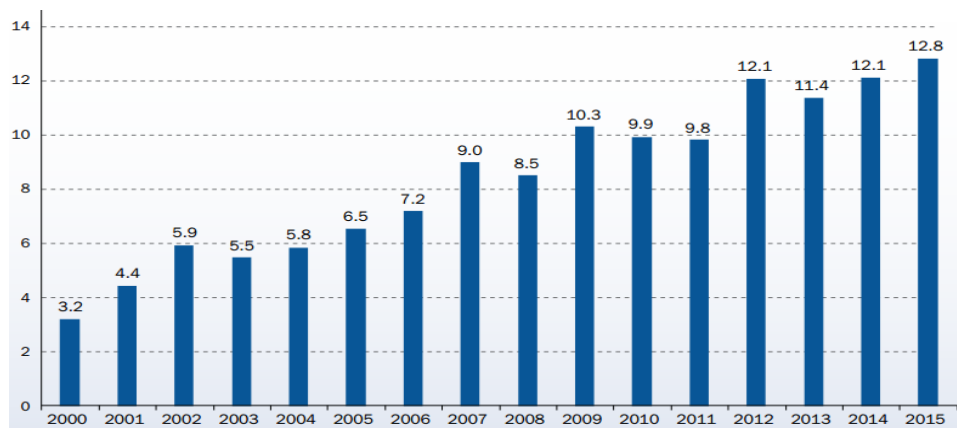


Figure 1.4 – Annual wind power installations in EU (GW), (EWEA, 2015)

In terms of the cumulative wind power installations, a total of 141.6 GW capacity is now installed in EU due to a growth of 9.7% in 2015, approximately 131 GW onshore and 11 GW offshore. Within the EU, Germany remains the country with the largest installed capacity (44.9 GW), followed by Spain (23 GW), the UK (13.6 GW), France (10.4 GW) and Italy (9 GW). Nowadays, Portugal has more than 5 GW installed (EWEA, 2015).

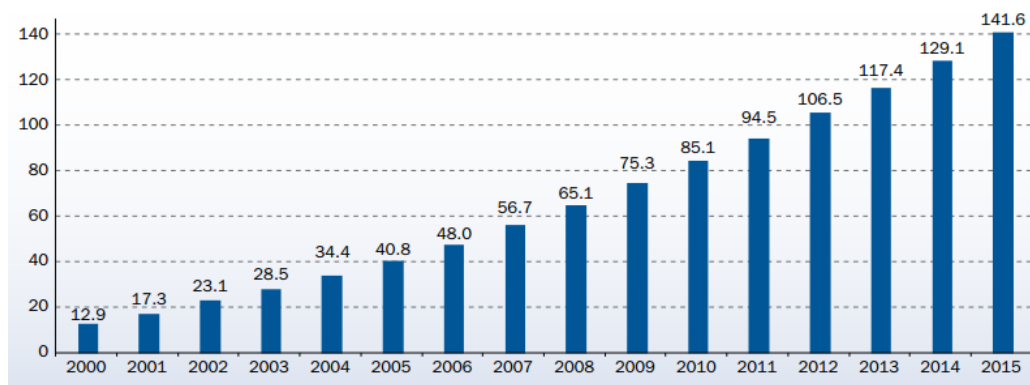


Figure 1.5 – Cumulative wind power installations in the EU (GW), (EWEA, 2015)

In fact, in Europe, by the end of 2015, the most installed kind of power generation was wind power. Since 2000, renewable capacity increased from 24.4% of total power capacity to 44.2% in 2015. Within the total energy, wind energy represents 15.6% in 2015, while in 2000 was only 2.4%. Wind energy has overtaken hydro as the third largest power generation in the EU with a 15.6% share of total power capacity, being now the first renewable energy technology in capacity installed.

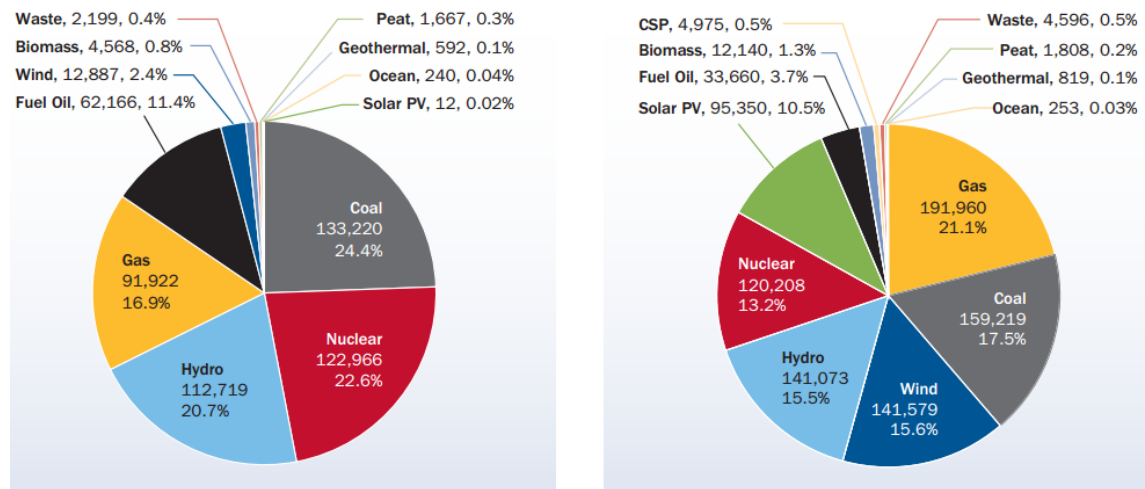


Figure 1.6 – Comparison of EU power mix in the year of 2000 and 2015, respectively (EWEA, 2015)

The wind power capacity installed in the EU at the end of 2015, in an average wind day, would be able to produce 315 TW of electricity, which cover 11.4% of the EU total consumption. (EWEA, 2015) APREN (Associação Portuguesa de Energias Renováveis), the Portuguese renewable energies association, claim that although wind power was insignificant 20 years ago, nowadays it represents over 20% of the Portuguese electric generation (APREN).

Initially, Portuguese wind sector had to overcome an amount of challenges such as obtaining funding for development and making electricity grid operators figure out the advantages of this industry. Nowadays, the industry has to face the ongoing financial crises while also meeting the country's commitments to reach the EU set goals for renewable energy. Despite that, António Sá da Costa, president of APREN, foresees that the share of wind electricity in Portugal should be around 25%, in 10 years.

According to International Energy Agency (IEA, 2015), wind is set to be the future in power system as it should represent a quarter of Europe's power demand by 2030. Thus, important developments which helps on addressing variability and maximise wind power's contribution to the energy system are needed, for example, turbines for low wind speeds.

Therefore, new technologies and new ways of construction are always being studied in order to get the maximum efficiency of this source and turn more competitive this source of energy. As the capacity of wind turbines increases, wind towers need to increase their structural strength and stiffness. According to Hau (Hau, 2013), the transportation and erection procedure are becoming a problem for the last generation of multi-megawatt wind turbines. Nevertheless, this problem stands as a strong incentive to find innovative solutions in tower design and connections, so that the wind energy continues to maintain or even develop its competitiveness in the future.

1.2 Objectives

The main objective of this thesis is to compare two different types of bolted connections between tubular steel segments of wind towers. The currently used ring flange connection is compared to a new one defined as friction connection with long open slotted holes, which has been recently developed in the scope of European research project HISTWIN (High-Strength Steel Tower for Wind Turbine) (Veljkovic et al, 2015). The purpose is to assess the potential benefits from implementing friction connection in tubular steel wind towers. The methodology used to assess the performance of the connections was the development of design tools based on *MS Excel* sheets, which are used to run examples and as basis for the implementation of the design procedures in apps running on iOS or Android devices (see Appendix D).

In order to fulfil the main objective, three different computer programmes were created with the help of *MS Excel*. For ring flange connection design verifications (resistance at Ultimate Limit State and Fatigue design) two different computer programmes were created. A third programme was created for fatigue design verification of friction connections. The Ultimate Limit State resistance of friction connections was computed using the *Excel-Tool* previously developed in the scope of HISTWIN project.

1.3 Outline of the thesis

This work is divided into 6 different chapters and appendixes aiming for a coherent organization of the document with technical descriptions of every step made to achieve the proposed goals.

Chapter 1 sums up the importance of the theme and the objectives of this work. It also presents a general overview of renewable energy consumption worldwide.

Chapter 2 focuses mainly on the tower and the physic concepts of wind energy converters. It is presented a brief historical development about wind towers and the currently used types.

Chapter 3 addresses the state of art introducing the two compared types of bolted connections and different kinds of bolts. Also, a brief explanation about fatigue is given.

Chapter 4 focuses on the design of ring flange connections and friction connections with long open slotted holes. A brief description of the different design loads taken is also provided.

In Chapter 5 two case studies are presented and compared.

Chapter 6 ends this thesis with some conclusions of the developed work and critical analysis of the results. It also presents some recommendations for future work.

In the appendixes are shown the computer programmes developed with *MS Excel* during this work and also the existing tools created by HISTWIN programme.

2 BACKGROUND THEORY

2.1 Historical development

Wind is a never ending, widely available source of energy and people soon learnt how to use it to their own benefit. The earliest known use of wind power is the sail boat. Ancient sailors understood lift, even though they did not have the knowledge to explain how or why it worked. Afterwards wind-powered machines have been used to grind grain and pump water. Nowadays, the resurgence of wind power is an unavoidable consequence in order to meet the energy requirements of industrial societies. The use of wind energy is not a new technology, thus, when investigating modern wind towers and turbines, comprehending the background of wind power technology is imperative. Therefore, this subchapter starts with a look at the past.

2.1.1 The Origins of Windmill

Although there are no certainties about the origins of windmills, some authors claim that remains of stone windmills were discovered near Alexandria (Egypt) with nearly 3000 years. The first reliable information from historical sources dates the year of 644 A.D. and came from the region of Sistan (Persian-Afghan border). A later report from the year of 945, including a sketch, describes a vertical axis windmill used for milling grain. Similar windmills can also be found in Afghanistan up to the present date (Fig. 2.1). Some centuries later the Chinese were also using windmills to drain rice fields. Those were simple structures made of bamboo sticks and fabric sails with a vertical rotation axis (Fig. 2.2) (HAU, 2006).



Figure 2.1 – Vertical-axis windmill for milling grain, Afghanistan (Deutsches Museum), (Hau, 2006)



Figure 2.2 – Ancient Chinese windwheel for pumping water (Deutsches Museum), (Hau, 2006)

The first verifiable information of the traditional windmill with a horizontal axis dates the year of 1180 in the Duchy of Normandy. They rapidly spread all over North and Eastern Europe and in the 13th century, numerous windmills could be found in Germany. About two centuries later,

aside from the windmills entirely made of wood, “tower windmills” appeared. In those, the wind wheel stands on a round tower made of stone. In the 16th century, in Holland, significant improvements were made leading to a new type of windmills, “Dutch windmill”. In the 19th century there were nearly 200.000 windmills scattered in Europe (Hau, 2006).

The initial attempts to produce electricity from wind took place in America. However, it was in Denmark that the first large scale attempt happened. Poul La Cour was a pioneer of electricity generation using wind power. He sets the turning-point from traditional windmill to the modern technology of power generating wind turbines. In 1891, La Cour built an experimental wind turbine in Askov, Denmark (Fig. 2.3). Albert Betz also played a significant role in the history of wind energy. He is responsible for the contemporary physical principles of wind-energy conversion, postulated in 1920. His work enabled to determine how much mechanical energy could be harvested from a free airflow by an energy converter, see chapter 2.2.1.

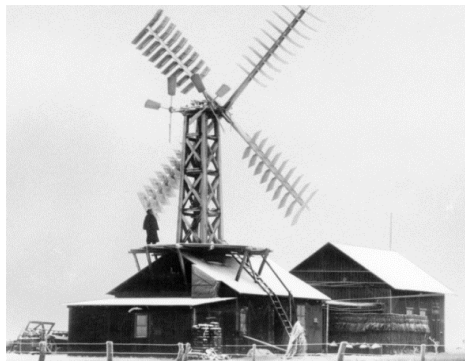


Figure 2.3 – Poul La Cour’s first electricity producing wind turbine (Hau, 2006)

With the development of technology and materials, windmills evolved to complex machines, capable to generate electricity to supply hundreds of houses. Steel and concrete replaced wood used to build millhouses (the oldest types of “wind turbines”, the windmills, had no towers but millhouses). Furthermore, to attain the most advantage of the wind in a higher altitude, the turbines have to be assembled in a high tower capable of supporting all the stresses, mainly the wind and self-weight. As they are in constant development, new types of towers and connections between tower segments are needed to improve their performance.

2.1.2 The tower

The height of the tower is a key feature of a horizontal-axis turbine. The optimum tower height depends on local variations of wind speed with height, energy and tower costs. Larger rotors generate further energy and economies of scale make them cheaper. But to fit larger diameters, higher towers are needed. In addition, with increasing height, higher and more uniform speeds are reached, which leads to higher energy outputs. The main disadvantage is the cost. Due to the increase height of the tower, manufacturing, transportation, assembly and erection became more laborious and expensive. Therefore, the optimum tower height must be determined from

the economy point, *i.e.*, the cost increase of a higher tower must be counterbalanced by an improvement of the energy yield of the turbine. Other important design factor of a tower is its stiffness. Thus, the main objective of the tower design is to obtain the desired tower height with the required strength and stiffness at the lowest construction cost (Hau, 2006).

In the early years of the development of modern wind energy technology, many materials and designs were tested but in the course of time, the range of different towers has narrowed down to a freestanding tubular steel tower, rarely made out of concrete. Usually, the towers of large turbines have a conical shape with increased diameter at the base, which saves weight for a given required stiffness when compared with a cylindrical geometry (Hau, 2006). Nowadays, the most common types of towers to support wind turbines are: lattice towers, pre-stressed tubular concrete towers or hybrid tubular steel-concrete towers and tubular steel towers.

2.1.2.1 Lattice towers

The simplest method of building high and stiff towers, required for large turbines sited in inland regions, is as a three-dimension truss. Steel lattice towers are also used in other kind of structures, *e.g.* for energy transmission lines. Lattice towers were the preferred design at the beginning of wind energy exploitation, which have been widely used in small turbines. Nowadays, this type of tower is a very competitive solution, mainly for high hub heights (above 100m). They require about half of the material of a tubular steel tower with a similar stiffness and can be welded or bolted together from angled sections. Despite of more complex assembly, this towers leads to significant cost advantages and easier transportation to the site.

Moreover, the assembly and erection process are being improved by the use of low-maintenance fasteners, which have a lower rate of pretension loss comparing to normal bolts and do not need maintenance, *e.g.* retightening (Veljkovic et al, 2015). According to Veljkovic (Veljkovic et al, 2015), the main advantages of lattice towers are: straightforward design, good dynamic behaviour (ideal for wind turbines), economy of fabrication and transportation (lattice angle sections are easier and lighter to transport comparing to tubular structures), simpler erection procedures and ecological advantages such ecological balance due to galvanizing and small concrete foundations.

2.1.2.2 Concrete towers

As the wind industry identified the need to increase turbine sizes, rotor diameters and towers height, concrete arises as a viable option. Concrete is an inherently durable material capable of maintaining its desired engineering properties under conditions of extreme exposure. It allows the construction of higher towers on site which simplifies transportation hurdle. Furthermore, the long construction time can be reduced by the use of prefabricated parts. Thus, they appear as an attractive solution for high hub heights where great diameters are needed (Husson, 2008).

Concrete towers can be divided into two groups: reinforced and prestressed concrete towers. In the first case, the steel reinforcement is installed but not prestressed, in the second one the

reinforcement is prestressed and sometimes with special tensioning elements, which can lead to an increase of the permissible tensile stresses in the concrete. Each case has advantages and disadvantages, therefore the decision for which is the best method depends on the characteristics of the site. Although these types of tower have a successful and long tradition in Europe, they have been mostly replaced by tubular steel towers. Considerable design and development efforts are still required for them to become more competitive (Husson, 2008).

2.1.2.3 Tubular steel towers

Tubular steel towers are now the standard solution for the support of the wind turbines. They are the adequate solution for wind turbines with hub height up to about 100m. They have a slightly conical shape, with diameter and plate thickness reducing from bottom to tower top. These towers are made of different sections manufactured in the workshop and then assembled on site by means of bolted ring flange connections (Husson, 2008). The main advantages of tubular steel towers are: tubular steel structure is relatively light and due to its circular cross section has the same bending stiffness in all direction, it has good torsional stiffness and it is relatively easy to install and has low maintenance costs. The possibility of pre-installing all the internal equipment of the tower is another advantage that makes tubular steel towers stand out as the best compromise between economical, aesthetical and safety (Husson, 2008).

As mentioned before, in order to reach higher energy outputs from wind turbines, higher towers are required. However, high wind power (turbine power) increases the loads, bending and torsional moments acting on the structure. Thus, to withstand these extraordinary loading, the dimension of the tower must also increase. Both diameter and thickness of tube wall must be greater, which leads, for example, to implications in transportation and cost. Therefore, the main limitation for tubular pre-fabricated towers (transportation) can be overcome by extra work on site, including the assembly of full diameter sections from smaller pieces.

2.2 Physics concepts of wind energy conversion

In order to transform the whole kinetic in the air stream (Fig. 2.4) the wind velocity should be reduced to zero when crossing the energy converter. However, as the same mass flow must pass through the cross-section, reduced velocity leads to a widening of it. There also would be a “stack” of the air mass near the converter, which is physically impossible. Therefore, there must be defined the “Theoretical Maximum” of energy that can be converted from wind.

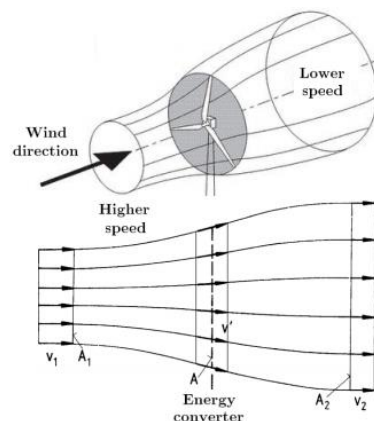


Figure 2.4 – Extracting energy from wind with a rotor disc (Veljkovic et al, 2015)

2.2.1 Betz's Elementary Momentum Theory

In the 20's, Albert Betz showed that, by applying elementary physical laws, the mechanical energy extractable from an air stream passing through a given cross-sectional area is limited to a certain proportion of the power contained in the air stream. He proved that the optimal power extracted from wind, regardless of the design of a wind turbine, could only be hit at a certain ratio between the flow velocity of air in front of the energy converter and the velocity behind it (Hau, 2006). Acc. to Betz's Momentum Theory, no turbine can capture more than $16/27$ (59.3%) of the kinetic energy in wind. The factor $16/27$ (0.593) is known as Betz's coefficient. Thus, the ratio of extractable mechanical work to the power contained in the wind is limited to a value of 0.593, *i.e.*, only $\approx 60\%$ of wind energy can be converted into mechanical power. It is worthwhile to recall that the relationships presented by Betz were derived for an ideal, frictionless flow, *i.e.*, Betz's law assumes an energy converter working without losses in a frictionless airflow. In real conditions the power that can be reached is not independent of the energy converter features and the power coefficient will always be smaller than the Betz's value. Despite that and some other simplifications, its results are useful for performing calculations in practical engineering.

2.2.2 Wind energy converters

Since the first attempt to build a wind turbine countless number of different solutions have been tested. The main component of a wind turbine is the energy converter, which transforms the kinetic energy contained in the moving air into mechanical energy. Wind energy converters can be classified by their constructional design and by the aerodynamic function. Classification according to constructional design is more practicable and thus more common. One of the most notable characteristic is the position of the wind rotor axis. However, what fairly influences the actual power is which of the aerodynamic forces are used to produce mechanical power.

The easiest type of wind energy conversion can be attained by means of pure drag surfaces, but achieves only one third of Betz's ideal power coefficient. Higher power coefficients can be hit

with aerodynamic lift. Modern wind rotors are designed to use the effect of aerodynamic lift, with the best solution being horizontal axis propellers. Vertical axis rotors were mostly from older designs using the drag effect only. Although it is possible to use also the lift effect, the production costs of vertical axis wind turbines are much higher than those with horizontal axis.

A horizontal-axis wind turbine (HAWT) is a wind turbine in which the rotation axis of the rotor is parallel to wind stream and the ground. Nowadays, almost all grid-connected wind turbines are built with a propeller-type rotor on a horizontal axis, which is now the standard design. Most of the HAWT are two or three-bladed. The rotor converts the linear wind motion into rotational energy which is used to propel a generator. This design brings incontestable advantages, such as the possibility to control the pitch of the rotor blades according to the flow of the wind and the ability to protect against extreme wind speeds. As the blades are constantly being optimized and, considering the ongoing research into aerodynamic lift, better performances are expected.

3 STATE OF ART

As the demand for renewable energy sources is constantly growing due to global climate change and the wind power generation has achieved competitive prices, obtaining electric power from the wind became even more appealing. During the last decades, wind farms have been built all over the world, mainly in Europe. Tubular towers are now the most common solution for onshore wind farms. Their main drawbacks are: relatively low fatigue resistance, high production costs and time consuming assembly. Therefore, to rise the competitiveness of wind energy, the construction's costs of wind farms must be reduced.

According to Heistemann (Heistemann, 2014) the capital cost for constructing a wind power plant and connecting it into the electric grid accounts for 75-90% of the total cost. The tower itself accounts for about 15-20% of the installation cost and its optimization may lead to significant savings regarding costs and material usage. Building higher towers, in order to reach zones of higher and more uniform wind speeds, can be seen as a solution. Higher towers significantly increase the amount of energy yield of a wind turbine generator but, on the other hand, they represent higher costs and challenges in terms of transportation and erection. They also lead to another important design aspect: the connection between tower's sections. The currently used solution with bolted ring flanges with low fatigue resistance imposes limitations that affect the overall efficiency.

Tubular steel towers are made of 20-30m high segments and flange connections are the most common solution to assemble them. The main focus is to enhance competitiveness of the steel tubular tower with hub-height up to 80-90m. The height is limited by transportation viability, which means that the diameter of the bottom segment of the tower is limited to about 4.3m to pass under road bridges (Husson, 2008), and by the fatigue resistance in the flange connections. Flange connections fabrication process is quite laborious and expensive, and their design is based on a complex model. Depending on the fabrication process and connection detailing, the fatigue class is often between 36* and 71, defined by Eurocode (EC 3-1-9).

Nevertheless, recent research projects have shown that improvement could be achieved by implementing friction connections with long open slotted holes, decreasing time and costs needed for installation and maintenance of the bolts. This solution can also be implemented in lattice towers. Long open slotted holes are used to simplify the assembly process. The segments are clamped with, *e.g.* Tension Control Bolts (TCB) which can be tightened from within the tower in a safe and easy way. More bolts will be presented later on this chapter. This solution

is a competitive alternative and has many advantages concerning costs for design, material, manufacturing, assembly and maintenance of the tower. It is estimated to reduce the total tower costs by 10–15%. The main advantage stated is definitely the much higher fatigue resistance.

3.1 Fatigue

When structures are exposed to cyclic loadings they can go through progressive damage which shows itself in form of cracks evolving at particular locations of the structure. This phenomenon is called fatigue and is represented by a loss of resistance in time. The cracks can initiate on the material surface or where the maximum stresses appear, *e.g.* in connection between elements. The fatigue cracks start on a microscopically scale, followed by crack growing to a macroscopic size until the failure in the last cycle of the fatigue life (Veljkovic et al, 2015).

The physical effect of a repeated load on a material is different from a static load and they need to be studied separately. In addition, the majority of fatigue failures occurs at stresses of an intensity considerably below the static elastic strength of the material. Fatigue failure is always of the brittle type whether the material is brittle or ductile, thus is sudden and catastrophic. The increase in stress difference (stress range) results in accelerated fatigue damage. This damage is cumulative – materials do not recover when rested.

The fatigue life of a structural component under repeated cyclic loadings is established by the number of stress cycles it can stand before failure. It depends mainly on stress range and stress concentration, including residual stresses. The environment, fabrication and structure geometry also affect the fatigue life – square holes or sharp corners lead to high local stresses where fatigue cracks can start, unlike round holes and smooth transitions that increase fatigue strength. Note that although different steel grades are expected to behave differently when exposed to fatigue loading, Eurocode (EC 3-1-9) disregard those differences concerning fatigue resistance.

3.1.1 S-N curves

In high-cycle fatigue situations, the usual way to express fatigue damage on a structural detail is by means of S-N curves, also known as Wöhler curve or Fatigue Spectrum. They relate stress range (S) with the number of cycles to failure (N) in a logarithmic scale. S-N curves derive from tests on samples of the material that has to be rated. This tests are based on a regular sinusoidal stress applied by a machine that counts the number of cycles until failure, *i.e.*, fatigue life.

Table 3.1 – Main parameters used to define S-N curves

Stress range	Stress amplitude	Stress ratio	Stress mean value
$S = \sigma_{max} - \sigma_{min}$	$A = \frac{\sigma_{max} - \sigma_{min}}{2}$	$R = \frac{\sigma_{min}}{\sigma_{max}}$	$\sigma_m = \frac{\sigma_{max} + \sigma_{min}}{2}$

Figure 3.1 illustrates a typical S-N curve. Some curves (for certain ferrous alloys and titanium) become horizontal at large N which represents the fatigue limit. The material never fails under

that stress amplitude, no matter the number of cycles– endurance limit. Nevertheless, some S-N curves show a different behaviour (nonferrous alloys and some high strength steels), their graph shows a continuous reduction of fatigue strength for high fatigue lives (S decreases with N), *i.e.*, the material does not present a fatigue limit. The progression of a S-N curve can be affected by many factors such as corrosion, temperature, residual stresses, *etc.*

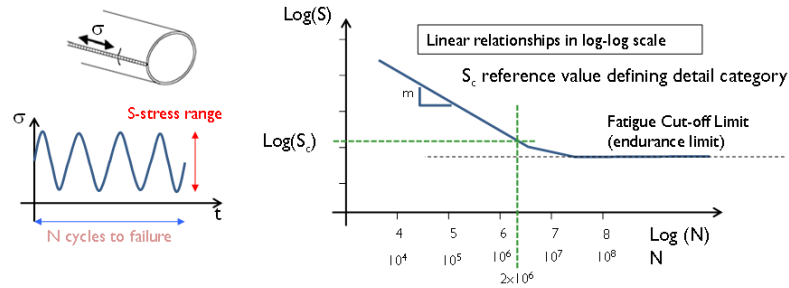


Figure 3.1 – Relationship between constant stress amplitude and number of cycles until failure (Veljkovic et al, 2015)

3.1.2 Fatigue safety assessment

In Europe, the most relevant standard for steel structural design is Eurocode 3, which includes a part (EC 3-1-9) dedicated to fatigue resistance calculations. This standard proposes two kinds of safety assessment: damage tolerant method and safe life method. The design of wind towers follows the second one and, in case of a steel tower, fatigue strength is represented by a series of S-N curves given in it. Different curves correspond to typical detail categories, depending on structure and manufacturing process. Each detail category is designated by a number which represents, in N/mm^2 , the reference value $\Delta\sigma_C$ for the fatigue strength at 2 million cycles. An overview of such curves is given in Figure 3.2. If the stress amplitudes are under the fatigue strength of the material, the number of load cycles no longer interests. On the other hand, if the stress amplitudes are above, only a certain number of load are supported (Veljkovic et al, 2015).

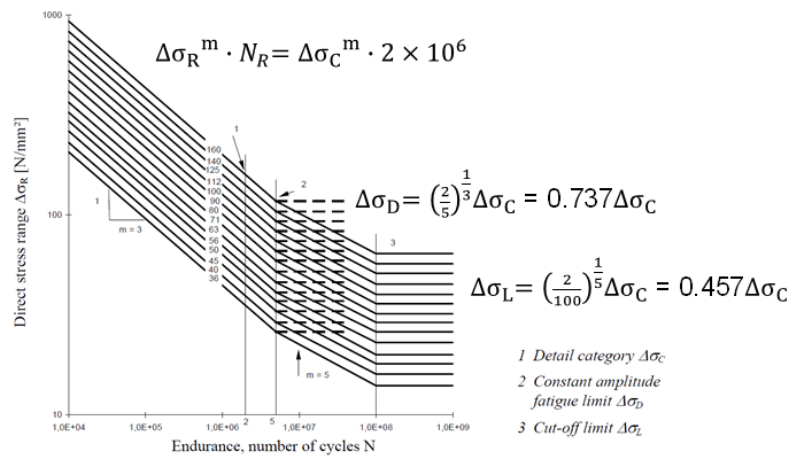


Figure 3.2 – Fatigue strength for nominal stress ranges represented by a series of $\log_{\Delta\sigma_R}$ vs $\log N$ curves (EC 3-1-9)

The fatigue design verification shall be based on damage accumulation based on linear cumulative damage calculation using for *e.g.* the Palmgren-Miner rule, or based on equivalent stress range. The Palmgren-Miner rule needs the full fatigue spectra of the load (effect) and of the resistance. The design verification is usually performed acc. to Eurocode (EC 3-1-9) by ensuring that the Palmgren-Miner damage accumulation is lower than unity:

$$D_d = \sum_i^m \frac{n_i}{N_i} \leq 1$$

The fatigue loads must be defined as Rainflow matrices, which contain information on load range and amplitude and also on its average. For linear systems, only the load range is required, thus the matrix can be replaced by a load spectrum. Therefore, the approach based on equivalent stress range, is simpler and only requires the comparison of the load (effect) range with the respective resistance range for a reference number of cycles. It is based on the concept of equivalent constant amplitude load range – Damage Equivalent Load (DEL). DEL can be defined as the single load range that would lead, at the considered number of cycles, to the same fatigue life (damage) as the considered load spectrum, when the comparison is based on a Miner's summation (Veljkovic et al, 2015). These approaches will be detailed in chapter 4.

3.2 Bolted ring flange connections

Nowadays, ring flanges connections are the most common solution to assemble tubular steel tower segments. Ring flange connections with preloaded high strength bolts are used for *in-situ* execution. To connect tubular steel profiles to each other, steel rings are welded to both tube ends and connected by preloaded high strength bolts. According to shape, there are two types of flanges: *L* and *T* model. *T* model is used in exceptional cases of large towers. In this thesis, *L* model is considered as this is the most common connection between tower segments, where pairs of steel flanges are welded on the inside of the tower and bolted together with pretensioned high strength bolts. Most flanges for onshore wind towers have diameters between 3m and 4.3m. Their width is established by the bolts and range between 100mm and 300mm, the thickness depends on the required stiffness and usually exceeds 100mm for the bottom flange. The bolts are usually M36 to M42, but they can reach M48 in some cases (Husson, 2008).

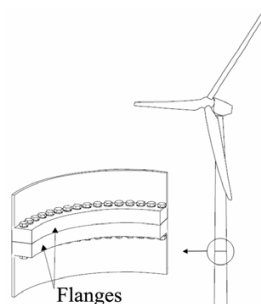


Figure 3.3 – Bolted L-flange connection (Husson, 2008)

3.2.1 Fabrication

Flange connections fabrication process is not only quite laborious but also very expensive. Flanges can be produced in two different ways, by welding or rolling. Flange imperfections may have a considerable influence on the resistance and, in order to meet the requirements for maximum imperfections, additional treatment is necessary, which undoubtedly leads to an increase of the production costs (Heistermann, 2011).

3.2.2 Theoretical background

The analytical determination of the structural behaviour of a preloaded ring flange connection under bending is quite complicated. Due to the high degree of contact surfaces needed, FE-simulations are too labour-intensive for the usual tower design (Veljkovic et al, 2015). During the last decades, several models for the design of the flange connections have been developed. The most common way is to use Petersen's model that was later on modified by Seidel. In this model the design of flange connections is simplified; it is assumed that the resistance of the three dimensional connection detail can be described by the resistance of only one segment of the tower flange. Therefore, the resistance is computed for a segment of a width, c , that equals the distance between two bolts, instead of considering the complete circumference, see Figure 3.4. Also, the tension force in the shell, Z , can be obtained by the integral of the axial stresses acting in the tower shell, σ_x , over the cross-sectional area of the shell segment, c . This bolt section has to fulfil the requirements of the Ultimate Limit State (ULS), Fatigue Strength (FLS) and Serviceability Limit State (SLS) (Heistermann, 2011). Due to this simplified 2-D model, the design for ULS and FLS can be done in a more practical way.

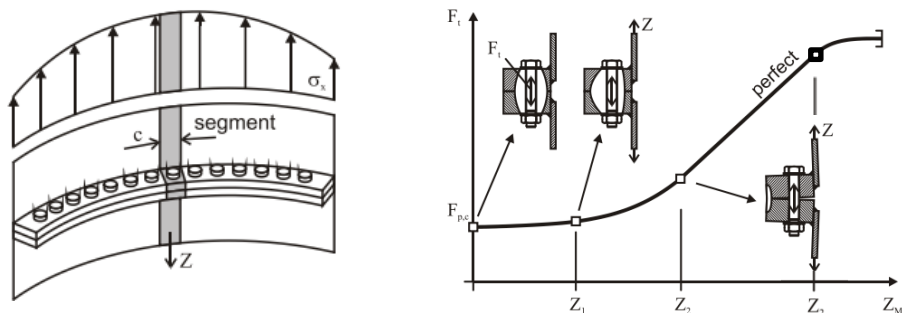


Figure 3.4 – Segment model of *L*-shaped ring flange connection (Veljkovic et al, 2015)

3.2.2.1 Load carrying behaviour of the segment – Fatigue resistance

As the fatigue loads are ranked in detail categories, 36*, 50 or 71, the design of the flange connections is generally governed by the fatigue resistance (Husson, 2008). The fatigue design for flange connections will be detailed later on this thesis, in the chapter 4.2.2. For the Fatigue Limit State (FLS) determination of the exact bolt load in function of the shell force, Z , plays a fundamental role. The applied loads are eccentric and the relationship between the load in the

shell and bolt force is not linear, as can be seen on the graph shown in Fig. 3.4. The general behaviour of a preloaded bolt in L -shaped ring flange connection can be described as follows:

- $Z \leq 0$ – for small tension forces, Z , in tower shell, the flange compressed zone (clamp solid) has the shape of a paraboloid of revolution and the bolt load, F_t , remains almost constant (slope is quite low) and equivalent to pretension force, $F_{p,c}$ ($F_t \approx F_{p,c} \approx \text{const.}$);
- $0 < Z \leq Z_1$ – as the load Z increases, the clamp solid begins to move in the direction of the flange edge and F_t slightly increases while the pressure acting in the contact zone between the flanges decreases progressively;
- $Z_1 < Z \leq Z_2$ – once the flange connection starts to open, an expeditious increase of bolt load, F_t , takes place;
- $Z_2 < Z \leq Z_3$ – the interface of the flanges stays only in contact at the flange edges; the slope of the opened connection depends on loads and geometry. The bolt load, F_t , increases linearly in function of the tension force in the shell, Z , until the yielding of the bolt starts and final rupture happens ($Z > Z_3$);
- $Z > Z_3$ – when reaching the elastic limit of the bolt (Z_3) the slope of the bolt-load function $F_t(Z)$ decreases and the connection reaches its limit due to the yielding of the bolt – failure of the connection.

Although fatigue failure of flange connections is governed by failure of the bolts, the resistance of the bolt is not sufficient to define the resistance of the whole connection. Actually, the connection solicitations depend on its geometry and pretension (Heistermann et al, 2009).

3.2.2.2 Influence of flange imperfections

Accuracy of the flatness of the flange itself is crucial for the connection resistance, but slops or gaps between the flanges cannot be avoided. In addition to manufacturing imperfections, further ones can appear from welding of the flanges to tower shell. In Fig. 3.5, the qualitative shape of the clamp solid after the preloading for different kinds of imperfections can be seen.

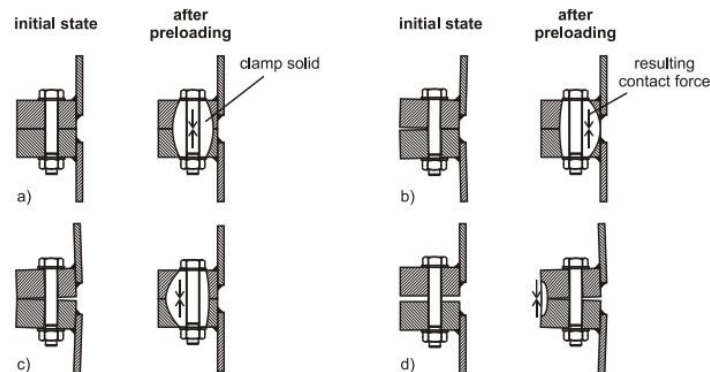


Figure 3.5 – Position of clamp solid in L -flange in a perfect (a) and different imperfect connections (b)(c)(d) (Veljkovic et al, 2015)

According to Jakubowski *apud* Veljkovic (Veljkovic et al, 2015), there are three types of imperfections that can occur in any combination:

1. Rotation symmetric or local taper with flange sided gap, Figure 3.5 case b)
2. Rotation symmetric or local taper with tube sided gap, Figure 3.5 case c)
3. Local parallel gap, Figure 3.5 case d). (Veljkovic et al, 2015)

All these imperfections can considerably affect the actual loads in the bolts near the region affected and consequently the performance of the entire connection. Therefore, imperfections radically reduce the lifetime of a connection (Heistemann, 2014).

3.2.2.3 Ultimate Limit State

The Ultimate Limit State (ULS) verification is normally done according to the plastic hinge theory. The flange behaves like a beam and failure modes are established with plastic hinges developing at different locations. The connection may fail by exceeding the resistance of the bolt, due to the development of plastic hinges either in shell or in flange or both at the same time. According to Petersen *apud* Veljkovic (Veljkovic et al, 2015), three failure mechanisms must be verified in *L*-shaped ring-flange connections and the lowest resistance, $Z_{ult,i}$, is controlling the design:

- Failure of the bolt – this governs failure mechanism when flanges and shells are stiff compared to the bolt;
- Failure of the bolt and plastic hinge in the shell at the same time;
- Plastic hinge in the shell and flange – the bolt load stays below its tensile resistance ($F_{t,Ed} < F_{t,Rd}$).

The last one, failure in the flange, has been separated into two new failure modes by Seidel. Based on experiments and numerical analysis, his model differentiates whether the plastic hinge occurs at the bolt axis or close to the shell, in the centre of the washer (Husson, 2008). However, in this document, only three failure modes will be considered and detailed in chapter 4.2.1.

3.3 A new type of connections

To overcome the disadvantages of flange connections such as complex design, laborious and cost intensive fabrication process and low fatigue resistance, an innovative solution for assembling segments of tubular steel towers for wind turbines has been studied and proposed – slip resistant connections with long open slotted holes. The HISTWIN project provides a guideline for the design of these connections claiming that this solution is not only simpler to produce but also 80% less expensive than traditional flange connections (Veljkovic et al, 2010).

Standard friction connections with normal clearance holes have been used in structural engineering for years. Slip resistant connections draw on load transfer between the joined parts

due to friction, which is guaranteed by a clamping force provided by preloading high strength bolts, see Fig 3.6. In addition to the force in the bolt, other important factor for load transfer is the surface condition of the clamping package, given by the slip coefficient, μ .

In this type of connection, all bolts are supposed to carry the same load and the maximum capacity of the connection is reached when the whole joint slips and the clamped plates move towards the bolt leading to bolt bearing (Heistemann, 2014). These joints not only have higher stiffness but also good energy dissipation properties, which improves the overall structure efficiency (Veljkovic and Husson, 2009).

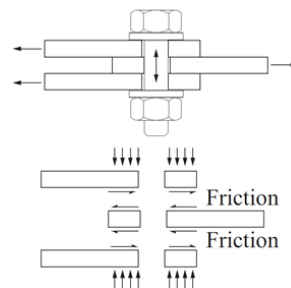


Figure 3.6 – Schematic view on load transfer in friction connections (Veljkovic et al, 2015)

Friction connections show as an efficient solution when movement in the connections with loads floating between tension and compression, *e.g.* wind loads, has to be prevented. However, this conventional friction connection is not practical for assembling tubular steel towers where some requirements arise: “for practical and safety reasons the fasteners shall be tightened from within the tower only, and the holes shape and clearance shall be adapted to facilitate alignment of the sections and installation of the fasteners” (Husson, 2008). (Veljkovic et al, 2012) proposed the replacement of the standard clearance holes on the lower tower segment (inner shell) with long open slotted holes with a cover plate, see Figure 3.7. Their width is equal to the normal clearance hole diameter, see chapter 3.3.2.2.2.

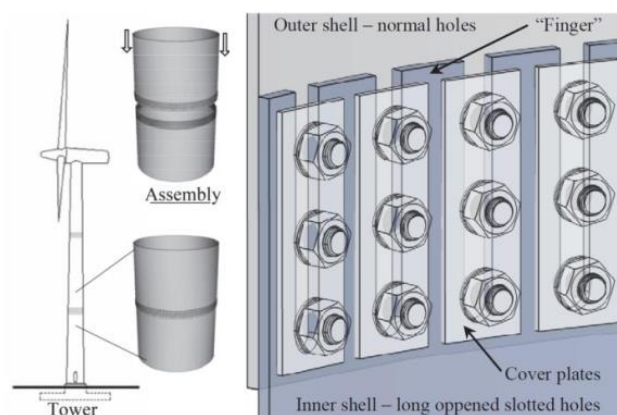


Figure 3.7 – Friction connection with long open slotted holes (Veljkovic et al, 2015)

The steel sections between the long slotted holes are called “fingers” due to their appearance. Moreover, there must be a gap between the upper and the lower segment of the steel tower, which is closed by preloading of the bolts. The friction connection length is an important aspect; as finger length increases, the force needed to close the mentioned gap decreases, but the risk of global buckling of the fingers also rises, which can affect the resistance of the friction connection. Consequently, although this document does not focus it, attention to the design of the connection length (finger length) must be paid.

The use of standard washers was experimentally found to have lower resistance with slotted holes, when compared to normal holes (Veljkovic and Husson, 2009). This is related to the different contact distribution of higher contact pressure, which increases with reduction of contact area – slotted holes. Thus, instead of standard washers for each bolt, a common cover plate with normal clearance holes is used on the inside of the tower. Its purpose is to spread the clamping force in a more uniform manner, ensuring a more homogeneous pressure distribution, and to hold the bolt group together in order to facilitate the assembling process. If the friction connection has cover plates with the same finishing as the shells, the second friction surface is activated doubling the ultimate slip resistance of the connection.

3.3.1 Fabrication

The replacement of bolted ring flange connections for friction connections allows a more diverse choice of the cross-section shape, which also provides the possibility to construct tower segments in a modularized way, *i.e.*, by vertically combining pieces of one segment. Therefore, the transportation limit¹ is overcome as the segment-pieces can be assembled *in-situ* and larger diameters are achievable, which enable the increase of hub heights (Heistemann, 2014). Feasibility studies within HISTWIN projects proved that tower segments using friction connection would be easily fabricated and assembled. In addition, as this solution is simpler to produce, it is about 80% less expensive than the traditional bolted ring flange connections (Pavlovic et al 2015). According to Veljkovic (Veljkovic et al, 2012), due to replacement of flange connections for friction connections, the total reduction of tower costs is about 15%. This reduction relies not only on the elimination of laborious and time-consuming flange production, but also on material savings.

3.3.2 Theoretical background

Comparatively to the flange connections, friction connection design process is much easier and can also be performed faster. As for the design of flange connection, the design of a friction connection can be performed segment wise, *i.e.*, not the complete cross-section of the tower has

¹ Transportation restrictions enforce limits on the diameter and length of the elements – usually the diameter of the bottom segment should be lower than 4.3m to pass under bridges and the elements length is ranging between 20m and 30m (Husson, 2008).

to be considered but only a segment with a single bolts' row, assuming that longitudinal stresses are uniformly distributed over that segment width, c .

Slip resistance connections rely on load transfer between the joined parts due to friction. That is ensured by clamping together the plates of the joint with the help of the preloaded high strength bolts. These bolts are usually of grade 10.9 or higher. For friction connections design Eurocode (EC 3-1-8), for example, can be followed. The slip resistance of the connection is then considered as the ultimate resistance of the connection. The fatigue of the connection also needs to be checked, but it is not regarded as authoritative for the design of a tubular tower.

3.3.2.1 Fatigue resistance

Besides the referred cost savings due to technical simplicity of this solution, friction connections are less sensitive to fatigue. Dependant on the used method to determine the bolt-load function, different detail category must be used. If the bending moments in the bolts are considered by the model, a detail category 50 should be used for bolts, acc. to Eurocode (EC 3-1-9). The friction connection in steel tubular towers (shell) can be regarded as detail category 90 and should withstand a number of 10^8 load cycles. The fact that fatigue detail increases, comparing to fatigue detail class for common flange connections (71-36*), change the design limit from resistance of the connection (fatigue) to resistance of tower shell (stability), which justify the use of thinner plates and offers the opportunity to use higher strength steels (Heistemann, 2014).

Furthermore, a less complex design method applies for fatigue design, as in friction connection a linear behaviour of the connection can be considered. As the relation between fatigue loads and the response of bolts in friction connections (stress variation ranges) is linear, damage equivalent load (DEL) method can be applied. The DEL can be defined as the constant load range which would lead, at the considered number of cycles, to the same fatigue life (damage) as the considered load spectrum, but that will also be explained later on chapter 4.3.2.2.

For the fatigue design of the bolts, the load variation range, $\Delta F_{p,C}$, in the preloaded bolts has to be checked, see chapter 4.3.2. The final fatigue design verification is done by insuring that:

$$\frac{\gamma_{Ff} \Delta \sigma_{DEL}}{\Delta \sigma_R / \gamma_{Mf}} \leq 1.0$$

The applied load (effect) ranges ($\Delta \sigma_{DEL}$) should be multiplied by the safety factor for loads ($\gamma_{Ff} = 1.10$) and the reference fatigue strength values ($\Delta \sigma_R$) divided by the safety factor for materials ($\gamma_{mf} = 1.15$) to obtain the corresponding number of cycles n_i or N_i for each band in the spectrum (EC 3-1-9). The fatigue design of the shell is computed using the same methods of the bolts, but using a different detail category.

3.3.2.2 Ultimate Limit State

The Ultimate Limit State (ULS) verification is regulated in various standards and guidelines. In this document, the design is performed according to Eurocode (EC 3-1-8). The slip resistance of the connection is then considered as the ultimate resistance of the connection and its calculation mainly depends on friction properties of joined surfaces and the preload in the engaged bolts.

Although this kind of connections is a single lap joint, *i.e.*, providing one friction surface, recent findings in the HISTWIN2 project have shown that the second friction surface is activated – the interface between the cover plates and fingers – after the ULS is reached (Veljkovic et al, 2015). Initially, the load is carried by the friction force between the outer and inner (fingers) shell. When the slip resistance is reached the slip occurs and the friction force between the fingers and the cover plate is activated. As mention before, as the friction connection has cover plates with the same finishing as the shells, the second friction surface activation doubles the ultimate slip resistance of the connection.

3.3.2.2.1 Slip factor, μ

For a good performance of friction connection, ensuring sufficient friction between facing surfaces is essential. That is taken into account by the slip factor or by the friction coefficient. The slip factor is defined as the ratio between slip load and initial pretension (clamping force) – nominal value – while the friction coefficient is defined as the slip load over the actual clamping force – considering true physical properties (Heistemann, 2014). Both vary depending on the type of surface finishing, the steel grade of the clamped plates of the connection and the thickness of the primer (Heistemann, 2011), (Veljkovic et al, 2012). The slip load is defined in EN 1090-2 as the load at which the maximum permitted slip of 0.15mm occurs.

Establishment of the slip factor is essential. Surface classification and corresponding slip factor for steel grades up to S460 are defined in Eurocode (EC 3-1-8). Alternatively, the slip factor can be identified by specific friction tests regulated in EN 1090-2, Annex G, which prescribes the specific specimen and the necessary procedure. Evaluation of test results follows the procedure presented in Eurocode (EC 0), (Heistemann, 2014). Depending on the used method to obtain the slip factor, different values may result for the same type of coating. In this document, two different contact surfaces are studied: contact surface painted with primer → Zinc coating $\mu=0.45$; tower shell made of weathering steel → Weathering steel $\mu=0.79$. These values are used in HISTWIN project (Veljkovic et al, 2015).

It has been found that the friction coefficient of the friction connections with long open slotted holes decreases when compared to standard round holes (Heistemann, 2014). This is related to the reduced contact area and complies with the correction factor, k_s , which consider the shape of the hole, see chapter 3.3.2.2.3.

3.3.2.2.2 Open slotted holes

As mention before, to ease the assembling process of tubular sections on the construction site, Veljkovic (Veljkovic et al, 2012) proposed the replacement of the standard clearance holes on the lower tower segment with long open slotted holes, which have the same width of the normal clearance hole diameter, with a cover plate. The bolts can be preinstalled in the normal clearance holes of the upper tower segment and they can thus be used for the angular alignment of the upper section while it slid down on top of the lower segment, with open slotted holes, see Fig. 3.7. Thereby, bolts can be preassembled which facilitates not only the mentioned alignment of the segment towards the open slotted holes, but also the process of tightening the bolts. Temporary support must be provided to hold the sections during the tightening.

The (lower) shell bending stiffness is locally reduced, which provides good conformation between tower tubes without significantly affecting the contact pressure, which increases with reduction of contact area. Thus, this type of connections allows tight contact between cylinders (Husson, 2008), (Veljkovic et al, 2012). Furthermore, instead of standard washers for each bolt, a common cover plate with normal clearance holes is used on the inside of the tower. Its purpose is to spread the clamping force in a more uniform manner, ensuring a more homogeneous pressure distribution, and to hold the bolt group together, facilitating the assembling process.

3.3.2.2.3 k_s

According to Eurocode (EC 3-1-8), if the hole is not a “normal clearance hole”, a correction factor, k_s , must be considered. The value of the reduction factor varies with the hole’s geometry of the connection (shape and size of the hole) as described in Table 3.6 of the Eurocode (EC 3-1-8). According to it, the correction factor, k_s , should be taken as 0.63 for the studied connection with long slotted hole parallel to load action.

3.4 Bolts

A structural connection is composed of several parts that guarantee the continuity of a structure and efforts transmission along it. Bolts play the main role in a friction connection as they ensure if the connection withstands a load or not. Thus, is essential to understand their performance.

There are two well know problems of bolt connections: they tend to open by themselves and they lose some of their pretension over time. The first one, the self-loosening effect, requires regular control and maintenance of bolted connection. The continuously need of tighten up all bolts in a tubular steel tower would be reckless and too expensive. This raised the question if there were bolts available on the market that do not untighten by themselves (Heistermann, 2011). The second problem with bolts is that they lose some of their pretension over time and it is very important that the bolts constantly keep the pretension force that they were designed for. Therefore, it is important to understand the behaviour of the bolts and be able to compute the changes in bolt force. Usually, as mentioned by Sedlacek and Kammel *apud* Heistermann

(Heistermann, 2011), loss of pretension can appear due to: self-loosening, relaxation in the connection, insufficient pretension force at installation (*e.g.* poor execution), material creep, use of unsuitable coatings, yielding of the bolt in the threaded part of the engaged shaft. A brief explanation of these phenomenon are presented in chapter 3.4.1 and 3.4.2.

Therefore, four types of bolts will be presented, which are foreseen as a potentially competitive solution. These bolts are the Tension Control Bolt, the Huck BobTail LockBolts, a standard bolt combined with a pair of Nord-Lock washers and the Friedberg HV Rändel.

3.4.1 Self-loosening effect

Most of engineering products with some degree of complexity uses threaded fasteners. Threaded fasteners are a discrete piece of hardware that has external or internal screw threads. They are usually used for assembly multiple parts and in most of the cases they permit disassembly. The common threaded fasteners types are screws, bolts and nuts (Groover, 2010). One of the main advantages of threaded fasteners, over the majority of other joining methods, is that, they can be disassembled and reused, which is a significant source of problems in machinery and other assemblies (Eccles, 2011a). One of the reasons to those problems is due to them unintentionally self-loosening.

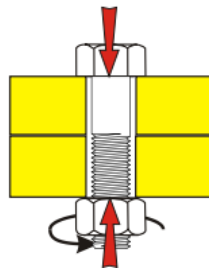


Figure 3.8 a) Preload induced by tightening the fastener (Eccles, 2011b)

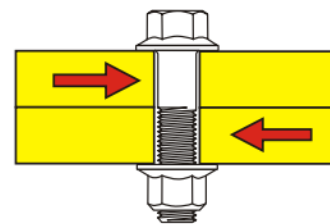


Figure 3.8 b) Transverse movement of a bolted joint (Eccles, 2011b)

Bolts are mostly used in clearance holes and, for their structural integrity, they rely on the preload induced by tightening the fastener (Figure 3.8 a)). If the fastener self-loosens, the preload will be reduced or even eliminated, which can lead to structural failure.

In 1969, Gerhard Junker published a technical paper (“New criteria for self-loosening of fasteners under vibration” SAE Paper 690055, 1969) showing why threaded fasteners self-loosen. He found that transverse dynamic loads create a far more tough condition for self-loosening than dynamic axial loads and it’s because the radial movement under axial loads is considerably smaller than that which is sustained under transverse loading. Gerhard Junker found that transverse joint movement was the cause of self-loosening of threaded fasteners (Fig. 3.8 b)). That relative movement occurs when the transverse force acting on the joint is bigger

than the frictional resisting force generated by the bolt's preload. Therefore, the mechanism can completely loosen fasteners under repeated transverse movements (Eccles, 2011a).

It is also worth mentioning that, if sufficient preload can be obtained from the bolts to prevent joint movement, no locking device would be needed, since friction would hold the parts together. However, when variations in frictional conditions are taken into account, the main problem of designing with threaded fasteners is guaranteeing that the preload is enough to hold the parts effectively together. Thus, designing the joint using the mean value of preload with no "safety factor" applied, would possible result in a number of bolts losing. However, designing with the minimum estimated preload provided by the bolt would remove the risk of self-loosening (Eccles, 2011a).

3.4.2 Loss of pretension

There are some cases where the slip resistance is governing the entire resistance of a structure and an underestimated or carelessness loss of preload may have huge consequences. Therefore, is reasonable to assume the loss of preload during the life time of a structure, whereas the remaining preload in the engaged bolts is crucial for the performance of a friction connection (Heistermann, 2014). In a slip resistance connection, when the loss of pretension in the bolts reaches a certain level and the bolts do not provide the pretension force which the connection has been designed for, slip may occur and the connection fails. The reduction of bolt force is usually divided into 3 phases (Heistermann, 2014):

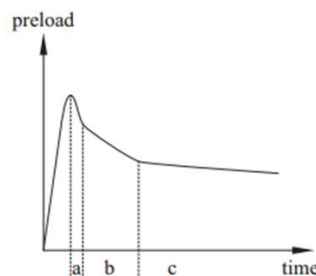


Figure 3.9 – Time dependent development of preload (Heistermann, 2014)

- a) The initial loss of pretension happens within the first couple of seconds after tightening the bolts – mainly depending on the tightening;
- b) The short term loss appears. This occur during the first twelve hours after tightening;
- c) The long term loss stars and develops asymptotically during the life time of the bolt.

The first drop in pretension force (initial loss) depends on the installation process of the bolts and it happens within the first ten seconds after the bolt is tightened. That loss increases with bigger initial preload, especially if the bolt has been tightened beyond its yield limit. In case of faster tightening process, the reduction in clamping force has been observed to increase

(Heistermann, 2011), therefore the loss of preload rises. It is also worth mention that when groups of bolts are tightened they usually influence each other; the bolt tightened initially will show the first drop in pretension force while the second bolt is being pretensioned. This is examined and explained by Husson, with Tension Control Bolts (TBCs) (Husson, 2008).

After the initial loss happened, the short term loss happens. Usually, it occurs in a bolted joint because of loading passing their yield point; the members of the joint may creep and thereby incite a reduction of elongation in the bolt, leading to a loss of clamping force (Bickford, 1998) (Heistermann, 2011). However, the most common phenomena that causes relatively short term relaxation is embedment. Under initial contact forces, high spots on thread and other contact surfaces yield and creep. Thus, the surfaces settle into each other until enough surface area has been brought into contact to stabilize the joint. This is known as embedment and is illustrated in Figure 3.10 (Bickford, 1998). Short term relaxation is known to be terminated 12 hours after tightening. The remaining force in the bolts is called residual preload (Heistermann, 2011).

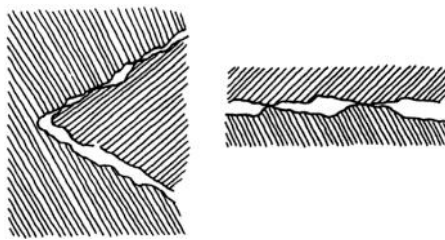


Figure 3.10 – Embedment (Bickford, 1998)

Long term relaxation describes the reduction of the residual preload during the life time of the connection. Generally, this happens due to stress relaxation of the bolt and clamping package, lateral contraction and external tensile loads. It also depends on self-loosening of the bolt, which is caused by vibration provoked by dynamic loads acting on the structure (Heistemann, 2014).

3.4.3 Tension Control Bolts

Tension Control Bolts (TCBs) are heavy duty bolts used in structural steelwork connections, generally to provide the clamping force. They are a special type of strength fastener with tightening carried out entirely at the nut end with a special electric wrench. As tightening is performed specifically at the nut end, no torsion is introduced in the shank. This property lowers the risk of self-loosening and the amount of torsional relaxation. Their primary advantage over other types of friction bolts is the ease of preloading the bolts (Cosgrove, 2004). Other advantages are presented in the table at the end of this subchapter, Table 3.2.

TBCs are available in metric sizes up to M30. They have mechanical properties similar to High Strength Bolts: grade S10T can be considered as bolt grade 10.9 (Cosgrove, 2004).

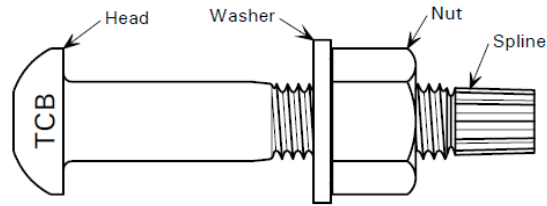


Figure 3.11 – Tension Control Bolt (Heistermann et al, 2009)

The end of the shank has a spline on it which is attached with an electric shear wrench which prevents the bolt from turning while the nut is tightened. Outer socket rotates clockwise and tighten the nut. When the correct preload/proper tension is reached the outer socket stops rotating and the inner socket counter rotates and shear the spline off (UK TCB Brochure).

Table 3.2 – Advantages of TCB (UK TCB Brochure)

TCB Advantages	
Technical	<ul style="list-style-type: none"> • Consistent tension • Visual Inspection • Higher grade steel and increased pre-load enables the use of smaller diameter bolts • TCBs can be used in Shear and Tension • No bolt relaxation since no torsional shear is induced during tightening • Does not loosen with vibration - no locknut required
Cost Saving	<ul style="list-style-type: none"> • Quick, safe and easy to install • One man installation on one side of the structure • Reduced tool maintenance • One tool can install several diameters
Safety	<ul style="list-style-type: none"> • Non-impacting electric shear wrenches • No heavy calibrated torque wrenches required • Light weight electric wrenches of various shapes and sizes • No risk of HAVS (hand-arm vibration syndrome) • Reduced operator fatigue • No air compressors with dangerous pipes and cables • Low on-site noise - under HSE minimum levels

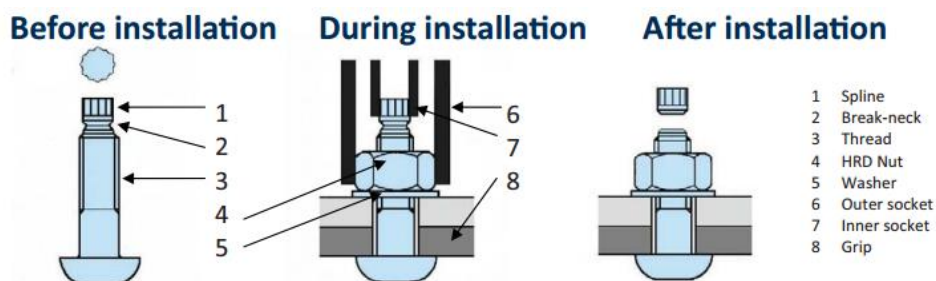


Figure 3.12 – Installation of TCB (UK TCB Brochure)

3.4.4 Huck BobTail Lockbolts

The Huck BobTail lockbolt is a special type of high strength fastener produced by Alcoa Fastening Systems in Great Britain, see Figure 3.13. This type of bolts is formed by a smoother thread part, without sharp thread edges, which provides the bolt a larger core diameter and less stress concentration in the thread. In order to allow the coupling of the tightening equipment, the bolt body has a thinner part.

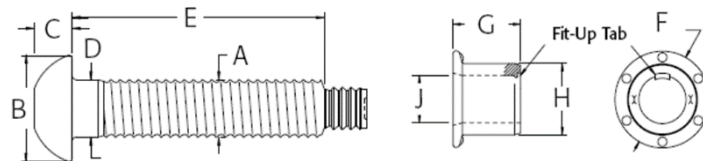


Figure 3.13 – Huck BobTail lockbolt (Heistermann, 2011), (Alcoa, 2015)

BobTail offers safe, quiet, swaged-on installation technology. They are designed to deliver superior joining strength even in the most extreme environments and to provide a high level of reliability. They are also engineered to have a vibration-resistance performance (Alcoa, 2015), (Fric et al 2014). One prominent property is a threadless nut, which gets swaged to the shank of the bolt. As mention before, the effective diameter of the bolt is reduced in order to allow it to stretch more when installed. Thus, the fastener has less preload loss caused by the seating of the joint (Fric et al 2014). Huck BobTail lockbolts are available in a wide range of sizes and grades (Alcoa, 2015). They are also easy and faster to install. The tightening of the bolt can only be made from the nut end and is carried out with the help of the installation tool. The tightening system is composed by four steps as presented in Fig. 3.14.

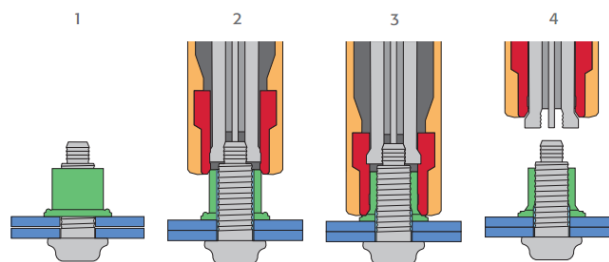


Figure 3.14 – Huck BobTail installation (Alcoa, 2015)

The bolt is placed into the hole and the threadless nut is manually tightened into the threaded part of the bolt (1). Then, the installation tool is applied and activated (2), a puller in the nose assembly comes down. Thus, the bolt gets prestressed by the installation tool and by the cold forming of the collar into the bolt thread grooves, drawing up any sheet gap, until desired load (3). When swaging of the collar is complete, the equipment is automatically uncoupled (4).

To open the bolt again, the same tool used in installation is needed, plus a special cutting device (Heistermann, 2011). The six circular spots in the collar flange, which can be seen in view F of Figure 3.13 and in Figure 3.15, function as marks for the installation process to indicate whether

the BobTail collar has been fully swaged on or not. Even if only one indicator has been marked, we can establish that a full swage has been achieved (Alcoa, 2015). Another significant advantage, when compared to conventional nuts and bolts, is that they are up to 10 times the fatigue strength (Alcoa, 2015). Other advantages can also be seen in the next table.



Figure 3.15 – Installation indicators on collar flange before and after installation (Alcoa, 2015), (Fric et al 2014)

Table 3.3 – Huck BobTail Lockbolts Benefits (Alcoa, 2015), (Fric et al 2014)

Huck BobTail Lockbolts Benefits	
Technical	<ul style="list-style-type: none"> • High fatigue strength thread ensuring vibration resistant installation, then: <ul style="list-style-type: none"> _ Superior strength (fatigue) _ Vibration resistance • Large bearing flanged head adds strength to the joint • "Fit-up" tab ensures alignment of collar on the pin • Large bearing flange eliminates need for hardened washers
Installation	<ul style="list-style-type: none"> • Secure/Fast Installation • Silent installation • No special training or skills required to install – easy installation • Quick visual inspection is all that's needed for a quality-assured joint: <ul style="list-style-type: none"> _ The installation in the collar flange indicates if the BobTail collar has been fully swaged on (see Figure 3.15)
Cost Saving	<ul style="list-style-type: none"> • Low overall installation cost

3.4.5 Standard Bolts with Nord-Lock washers

The Nord-Lock security system is a wedge locking system that includes a pair of lock washers that has cams on one side and radial teeth on the opposite side, see Figure 3.16 b), which must be used in combination with standard structural bolts. The shape of the wedge is selected so that the angle of the wedge surface is always greater than the thread angle, see Figure 3.16 b). The wedge lock washers are installed in pairs, cam face to cam face (Nord-Lock Group, 2014).

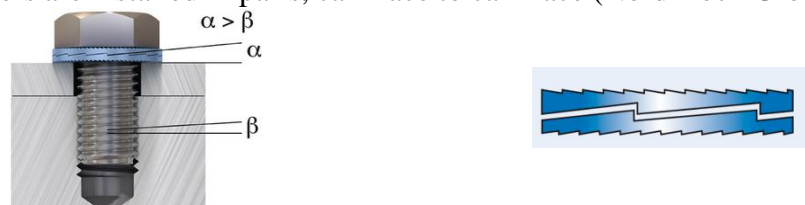


Figure 3.16 – a) Nord-Lock wedge-locking technology; b) Nord-Lock wedge lock washer (Nord-Lock Group, 2014)

Nord-Lock wedge-locking has the ability to secure bolted joints exposed to severe vibration and/or dynamic loads. Nord-Lock washers lock bolted joints with tension instead of friction. This means that when the bolt and/or nut is being tightened, the washer-pair is pressed together, gripping and embedding themselves into the mating surfaces. Therefore, the paired washers are firmly embedded in their position allowing movement only across the face of the cams. Even the lesser rotation of the screw during vibration causes an enhancement in preload strength due to the wedge effect - the screw locks itself (Nord-Lock Group, 2014).

Whenever the bolt begins to open, the washer pair does the same. But due to different angles in the washer and the bolt thread, see Fig. 3.16 a) (the cam angle " α " is larger than the thread pitch " β "), the pair of wedge lock washers expands more than the corresponding pitch of the thread, preventing the bolt from loose and keeping it preloaded (Heistermann, 2011), (Nord-Lock Group, 2014). If the bolt is untightened with a wrench, the pair of washers expands more than the corresponding pitch of the thread allowing the bolt/nut to rise (Nord-Lock Group, 2014).

Due to the extreme hardness of the washers it is possible to use them with a screw in a property class up to 12.9 (Nord-Lock Group, 2014). Some of the benefits of using this type of connection are presented in Table 3.4.

Table 3.4 – Benefits of using Nord-Lock wedge-locking solutions (Nord-Lock Group, 2014)

Benefits of using Nord-Lock wedge-locking solutions	
Technical / Installation	<ul style="list-style-type: none"> • Maintains high clamp load and thereby ensures the function of the joint • Reliable security against loosening • Quick/easy to install and remove with standard tools • Verifiable locking function • Locking function not affected by lubrication • Defined and uniform friction conditions which result in a more accurate preload • Same temperature characteristics as standard bolt/nut • Reusable – in addition, Nord-Lock wedge lock washers do not affect the reusability of fasteners • The washers are hardened and can support and distribute great loads • Washers with enlarged outer diameter available for flanged bolts/nuts • High corrosion resistance • Can be used with fasteners up to grade 12.9 (ASTM A574) • Reliable screw locking, even for joints with short clamp length and under conditions of extreme vibration and dynamic stress • Secures fasteners at both high and low preloads • No retighten needed

3.4.6 Friedberg HV Rändel

The Friedberg HV Rändel is a press fitted bolt produced in Germany by August Friedberg GmbH. It is a high strength bolt with a knurl at the shank, under the bolt head, which fixes the bolt in the hole ensuring its position. Those bolts are tightened only using conventional tools (Heistermann, 2011). As they are press fitted bolts, they are not fully comparable to the other bolts described above. Press fitted bolts transfer some of their clamping force by pressuring the clamping package (as TCB, Huck BobTail Lockbolts and standard structural bolts also do) but the remaining force is transferred by friction of the fitted bolt shank (Heistermann, 2011).

Studies made by (Heistermann, 2011) proved that installing those bolts was complicated since, due to the inserted strain gauges, a special carefulness was necessary. The bolts must be pulled into the hole by tightening the nut from the other side. Those gauges inserted into the bolts' shank served to measure all of the bolt forces.

Furthermore, research studies (Heistemann, 2014) reveal that the tests with Tension Control Bolts (TCBs) presented the best results. Therefore, the designed friction connection presented on chapter 5.5 will be using this type of bolts (S10T).

4 CONNECTIONS

In this chapter all formulas needed for design verification will be presented. In the next chapter an *Excel* tool programmed for each verification will also be presented. Note that, the *Excel* tool for friction connection (ULS) was programmed by HISTWIN project, the other three (flange connection ULS and SLS and friction connection SLS) were made based on the existing one.

4.1 Design Loads

Wind turbines are subjected to specific loads and stresses. The main loads acting on a wind tower are: self-weight of different elements, actions of wind (thrust and drag) on the blades and wind pressure on the tower (Husson, 2008). Wind loads are highly variable in time. Obviously, varying loads are difficult to handle, when compared to static loads, as the material becomes fatigued. For this thesis, as the design of the connections is done for an existing MM92 tower produced by *REpower*, the connections were designed according to the loads provided by them.

4.1.1 Wind Loads

The starting point for a wind turbine load spectrum are the loads acting on the rotor blades, which are then passed on to the other components and to a large extent, determine their loading. Comparing to these loads, the loads originated directly from downstream components are less significant. Therefore, the loads acting on a wind turbine can be represented by the ones acting on the rotor (Hau, 2006). During steady and symmetrical flows, the wind loads on the rotor blade are established by the effective wind speed varying from the blade root to the tip, and by the geometric shape of rotor blades (Veljkovic et al, 2015).

For design, establishing limit loads is a matter of detecting infrequent load situations that can damage structure or its mechanical components. The life of a wind turbine is then represented by a set of design situations covering the most significant, but realistic, combinations of external wind conditions and machine states that the wind turbine may experience. The wind regime for load and safety concerns is divided into normal wind conditions, which occur frequently during normal operation of a wind turbine, and extreme wind conditions that are defined as having a 1-year or 50-year recurrence period (GL, 2010). The combination of design situations with safety factors is presented using 22 Design Load Cases, although only some of them are usually relevant for the structural safety assessment of the support structure (Veljkovic et al, 2015). The most relevant load cases for the design of tubular wind towers are those that cause maximum loads (effects) along the tower height, *e.g.* cross-section forces, when the ULS are expected.

Maximum loads (effects) on different structural components along the tower may be achieved with distinct load cases. It is necessary to have a large number of load cases as it cannot be foreseen, *e.g.* whether it is the load cases leading to fracture stress or the fatigue strength under continuous load that will be controlling design. However, some cases are expected like the load case that delivers maximum shear force at the top of the tower will normally be designed driving for the bending moment along the tower, except for the upper part, where the load case leading to maximum bending moment will be designed driving. On the other hand, for fatigue check, conclusions about controlling design load case are usually not possible. Thus, information about fatigue spectra for each tower section must be provided (Hau, 2006), (Veljkovic et al, 2015).

Generally, to calculate wind turbine loads, dynamic simulations using a structural dynamic model are used. The designers rely on models simulating loading conditions over a range of operational and extreme wind speeds and fault states, in order to consider the extrapolation to 20 years of extreme and fatigue loads (Veljkovic et al, 2015).

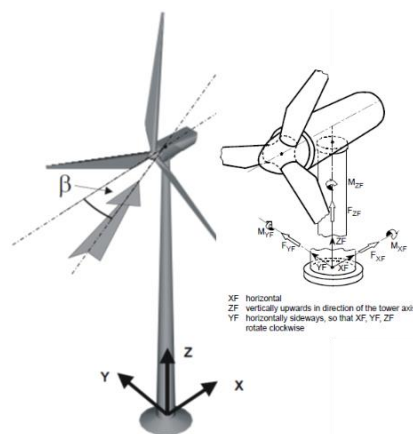


Figure 4.1 – Coordinate system to define design loads and wind direction (Veljkovic et al, 2015)

4.1.1.1 Extreme loads

The design loads are usually summarized in load tables. According to GL-Guideline (GL, 2010) the result of extreme load evaluations, including partial safety factors, should be presented in tabular form for each position investigated, *e.g.* blade sections, blade root, rotor shaft, tower, *etc.* Those tables must contain a brief description of the load case with statement of the partial safety factor applied. The recommended presentation format is: the extreme values (maxima and minima) of the corresponding load component are located on the diagonal and the simultaneous loads of the other load components are given in the rows. For the extreme loads in tower coordinate system, a column should be added to the table for the wind speed and wind direction belonging to extreme load situation. The sign of wind direction must be indicated in a sketch or stated in accordance with the coordinate systems (Fig. 4.1).

The tower considered for the case studies presented in chapter 5 is an existing MM92 tower produced by *REpower*. *REpower* provided the design loads of that wind tower as load tables, which includes the results for the load cases that lead to the maxima of each load component.

The given loads are design loads, *i.e.*, the displayed values already include a safety factor. For a specific load case, design loads can be linearly interpolated between two given sections. An excerpt is presented below which shows the decisive internal forces at the tower bottom section.

section	FxTS01	FyTS01	FzTS01	Fr01	MxTS01	MyTS01	MzTS01	Mr01	VcupHC	VdirHC	safety
0	kN	kN	kN	kN	kNm	kNm	kNm	kNm	m/s	deg	factor
MAX:	725.2	37.6	-3266.2	726.2	-743.6	54973.6	1125.3	54978.8	16.5	-7.9	1.35
MIN:	-873.2	27.6	-3174.7	873.6	521.1	-67796.3	-1363.1	67798.3	9.0	-0.1	1.35
MAX:	177.6	958.3	-2495.2	974.6	-64868.7	10167.4	-1043.1	65660.7	55.8	-59.2	1.10
MIN:	-217.4	-933.0	-2602.6	958.0	64537.7	-14579.7	1339.3	66164.0	56.4	120.7	1.10
MAX:	188.3	-495.9	-2220.2	530.4	35316.9	6203.4	24573.0	35857.5	57.8	4.4	1.10
MIN:	56.9	-249.6	-3507.7	256.1	18529.1	-234.7	590.7	18531.0	37.5	14.7	1.50
MAX:	177.6	958.3	-2495.2	974.6	-64868.1	10167.4	-1043.1	65660.7	55.8	-59.2	1.10
MIN:	0.1	-0.1	-3205.9	0.2	18.5	-962.5	-70.0	962.8	0.8	-63.5	1.35
MAX:	-217.4	-933.0	-2602.6	958.0	64537.7	-14579.7	1339.3	66164.0	56.4	120.7	1.10
MIN:	177.6	958.3	-2495.2	974.6	-64368.7	10167.4	-1043.1	65660.7	55.8	-59.2	1.10
MAX:	722.2	64.7	-3266.6	725.1	-1668.7	55329.4	1130.3	55354.4	16.5	-7.9	1.35
MIN:	-873.2	27.6	-3174.7	873.6	521.1	-67796.3	-1363.1	67798.3	9.0	-0.1	1.35
MAX:	462.4	-178.8	-2695.1	495.8	15718.7	32538.1	5556.6	36135.5	24.0	-7.5	1.10
MIN:	-262.0	85.9	-3010.3	275.8	-6287.4	-25287.7	-6476.2	26056.9	32.9	-8.5	1.35
MAX:	-873.2	27.6	-3174.7	873.6	521.1	-67796.3	-1363.1	67798.3	9.0	-0.1	1.35
MIN:	17.1	4.8	-2629.3	17.8	-3.4	-0.3	-132.5	3.4	14.0	-8.0	1.10

Table 4.1 – Example of extreme loads at tower bottom

4.1.1.2 Fatigue Loads

The loads are initially derived in time domain by a simulation programme. These simulations provides times series of the load effect, which in case of the support structure are time series for several load cases and for all load components. In order that the time phase between different load components can be considered, time series include information on load range and its level as well as how often an event occurs and when it does. Although time series are the most accurate source of providing loads for fatigue analysis, they are very complex to handle. When load amplitude is needed, to simplify the fatigue design, a Rainflow count is performed. The information given by the time series calculated for each of the design load cases is condensed in a Rainflow matrix or a Marcov matrix that includes information on the load range, mean and number of occurrence. For linear systems only information about the range value and the respective number of cycles is needed. That can be obtained through established algorithms for Rainflow counting, resulting in the Whöler or S-N curves, which are defined based on a constant loading range related to the number of cycles until failure, *i.e.*, fatigue life.

A further simplification can be done replacing the fatigue load spectrum by the use of a Damage Equivalent Load (DEL). DEL method is only applicable for linear systems, *i.e.*, as long as a linear relation between load-actions and member stresses exists. For the friction connections design, as the relation between fatigue loads and the response of bolts is linear, DEL method

can be used. Damage equivalent fatigue loads can be presented in load table for different tower sections height for all material relevant slope parameters of the S-N curves (GL, 2010).

DEL presented in load tables can be taken as a static load case in combination with the reference number of cycles (*e.g.* $N_{ref}=2 \times 10^8$). and a S-N curve with constant Wöhler slope m . Generally, only one slope is of interest for a certain kind of structural material, for steel structures $m=4$ is relevant. Fatigue loads for the considered tower were also provided by *REpower* in the form of load tables with DEL effects, Table 4.2. The columns give information about different load components and the different rows include fatigue load calculated for different tower sections.

Table 4.2 – Example of Damage Equivalent Load effects (Veljkovic et al, 2015)

section 0	Nref: 2.0E+08 Tower Base					
	FxTS01 kN	FyTS01 kN	FZTS01 kN	MxTS01 kNm	MyTS01 kNm	MzTS01 kNm
m						
3	92.2	47.9	26.4	3239.6	5057.2	1104.0
4	102.6	67.8	28.9	4774.0	6204.1	1228.7
5	115.5	91.0	32.7	6443.5	7353.9	1383.6
section 21.46	Nref: 2.0E+08					
	FxTS13 kN	FyTS13 kN	FZTS13 kN	MxTS13 kNm	MyTS13 kNm	MzTS13 kNm
m						
3	85.0	46.4	26.4	2270.8	3376.7	1104.1
4	96.6	66.9	28.9	3361.6	4267.4	1228.8
5	110.5	90.2	32.7	4526.7	5109.7	1383.7
section 48.08	Nref: 2.0E+08					
	FxTS29 kN	FyTS29 kN	FZTS29 kN	MxTS29 kNm	MyTS29 kNm	MzTS29 kNm
m						
3	65.7	41.1	26.4	1179.1	1910.0	1104.2
4	81.2	60.8	28.9	1725.6	2379.4	1228.8
5	96.3	81.9	32.7	2321.3	2824.4	1383.8
section 75.64	Nref: 2.0E+08 Tower Top					
	FxTS45 kN	FyTS45 kN	FZTS45 kN	MxTS45 kNm	MyTS45 kNm	MzTS45 kNm
m						
3	65.4	37.8	26.4	235.3	1065.2	1104.4
4	80.5	55.1	28.9	312.9	1206.5	1229.1
5	95.4	74.4	32.7	393.3	1378.4	1384.1

However, for fatigue design of bolts in flange connections, as the relationship between the tension in tower shell and bolt force is non-linear, the simplification of the fatigue load spectrum into a DEL cannot be done. Therefore, the complete Rainflow matrix, has to be considered. As no complete matrices were available for the design of the given example (chapter 5), a computer

programme was created with *MS Excel* to determine the bolt-load function and the Rainflow matrices for damages caused by one cycle per load variation range ΔZ . The Rainflow matrix for the design example will be presented later on in this document. An *Excel* Tool for the fatigue design of friction connections with DEL method was also programmed and be presented.

4.2 Design of bolted ring flange connections

To simplify the design of flange connections only one segment of tower flange is considered, *i.e.*, the design is done assuming that the resistance of the three dimensional bolted ring flange connection can be described by the resistance of a segment of a width, c , that equals the distance (arc length) between two bolt holes instead of considering the complete circumference. Furthermore, the tension force in the shell, Z , can be obtained by the integral of the axial stresses acting in the tower shell, σ_x , over the cross-sectional area of the shell segment, c . This bolt section has to fulfil the following requirements: Resistance at the Ultimate Limit State (ULS); Fatigue design (FLS) and Resistance at the Serviceability State (SLS). Only ULS and FLS will be considered in this thesis for comparison with the friction connection.

4.2.1 Static resistance at ULS

The static resistance of a flange connection at the ULS is determined by the failure of the bolts and/or the flange and is usually done according to the plastic hinge theory developed by Petersen. The flange behaves like a beam and failure modes are established with plastic hinges developing at different locations. The connection may fail by exceeding the resistance of the bolt but also due to the development of plastic hinges either in shell or in flange. According to Petersen, three failure modes were defined and they are illustrated in Fig.4.2:

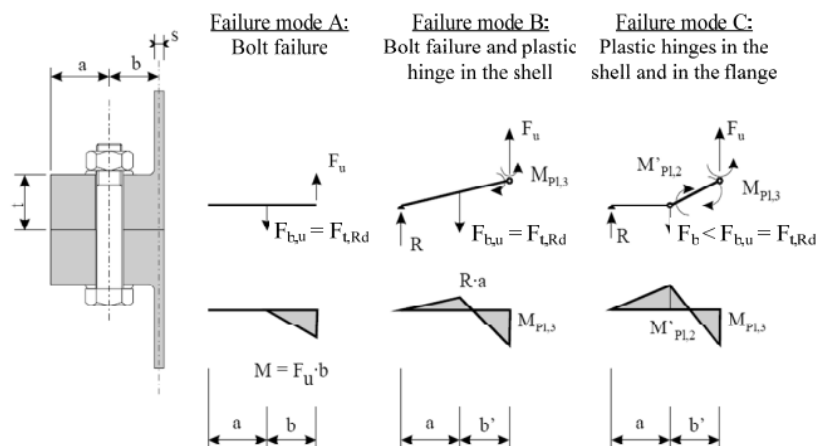


Figure 4.2 – Design failure modes by Petersen at the ULS (Husson, 2008)

This three failure modes correspond to bolt failure, plastic hinge in the shell and plastic hinge in the shell and in the flange. Obviously, the lowest resistance, $Z_{ult,i}$, is governing the design.

- A - Failure of the bolt – this governs failure when flange and shell are stiff compared to the bolt. Thus, the ultimate resistance of the segment is the tensional resistance of bolt:

$$Z_{ult,1} = F_{t,Rd}$$

- B - Failure of the bolt and plastic hinge in the shell at the same time:

$$Z_{ult,2} = \frac{F_{t,Rd} \cdot a + M_{N,pl,Rd,sh}}{a + b}$$

$$= -\frac{N_{pl,Rd,sh}^2 (a + b)}{2 \cdot M_{pl,Rd,sh}} + N_{pl,Rd,sh} \cdot \sqrt{1 + \frac{N_{pl,Rd,sh}^2 \cdot (a + b)^2 + 4 \cdot F_{t,Rd} \cdot a \cdot M_{pl,Rd,sh}}{4 \cdot M_{pl,Rd,sh}^2}}$$

- C - Plastic hinge in the shell and flange –the bolt load stays below its tensile resistance ($F_{t,Ed} < F_{t,Rd}$)

$$Z_{ult,3} = \frac{M_{N,pl,Rd,sh}(Z_{ult,3}) + M_{pl,Rd,fl,net}}{b}$$

$$= -\frac{N_{pl,Rd,sh}^2 \cdot b}{2 \cdot M_{pl,Rd,sh}} + \sqrt{\frac{N_{pl,Rd,sh}^4 \cdot b^2}{4 \cdot M_{pl,Rd,sh}^2} + \frac{M_{pl,Rd,fl,net} + M_{pl,Rd,sh}}{M_{pl,Rd,sh}} \cdot N_{pl,Rd,sh}^2}$$

With:

a	distance between flange edge and axis of bolt
b	distance between axis of bolt and shell
Z_{ult}	ultimate tensile resistance force of the segment
$F_{t,Ed}$	design tensile force in bolt
$F_{t,Rd}$	design tensile resistance of the bolt: $F_{t,Rd} = \frac{0.9 \cdot f_{ub} \cdot A_s}{\gamma_{M2}}$
f_{ub}	bolt ultimate strength
A_s	stress area
$M_{pl,Rd,sh}$	design plastic bending resistance of the shell: $M_{pl,Rd,sh} = \frac{W_{pl,sh} \cdot f_{y,sh}}{\gamma_{M0}} = \frac{c \cdot s^2 \cdot f_{y,sh}}{4 \cdot \gamma_{M0}}$
$f_{y,sh}$	shell yield strength
$N_{pl,Rd,sh}$	design plastic resistance of shell: $N_{pl,Rd,sh} = \frac{A_{sh} \cdot f_{y,sh}}{\gamma_{M0}} = \frac{c \cdot s \cdot f_{y,sh}}{\gamma_{M0}}$
$f_{y,fl}$	flange yield strength
$M_{N,pl,Rd,sh}$	design plastic bending resistance of the shell considering M-N-interaction
	$M_{N,pl,Rd,sh} = \left[1 - \left(\frac{Z_{ult}}{N_{pl,Rd,sh}} \right)^2 \right] \cdot M_{pl,Rd,sh}$
$M_{pl,Rd,fl,net}$	design plastic bending resistance of net cross-section of flange
	$M_{pl,Rd,fl,net} = \frac{W_{pl,net,fl} \cdot f_{y,fl}}{\gamma_{M0}} = \frac{(c - d_0) \cdot t_{fl}^2 \cdot f_{y,fl}}{4 \cdot \gamma_{M0}}$

γ_{M0}	partial safety factor taken as 1.10
γ_{M2}	partial safety factor taken as 1.25

4.2.2 Fatigue resistance

Fatigue failure of bolted ring flange connections is controlled by failure of the bolts. However, the resistance of the bolts exclusively is not enough to establish the resistance of the connection. Actually, the solicitations depend on the geometry and pretension. Regarding to a high fatigue safety, flange connections should be designed in order that the bolted joint does not open during relevant fatigue cycles, which requires a sufficient high preloading of the bolts (Veljkovic et al, 2012). The design verification is usually performed acc. to Eurocode (EC 3-1-9) by ensuring that the Palmgren-Miner damage accumulation is lower than unity:

$$D_D = \sum_i^m \frac{n_i}{N_i} \leq 1$$

With:

D_d	damage index of entire life time
n_i	number of cycles from load (effect) fatigue spectrum
N_i	number of cycles from the design fatigue resistance spectrum
m	slope of fatigue strength curve

The applied load (effect) ranges ($\Delta\sigma$) shall be multiplied by the safety factor for loads ($\gamma_{Ff}=1.10$) and the reference fatigue strength values ($\Delta\sigma_c$) divided by the safety factor for materials ($\gamma_{mf}=1.15$) to obtain the number of cycles n_i or N_i for each band in the spectrum (EC 3-1-9).

As Figure 3.4 illustrates, due to pretension, the relationship between the tension in the tower shell, Z , and the bolt force, F_S , is non-linear. This non-linearity prevents the simplification of the fatigue load spectrum to a DEL. That means that the fatigue loads must be defined as Rainflow matrices, which contain information on the load range and amplitude and also on its average. As no complete Rainflow matrices are available for the design of the given example (chapter 5), Rainflow matrices for damages caused by one cycle per load variation range ΔZ will be determined in chapter 5.4.3.

Dependant on the method used to determine the bolt-load function, different detail category must be used. If the bending moments in the bolts are considered by the model, a detail category 50 should be used acc. to Eurocode (EC 3-1-9). On the other hand, if a simplified method is used to determinate the bolt-load-function, GL-Guideline (GL, 2010) recommends the use of a detail category 36* for the bolt. For this document, as it is one of the most commonly used, the Schmidt/Neuper method has been chosen to determine bolt-load function – see chapter 4.2.2.2. This method does not consider bending stresses so the Wöhler curve for bolts in tension given in Eurocode (EC 3-1-9) has to be reduced to detail category 36*. Moreover, if bolts with nominal

diameters larger than 30mm are used, which happens in most flange connections for wind towers, all detail categories should be reduced by a reduction factor, k_s , acc. to GL-Guideline (GL, 2010): $k_s = (30/d)^{0.25}$

4.2.2.1 Elastic structural behaviour of L-flange connections

Despite several methods have been develop to establish the bolt force as a function of applied load, all of them are based on the bolt stiffness, C_S , and the clamp solid stiffness, C_D ,

- Bolt stiffness, C_S :

$$C_S = \frac{1}{\int_0^{l_S} \frac{1}{E_S A_S(x)} dx} \approx \frac{E_{bolt} A_{nom}}{2 \cdot t_{fl}}$$

- Clamp solid stiffness, C_D :

$$C_D = \frac{1}{2 \int_0^{t_f} \frac{1}{E_D A_D(x)} dx} \approx \frac{E_{fl} \cdot \pi}{4 \cdot 2 \cdot t_{fl}} \cdot \left[\left(d_{washer} + \frac{2 \cdot t_{fl}}{10} \right)^2 - d_0^2 \right]$$

With:

E_{bolt}	Young's-modulus of bolt material
A_{nom}	nominal cross section of bolt
t_{fl}	flange thickness
E_{fl}	Young's-modulus of flange material
d_{washer}	outside diameter of washer
d_0	diameter of bolt hole

4.2.2.2 Bolt-load function acc. to Schmidt/Neuper

As it is one of the most commonly used bolt-load function, the tri-linear model developed by Schmidt and Neuper, has been chosen to use in this thesis.

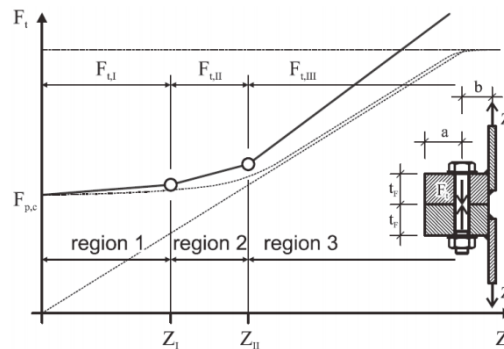


Figure 4.3 – Trilinear model developed by Schmidt/Neuper (Veljkovic et al, 2012)

The curve parameters are given by:

$$p = \frac{C_S}{C_S + C_D} ; q = \frac{C_D}{C_S + C_D} ; \lambda^* = \frac{0.7 \cdot a + b}{0.7 \cdot a} ; Z_I = \frac{a - 0.5 \cdot b}{a + b} \cdot F_{p,c} ; Z_{II} = \frac{1}{\lambda^* \cdot q} \cdot F_{p,c}$$

The final bolt-load is then given by:

$$\text{If } Z \leq Z_I \quad \rightarrow F_{t,I} = F_{p,c} + p \cdot Z$$

$$\text{If } Z_I \leq Z \leq Z_{II} \quad \rightarrow F_{t,II} = F_{p,c} + p \cdot Z_I + [\lambda^* \cdot Z_{II} - (F_{p,c} + p \cdot Z_I)] \cdot \frac{Z - Z_I}{Z_{II} - Z_I}$$

$$\text{If } Z \geq Z_I \quad \rightarrow F_{t,III} = \lambda^* \cdot Z$$

Application limit of this model is given by:

$$\frac{a + b}{t_f} \leq 3$$

a , b and t_f are geometric parameters that can be seen in Figure 4.3.

This method does not consider bending stresses in the bolt, therefore fatigue detail category 36* is recommended by design guidelines.

4.3 Design of friction connections

As for flange connection, to simplify the design of the friction connection, only one segment of the tower will be considered. Assuming a uniform longitudinal stress distribution over the shell, the resistance can be described by the resistance of a segment of a width, c , that equals the distance (arc length) between two bolt rows, instead of considering the complete circumference. Also, the tension force in the shell, Z , can be obtained by the integral of the axial stresses acting in the tower shell, σ_x , over the cross-sectional area of the shell segment, c .

The design of friction connections is ruled in various standards and guidelines. In this document the design is performed according to Eurocode (EC 3-1-8), which differentiates between slip resistance at serviceability limit state (category B) and ultimate limit state (category C). For this thesis, the second one is of main interest.

4.3.1 Static Resistance at ULS

The static resistance of the friction connection segment can be based on the design model from Eurocode (EC 3-1-8), given for a single bolt as:

$$F_{s,Rd} = \frac{k_s \cdot n \cdot \mu_s}{\gamma_{M3}} \times F_{p,c}$$

With:

k_s	reduction factor considering shape and size of hole taken as $k_s = 0.63$
n	number of friction surfaces
μ	slip factor

The characteristic preload force in bolt, $F_{p,C}$, is taken as:

$$F_{p,C} = \frac{0.7 \cdot f_{ub} \cdot A_s}{\gamma_{M7}}$$

With:

f_{ub}	ultimate tensile strength of the bolt depending on bolt class
A_s	tensile stress area of the bolt
γ_{M3}	partial safety factor at ultimate limit state (Category C), $\gamma_{M3} = 1.25$
γ_{M7}	partial factor for preload of high strength bolts, $\gamma_{M7} = 1.10$

Although in Table 3.7 of Eurocode (EC 3-1-8) states that “a loss of pre-load may occur over time” in case of painted surface treatments, the structural design for slip resistant connections, as it is presented in chapter 5.5, does not consider time dependent losses of preload explicitly.

Despite this thesis predominantly focus on creating computer programmes using *MS Excel* to perform design verifications, as the resistance at the Ultimate Limit State (ULS) is likely to be the design driving criterion, it is recommended to dimension the connection for the ULS and then perform the design checks. Assuming a uniform longitudinal stress distribution over the shell, which is similar to assuming a maximal, constant stress over the entire cross-section, the minimum number of bolts required in the connection is given as:

$$n_{Bolts} \geq \frac{Z_{Ed,max}}{F_{S,Rd}}$$

The maximum force in longitudinal direction, $Z_{Ed,max}$, can be obtained by the integral of the axial stresses acting in the tower shell, $\sigma_{ult,Ed}$, over the cross-sectional area of the shell.

From the design loads it's simple to reach the maximum design stress in the tower shell, $\sigma_{ult,Ed}$. As for flange connections, the effects of shear stresses on the resistance of the connection can be ignored and only loads introducing longitudinal stresses in the shell are considered. Furthermore, the highest design loads are found in the compressed zone, so it becomes clear that considering pure compression leads to an equivalent maximum stress. Thus, to derive the design load, only compressive longitudinal stresses originating from bending (M_r – tilting moment) and vertical load (F_z – self-weight) are considered:

$$\sigma_{ult,Ed} = \frac{M_r}{W_i} - \frac{F_z}{A_i}$$

With:

$M_r, F_z \rightarrow$	extreme design loads at height of flange section i acc. to Table 5.1
$W_i, A_i \rightarrow$	cross section resistances of tower tube at height of flange section i

The maximum number of bolt's rows is defined by the row spacing, which is determined either by the minimal bolt spacing defined in Eurocode (EC 3-1-8) or by the clearance necessary for

the tightening tools. As the electrical wrenches used to tighten Tension Control Bolts are compact tools (Husson, 2008), (Heistermann et al, 2009), the row spacing for this type of bolts is set by the norm. Therefore, the minimum distance between bolt's rows is: $p_2 = 2.4 \cdot d_0$

The maximum number of rows becomes: $n_{Rows} \leq \frac{\pi \cdot d_{tower}}{2.4 \cdot d_0}$

The minimum amount of bolts per row, n_s , should be rounded to next integer.

4.3.1.1 Design Verifications

The design resistance is given by the minimum value between the maximum slip resistance of the friction connection and the yield resistance of the finger, assuming a uniform longitudinal stress distribution over the shell segment width, c . Although is rather conservative, it is an acceptable assumption to consider loads from the compressed zone of the connection and resistance from the tensile zone (Veljkovic et al, 2015). Thus, the maximum allowable stress in gross cross section of the tower shell becomes:

$$\sigma_{ult,Rd} = \min \left\{ \frac{n_s \cdot \mu \cdot k_s \cdot F_{p,C}}{c \cdot s \cdot \gamma_{M3}}; \frac{c - d_0}{c} \cdot \frac{f_{y,shell}}{\gamma_{M0}} \right\}$$

With:

n_s	number of bolts per row
μ	slip factor
k_s	reduction factor considering shape and size of hole taken as $k_s = 0.63$
$F_{p,C}$	characteristic preload force in bolt
c	width of shell segment
s	shell thickness
d_0	diameter of bolt hole
$f_{y,shell}$	characteristic yield strength of tower shell material
γ_{M0}	partial factor for preload of high strength bolts, $\gamma_{M0} = 1.0$
γ_{M3}	partial factor for preload of high strength bolts, $\gamma_{M3} = 1.25$

4.3.2 Fatigue Resistance

For the fatigue design verification of the friction connections, the load variation range in the preloaded bolts, $\Delta F_{p,C}$, has to be checked. This load variation is due to lateral contraction of the tower shell under bending and it depends on the shell stresses and on the bolt and connection geometry. In accordance with Kammel 2001 *apud* Veljkovic (Veljkovic et al, 2012), the load variation range in the preloaded bolts, $\Delta F_{p,C}$, can be determined by the following equation:

$$\Delta F_{p,C} = \beta \cdot \frac{\nu \cdot \sum (\Delta \sigma_{z,i} \cdot s_i)}{\delta_{joint} \cdot E_{shell}}$$

With:

β	empirical determined correction factor taken as $\beta = 1.25$
ν	Poisson ration taken as $\nu = 0.3$

δ_{joint}	elastic resilience of bolted connection, see next chapter
E_{shell}	Young-modulus of tower shell material
$\Delta\sigma_{z,i}$	maximum stress variation range in the net cross section of the tower cross section i , taken as $\Delta\sigma_z = (c/c_{net}) \cdot \sigma_{ult,Rd}$
s_i	shell thickness of the tower cross section i

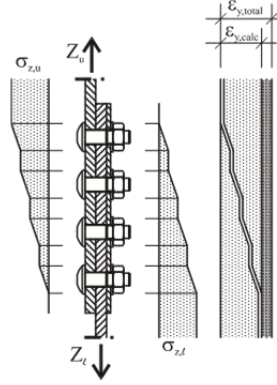


Figure 4.4 – Sketch of idealised stress distribution in tower shells within the friction connection zone and considered lateral contraction ($\varepsilon_{y,total} = 1.25 \cdot \varepsilon_{y,calc}$) of the shell (Veljkovic et al, 2015)

As the Figure 4.4 shows, the shell stresses are transferred from one tower segment to other stepwise within the friction connection. Thus, the sum $\sum(\Delta\sigma_{z,i} \cdot s_i)$ can be simplified:

$$\sum(\Delta\sigma_{z,i} \cdot s_i) \cong \Delta\sigma_{z,mean} \cdot s_{mean}$$

$\Delta\sigma_{z,mean}$	mean stress variation range of the net cross section of both tower cross sections
s_{mean}	mean shell thickness of both tower cross sections

4.3.2.1 – Elastic resilience acc. to VDI 2230

The Association of German Engineers (Verein Deutscher Ingenieure, VDI) published a guideline (VDI, 2003) which is a recognised helpful tool to analyse and calculate cylindrical steel bolts in high duty bolted joints. Although the calculation model is for a single-bolt-joint it can be used for more complex connections (Heistemann, 2014).

The elastic resilience of the bolted connection, δ_{joint} , acc. to VDI Guideline (VDI, 2003), is the sum of the elastic resilience of the bolt and the elastic resilience of the clamping package:

$$\delta_{joint} = \delta_{bolt} + \delta_{cp}$$

With:

δ_{bolt}	elastic resilience of the preloaded bolt
δ_{cp}	elastic resilience of clamping package (steel shells + cover-plate + washers)

According to VDI Guideline (VDI, 2003), the resilience of the bolt takes into account elastic deformation within the clamp length and any elastic deformations, which occur outside this region and have effect on the deformation behaviour of the bolt in the joint. Thus the geometry

of the whole bolt has to be taken into account. The bolt presented in Figure 4.5 is divided into individual cylindrical bodies of various lengths and cross sections. These individual cylindrical elements are: the bolt head, the shank, the unengaged loaded part of the thread (free thread), the part of the thread inside the nut (engaged thread) and the nut.

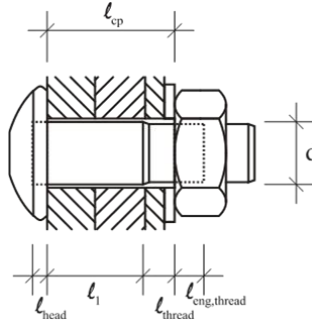


Figure 4.5 – Division of a bolt into individual cylindrical solids and deformation regions outside the bolt acc. to VDI (VDI, 2003), (Veljkovic et al, 2015)

The cylindrical elements are arranged in a row, thus the total resilience of the bolt is given by:

$$\delta_{bolt} = \delta_{head} + \delta_{shank} + \delta_{freethread} + \delta_{eng.thread} + \delta_{nut}$$

- δ_{head} – elastic resilience of bolt head: $\delta_{head} = \frac{l_{head}}{E_{bolt}A_{nom}}$

l_{head}	substitutional extension length of bolt head; $l_{head} = \alpha \cdot d$ ($\alpha = 0.5$ for hexagon head bolts and $\alpha = 0.25$ for rivet head bolts)
E_{bolt}	Young's modulus of bolt material
A_{nom}	nominal cross section of bolt, $A_{nom} = \frac{\pi}{4} \cdot d^2$
d	nominal diameter of bolt shank

- δ_{shank} – elastic resilience of shank: $\delta_{shank} = \sum \frac{l_i}{E_{bolt}A_i}$

l_i	length of shank body i
A_i	nominal cross section of bolt shank body i , $A_i = \frac{\pi}{4} \cdot d_i^2$

- $\delta_{freethread}$ – elastic resilience of unengaged loaded part of thread: $\delta_{freethread} = \frac{l_{thread}}{E_{bolt}A_{d_3}}$

l_{thread}	free length of unengaged loaded thread
A_{d_3}	nominal cross section of bolt thread, $A_{d_3} = \frac{\pi}{4} \cdot d_3^2$
d_3	minor diameter of bolt thread

- $\delta_{eng.thread}$ – elastic resilience of engaged bolt thread: $\delta_{eng.thread} = \frac{l_{eng.thread}}{E_{bolt}A_{d_3}}$

$l_{eng.thread}$	length of engaged loaded thread, $l_{eng.thread} = 0.5 \cdot d$
------------------	---

- δ_{nut} – elastic resilience of nut: $\delta_{nut} = \frac{l_{nut}}{E_{nut}A_{nom}}$

l_{nut}	substitutional extension length of nut, $l_{nut} = 0.4 \cdot d$
E_{nut}	Young's-modulus of nut material

Considering that the bolted joint is concentrically clamped² ($D_A > D_K$), see Figure 4.6, the elastic resilience of clamping package can be obtain according to:

$$\delta_{cp} = \frac{2 \cdot \ln \left[\frac{(d_w + d_0) \cdot (d_w + l_{cp} \cdot \tan \varphi - d_0)}{(d_w - d_0) \cdot (d_w + l_{cp} \cdot \tan \varphi + d_0)} \right]}{E_{cp} \cdot \pi \cdot d_0 \cdot \tan \varphi}$$

With:

d_w	outside diameter of the plane head bearing surface of the bolt, see Figure 4.6
d_0	diameter of bolt hole
l_{cp}	length of clamping package, see Figure 4.5
φ	angle of deformation cone taken as $\varphi = 35^\circ$
E_{cp}	Young's-Modulus of clamping package material (shell, cover-plate, washer)

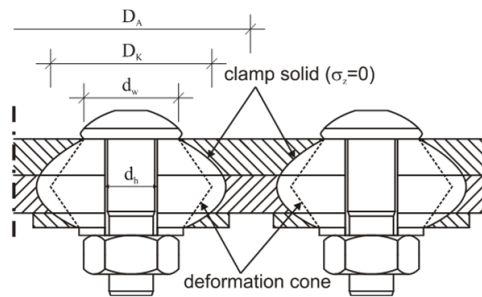


Figure 4.6 – Clamp solid and calculation model at a bolted joint (Veljkovic et al, 2015)

4.3.2.2 Damage Equivalent Loads

As the relation between fatigue loads and the response of bolts in friction connections (stress variation ranges) is linear, the design can be performed with Damage Equivalent Loads (DEL). DEL can be described as the single load range that would lead, at the considered number of cycles, to the same fatigue life (damage) as the considered load spectrum. To define DEL a reference number of cycles (N_{ref}) must be establish. Acc. to Eurocode (EC 3-1-9), the design value of DEL to be used for fatigue assessment should be the stress ranges $\gamma_{Ff} \Delta\sigma_{E,2}$ corresponding to $N_C = 2 \times 10^6$ cycles. The fatigue design is based on the constant amplitude DEL range ($\Delta\sigma_{E,ref}$), associated with a reference number of cycles (N_{ref}), ensuring that: $\Delta\sigma_{E,ref} \leq \Delta\sigma_C$

- $\Delta\sigma_C \rightarrow$ reference value of fatigue strength at $N_C = 2 \times 10^6$ cycles; detail category (EC 3-1-9)

If the load spectrum ($\Delta\sigma_i - n_i$) is available, the constant amplitude DEL range ($\Delta\sigma_{E,ref}$), associated with a reference number of cycles (N_{ref}) and a certain slope m of the resistance S-N curve, can be obtained using:

² According to Section 3.2.1 of VDI (VDI, 2003), a bolted joint is considered concentrically clamped if the deformation cone can spread without hindrance up to the interface within the plane of bolt axis/line of action of the working load or if the deformation solid can form in a laterally symmetrical manner.

$$\left(\frac{\Delta\sigma_i}{\Delta\sigma_{E,ref}}\right)^m = \frac{N_{ref}}{N_i} ; \quad D_d = \sum_i \frac{n_i}{N_i} = \sum_i \frac{n_i \Delta\sigma_i^m}{N_{ref} \Delta\sigma_{E,ref}^m}$$

As $D_d = 1.0$ is the admissible damage of the structure, the constant amplitude DEL range is:

$$\Delta\sigma_{E,ref} = \left(\sum_i \frac{n_i \Delta\sigma_i^m}{N_{ref}}\right)^{\frac{1}{m}}$$

A standard S-N curve for steel structures has two different Wöhler slopes, $m=3$ and $m=5$, for different number of cycles. Since DEL includes load cycles acting in the range of both slopes, in order to recalculate all load cycles on the same basis, a single S-N curve with a constant Wöhler slope has to be defined. The state of art is to use a Wöhler slope of $m=4$, that is connected to the standard S-N curve at $N = 2 \times 10^6$ (Veljkovic et al, 2012).

The applied load (effect) ranges ($\Delta\sigma_{E,2}$) should be multiplied by the safety factor for loads ($\gamma_{Ff} = 1.0$) and the reference fatigue strength values ($\Delta\sigma_C$) divided by the safety factor for materials ($\gamma_{Mf} = 1.15$). Acc. to Eurocode (EC 3-1-9), the fatigue check corresponds to the evaluation of:

$$\gamma_{Ff} \Delta\sigma_{E,2} \leq \sqrt[m]{D_d} \frac{\Delta\sigma_C}{\gamma_{Mf}}$$

If a different N_{ref} is defined for the constant amplitude DEL range, next conversion can be made:

$$\Delta\sigma_{E,2} = \left(\frac{N_{ref}}{2 \times 10^6}\right)^{\frac{1}{m}} \Delta\sigma_{E,ref}$$

To sum up, the final fatigue design verification then reads:

$$\frac{\gamma_{Ff} \Delta\sigma_{DEL}}{\Delta\sigma_R / \gamma_{Mf}} \leq 1.0$$

- $\Delta\sigma_R \rightarrow$ characteristic fatigue resistance associated with a reference number of cycles, N_{ref}

$$\Delta\sigma_R = \Delta\sigma_C \left(\frac{2 \times 10^6}{N_{ref}}\right)^{\frac{1}{m}}$$

Acc. to Eurocode (EC 3-1-9), detail category 50 is used for the pre-loaded bolts and 90 for the shell. The damage equivalent tensile stresses in bolts and in gross cross-section is obtained with:

$$\Delta\sigma_{bolt,DEL} = \frac{F_{p,C,DEL}}{A_s} ; \quad \Delta\sigma_{shell,DEL} = \gamma_M \cdot \frac{M_y}{W}$$

The damage equivalent tensile stress in the gross cross-section (shell) are derived considering only stresses from tilting moment, M_y (Heistermann et al, 2009), (Husson, 2008).

As the stresses are obtained using the cross-section, the fatigue strength is governed by the shell thickness and it is not influenced by the number of bolts or bolts row.

5 CASE STUDIES

5.1 Tower Geometry

The chosen tower for the case studies presented below is an existing MM92 tower produced by *REpower*, which hub height is 80m and supports a three blade turbine. It is made of three sections assembled with two intermediate *L*-flange connections. The tower is made of steel S460. The geometry is presented in Figure 5.1.

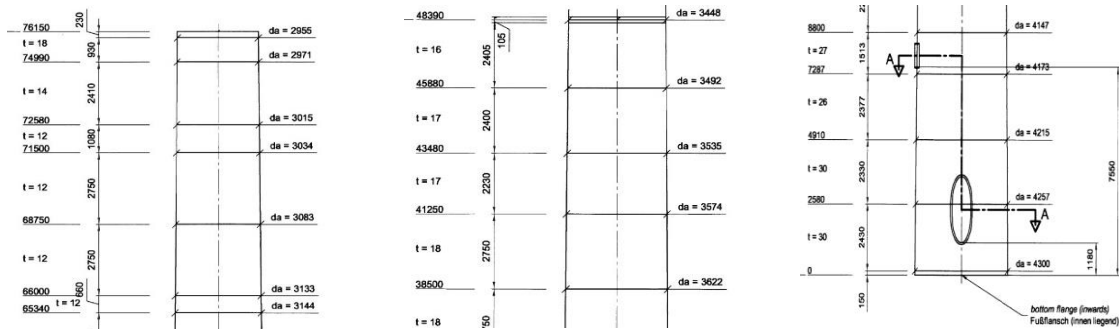


Figure 5.1 – a) Detail of tower upper segment

b) Detail of tower middle segment

c) Detail of tower bottom segment

5.2 Static design loads

The static design loads usually derive from information on the wind speed and direction, with help of simplified models which include the geometrical properties of the wind tower. Due to the long lever arm of the relevant sections in the design of the connections ($H=21770\text{mm}$ and $H=48390\text{mm}$), the extreme shear forces in the x - y plane usually correspond to the extreme resulting bending moment. Therefore, this load case is design driving. As mention before, for a specific load case, the design loads can be linearly interpolated between two given sections. The design loads for the two flange sections can be simplified as in Table 5.1.

Table 5.1 – Extreme design loads at the flange sections (Veljkovic et al, 2015)

	Height	F _x	F _y	F _z	F _r	M _x	M _y	M _z	M _r
	mm	kN	kN	kN	kN	kNm	kNm	kNm	kNm
Flange 1	21770	-886	27	-2443	886	1129	-48617	-1368	48631
Flange 2	48390	-864	7	-1846	864	1635	-25168	-1363	25221

The safety factor is taken as 1.35. To derive the design loads acting on a segment only the load components inducing compressive longitudinal stresses in the shell, originating from bending (tilting moment) and vertical load (self-weight), are considered. Thus, the maximum design stress in tower shell becomes:

$$\sigma_{ult,Ed} = \frac{M_r}{W_i} - \frac{F_z}{A_i}$$

With:

M_r, F_z → Extreme design loads at height of flange section i acc. to Table 5.1

W_i, A_i → Cross section resistances of tower tube at height of flange section i

This leads to:

Connection 1 → $\sigma_{ult,Ed} = 200 \text{ N/mm}^2$ Connection 2 → $\sigma_{ult,Ed} = 177 \text{ N/mm}^2$

5.3 Fatigue design loads

The fatigue loads were also provided by *REpower* and the complete load table for different tower sections is presented in chapter 4.1.1.2. The DEL were given for each load component for different Wöhler slopes. As mention before, the state of art is to use a single Wöhler slope of $m=4$. The fatigue loads for the two flange sections can be simplified as in Table 5.2.

Table 5.2 – Damage Equivalent Loads at the flange sections ($m=4$ and $N_{ref}=2 \cdot 10^8$)

	Height	ΔF_x	ΔF_y	ΔF_z	ΔM_x	ΔM_y	ΔM_z
	mm	kN	kN	kN	kN.m	kN.m	kN.m
Flange1	21770	96	67	29	3342	4243	1229
Flange2	48390	81	61	29	1707	2359	1229

Usually, if DEL are used, consideration of the rotor thrust (F_x), tilting moment (M_y) and tower torsional moment (M_z) is enough (Veljkovic et al, 2012). Tilting and torsional moment can be assumed to act orthogonally, which means that the damages resulting from the tensile stresses (due to M_y and F_x) can be calculated separately from the damage resulting from shear stresses (due to M_z). At tubular steel towers, the damage from shear stresses (M_z) is usually much smaller and it can be neglected, the component from rotor thrust (F_x) can also be neglected. Then, the damage equivalent tensile stress in gross cross-section are calculated considering only stresses from tilting moment (M_y) (Veljkovic et al, 2015):

$$\sigma_{shell,DEL} = \gamma_M \cdot \frac{M_y}{W}$$

Connection 1 $\rightarrow \sigma_{z,DEL} = 18.3 \text{ N/mm}^2$ Connection 2 $\rightarrow \sigma_{z,DEL} = 17.2 \text{ N/mm}^2$

The partial factor for material properties was taken as $\gamma_M = 1.10$. Note that DEL method is only applicable as long as the relationship between the tension in the tower shell and the bolt force is linear – friction connections. For flange connections an extremely non-linear relation has to be taken into account. Thus, the complete Rainflow matrix, has to be considered.

5.4 Flange connection

The static resistance at the Ultimate Limit State (ULS) and the fatigue strength of the two intermediate flange connections (H=21770mm and H=48390mm) are calculated using the methods described previously. For flange connection design verifications (ULS and fatigue) two different computer programmes were created with *MS Excel*. This chapter only presents the results obtained with it and some guidelines to use it. The complete *Excel* sheet is presented in Appendix A and B.

5.4.1 Flange geometry

The dimensions and material properties of the both flanges are shown in Figure 5.2.

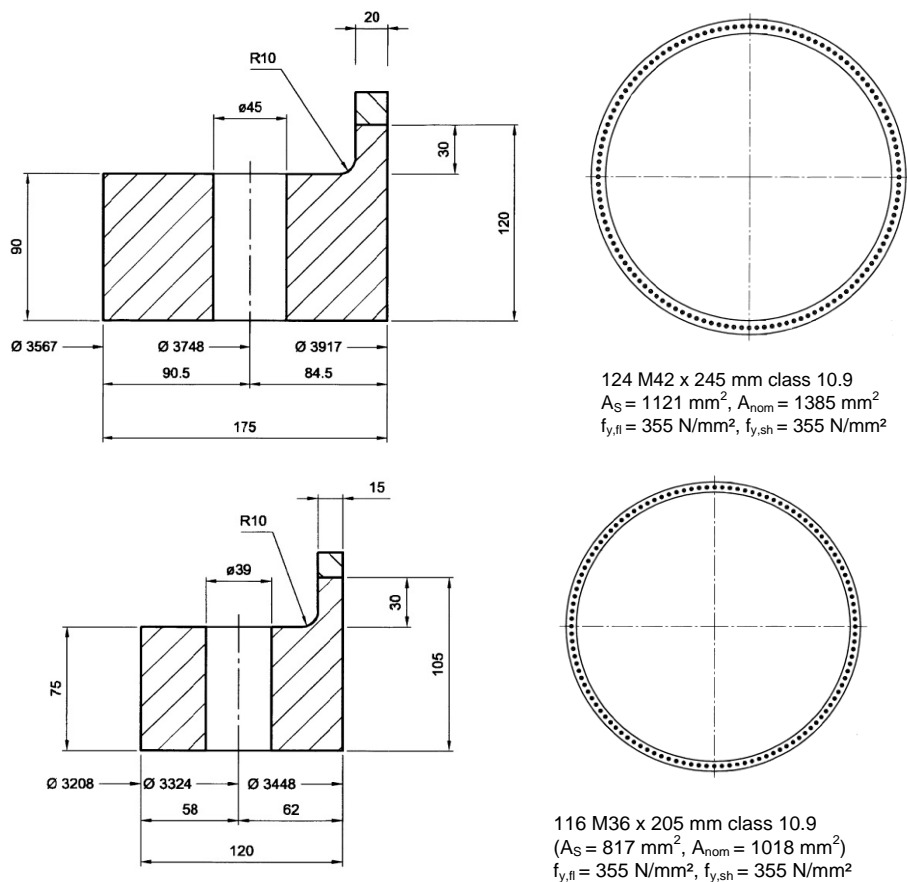
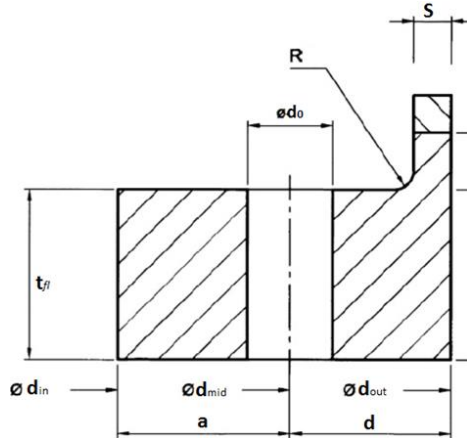


Figure 5.2 –Dimensions and material properties of bottom (1) and upper flange (2)

5.4.2 ULS

The ultimate resistance of the flange connection can be determined acc. to the plastic hinge theory described on chapter 3.2.2.3, using the formulas presented in chapter 4.2.1 of this thesis. The given dimensions of flanges are:



Flange 1	Flange 2
$a = 90,5 \text{ mm}$	$a = 58 \text{ mm}$
$b = 74,5 \text{ mm}$	$b = 54,5 \text{ mm}$
$c = 95 \text{ mm}$	$c = 90 \text{ mm}$
$d = 84,5 \text{ mm}$	$d = 62 \text{ mm}$
$t_{fl} = 90 \text{ mm}$	$t_{fl} = 75 \text{ mm}$
$s = 20 \text{ mm}$	$s = 15 \text{ mm}$

Figure 5.3 – Dimensions of flange connection

$b \rightarrow$ distance between flange axis of bolt and shell; $b = d - s/2$

$c \rightarrow$ shell strip width;

Table 5.3 – Design resistances of the single components and possible failure modes

Description	Parameter	Connection 1	Connection 2
Design tensile resistance of bolt	$F_{t,Rd} = \frac{0,9 \cdot f_{ub} \cdot A_s}{\gamma_{M2}}$	807.1 kN	588.2 kN
Design plastic bending resistance of shell	$M_{pl,Rd,sh} = \frac{c \cdot s^2 \cdot f_{y,sh}}{4 \cdot \gamma_{M0}}$	306.6 kNcm	163.4 kNcm
Design plastic resistance of shell	$N_{pl,Rd,sh} = \frac{c \cdot s \cdot f_{y,sh}}{\gamma_{M0}}$	613.2 kN	435.7 kNcm
Design plastic bending resistance of net cross-section of flange	$M_{pl,Rd,fl,net} = \frac{(c - d_0) \cdot t_{fl}^2 \cdot f_{y,fl}}{4 \cdot \gamma_{M0}}$	3267.6 kN	2314.6 kNcm
Yielding (failure) of the bolt	$Z_{ult,1} = F_{t,Rd}$	807.1 kN	588.2 kN
Yielding (failure) of the bolt and at the same time plastic hinge in shell	$Z_{ult,2} = \frac{F_{t,Rd} \cdot a + M_{N,pl,Rd,sh}}{a + b}$	451.2 kN	310.4 kN
Plastic hinge in shell and flange (failure of the connection)	$Z_{ult,3} = \frac{M_{N,pl,Rd,sh}(Z_{ult,3}) + M_{pl,Rd,fl,net}}{b}$	456.9 kN	426.0 kN

The ultimate resistance of the flange connection is given by:

$$\text{Min}\{Z_{ult,1}; Z_{ult,2}; Z_{ult,3}\}$$

Table 5.4 – Ultimate resistance of flange connection 1 and 2

	Failure mode acc. to plastic hinge theory from Petersen Error! Reference source not found.	Ultimate tensile force in segment shell $Z_{ult,Rd}$ [kN]	Ultimate tensile stress in tower shell $\sigma_{ult,Rd}$ [N/mm ²]
Flange 1	“2” = Yielding of bolt in combination with a plastic hinge in shell	451.2	237.5
Flange 2	“2” = Yielding of bolt in combination with a plastic hinge in shell	310.4	299.9

Table 5.5 – Design verification of flange connection 1 and 2

	Resulting maximum tensile stresses in tower shell $\sigma_{ult,Ed}$ [N/mm ²]	Design verification $\sigma_{ult,Ed} / \sigma_{ult,Rd}$ [-]
Flange 1	200.2	0.8
Flange 2	177.4	0.8

5.4.3 Fatigue

The fatigue design of flange is performed acc. to chapter 3.2.2.1 using the formulas presented in chapter 4.2.2. As no complete Rainflow matrices were available for the design of the given example, a computer programme was created with *MS Excel* to determine the bolt-load function and the Rainflow matrices for damages caused by one cycle per load variation range ΔZ .

Despite the method chosen to establish the bolt force as a function of applied load, all of them are based on the required stiffness. The bolt stiffness, C_s , and the clamp solid stiffness, C_D are presented in Table 5.6, for both flange connections.

Table 5.6 – Required stiffness

Description	Parameter	Connection 1 [N/mm]	Connection 2 [N/mm]
Bolt stiffness	$C_s \approx \frac{E_{bolt} A_{nom}}{2 \cdot t_{fl}}$	1615833	1425200
Clamp solid stiffness	$C_D \approx \frac{E_{fl} \cdot \pi}{4 \cdot 2 \cdot t_{fl}} \cdot \left[\left(d_{washer} + \frac{2 \cdot t_{fl}}{10} \right)^2 - d_0^2 \right]$	6589098	5541769

The bolt-load function of the considered connections were determinate acc. to the tri-linear model developed by Schmidt and Neuper presented in chapter 4.2.2.2. All required curve parameters of this tri-linear model are summarized in Table 5.7.

Table 5.7 – Curve parameters of tri-linear Schmidt/Neuper bolt-load function model

Curve parameter	Flange 1	Flange 2
$p = \frac{C_S}{C_S + C_D}$	0.197	0.205
$q = \frac{C_D}{C_S + C_D}$	0.803	0.795
$\lambda^* = \frac{0.7 \cdot a + b}{0.7 \cdot a}$	2.176	2.342
$Z_I = \frac{a - 0.5 \cdot b}{a + b} \cdot F_{p,C}$	230.2 kN	142.1 kN
$Z_{II} = \frac{1}{\lambda^* \cdot q} \cdot F_{p,C}$	408.2 kN	279.0 kN

The final bolt-load is then given by:

$$\text{If } Z \leq Z_I \quad \rightarrow F_{t,I} = F_{p,C} + p \cdot Z$$

$$\text{If } Z_I \leq Z \leq Z_{II} \quad \rightarrow F_{t,II} = F_{p,C} + p \cdot Z_I + [\lambda^* \cdot Z_{II} - (F_{p,C} + p \cdot Z_I)] \cdot \frac{Z - Z_I}{Z_{II} - Z_I}$$

$$\text{If } Z \geq Z_{II} \quad \rightarrow F_{t,III} = \lambda^* \cdot Z$$

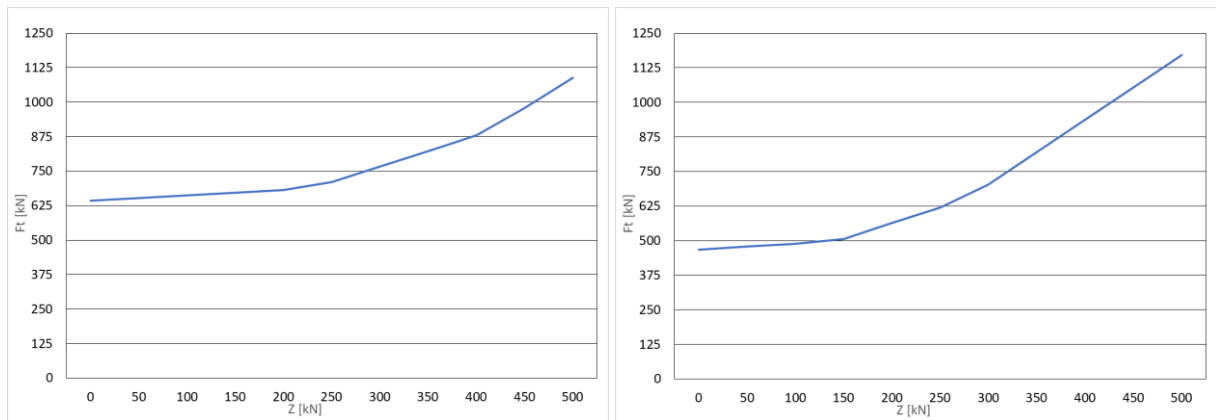


Figure 5.4 – Bolt-load function of flange connection 1 and 2 acc. to Schmidt/Neuper

A re-adjustment of the pre-load, $F_{p,C}$, of all bolts within 6-month is assumed. Thus, acc. to DIBt-Guideline (DIBt, 2005), 90% of the nominal pre-load can be taken into account. Figure 5.4 shows the resulting bolt-load functions for flange connection 1 and 2.

For the determination of Rainflow matrices, only loads which produce stresses up to $\approx 80\%$ of the bolts yield strength will be considered, *i.e.*, $Z_{max} = 300\text{kN}$ for flange 1 and $Z_{max} = 200\text{kN}$ for flange 2. It is assumed that the probability of occurrence of higher loads is too small to be considered in fatigue design (Veljkovic et al, 2015). The results are presented in Table 5.8.

Table 5.8 – Relationship between load Z_{Ed} in shell segment and resulting bolts force $F_{t,Ed}$ in load steps of 50 kN

	Flange 1	Flange 2
Z [kN]	$F_{t,Ed}$	$F_{t,Ed}$
0	642.0	467.9
50	651.9	478.1
100	661.7	488.4
150	671.6	506.0
200	681.4	563.2
250	709.7	-
300	766.1	-

With the tensile stress area of the bolts, A_s , matrices can be determined. They summarize the bolt stress variation ranges, $\Delta\sigma_N$, in function of the shell stress variation, $\Delta Z = Z_{max} - Z_{min}$. The resulting matrices for flange 1 and 2 are presented below in Table 5.9 and Table 5.10.

Table 5.9 – Resulting axial stress variation ranges $\Delta\sigma_N$ in bolts in function of load ranges $Z_{max} - Z_{min}$ in Flange 1

$\Delta\sigma_N$ [N/mm ²]	from Z_{min} [kN]					
to Z_{max} [kN]	0	50	100	150	200	250
0						
50	8.8					
100	17.6	8.8				
150	26.4	17.6	8.8			
200	35.1	26.4	17.6	8.8		
250	60.4	51.6	42.8	34.0	25.2	
300	110.7	101.9	93.1	84.4	75.6	50.3

Table 5.10 – Resulting axial stress variation ranges $\Delta\sigma_N$ in bolts in function of load ranges $Z_{max} - Z_{min}$ in Flange 2

$\Delta\sigma_N$ [N/mm ²]	from Z_{min} [kN]			
to Z_{max} [kN]	0	50	100	150
0				
50	12.5			
100	25.0	12.5		
150	46.6	34.1	21.6	
200	116.6	104.1	91.6	70.0

This method used to determine bolt-load function does not consider bending stresses in the bolt, therefore the Wöhler curve for bolts in tension given in Eurocode (EC 3-1-9) has to be reduced to detail category 36*, acc. to GL-Guideline. Also, if bolts with nominal diameters larger than 30mm are used, all detail categories should be reduced by a reduction factor: $k_s = (30/d)^{0.25}$

Table 5.11 – Properties of the considered Wöhler curves 36*

Bolt	k_s	$\Delta\sigma_C$ with $N_c=2.10^6$	$\Delta\sigma_D$ with $N_c=10^7$
M42	0.919	36.8	21.1
M36	0.955	38.2	22.0

Following the recommendation of GL-Guideline (GL, 2010), the cut-off limit for endurance given in Eurocode (EC 3-1-9) was neglected.

The single damages can be derived by: $D_i = \frac{n_{E,i}}{N_{R,i}}$

With:

$$N_{R,i} = \begin{cases} N_c \cdot \left(\frac{\Delta\sigma_C/\gamma_{Mf}}{\gamma_{Ff}\Delta\sigma_N} \right)^3 & \text{if } \Delta\sigma_N \geq \Delta\sigma_D/\gamma_{Mf} \\ N_D \cdot \left(\frac{\Delta\sigma_D/\gamma_{Mf}}{\gamma_{Ff}\Delta\sigma_N} \right)^5 & \text{if } \Delta\sigma_N < \Delta\sigma_D/\gamma_{Mf} \end{cases} \quad \text{With } \begin{cases} \gamma_{Mf} = 1.15 \\ \gamma_{Ff} = 1.0 \end{cases}$$

Usually, matrices should include information on the occurrences, $n_{E,i}$, of the single load variation ranges, $\Delta\sigma_N$. As this information was not given, Rainflow matrices are presented for the damages produced by a single load cycle. The matrices are built as tables where columns represent the load range starting load and the rows represent the ending load. Due to symmetry only half of the matrix needs to be considered. The results are presented in Table 5.12 and 5.13.

Table 5.12 – Rainflow matrix for damages caused by one cycle per load variation range ΔZ in flange 1

D_i [cycle ⁻¹]	from Z_{\min} [kN]					
to Z_{\max} [kN]	0	50	100	150	200	250
0						
50	2.5E-09					
100	8.0E-08	2.5E-09				
150	2.8E-07	8.0E-08	2.5E-09			
200	6.6E-07	2.8E-07	8.0E-08	2.5E-09		
250	3.4E-06	2.1E-06	1.2E-06	6.0E-07	2.5E-07	
300	2.1E-05	1.6E-05	1.2E-05	9.2E-06	6.6E-06	2.0E-06

Table 5.13 – Rainflow matrix for damages caused by one cycle per load variation range ΔZ in flange 2

D_i [cycle ⁻¹]	from Z_{\min} [kN]			
to Z_{\max} [kN]	0	50	100	150
0				
50	1.2E-08			
100	2.1E-07	1.2E-08		
150	1.4E-06	5.4E-07	1.4E-07	
200	2.2E-05	1.5E-05	1.0E-05	4.7E-06

5.5 Friction connection

The tower geometry and design loads remain the same. However, frictions connections were designed in order to replace the two intermediate flange connections presented before.

5.5.1 Geometry

Studies made by Heistemann (Heistemann, 2014) reveal that the tests with Tension Control Bolts (TCBs) showed the best results. Therefore, the design of both friction connections was made using TCB of type M30 S10T. As they have mechanical properties similar to High Strength Bolts, grade S10T can be considered as bolt grade 10.9 (Cosgrove, 2004). A sketch of the clamping package geometry is shown in Figure 5.5. The dimensions of the clamping packages for both friction connections can be consulted in Table 5.14. Those values were suggested and used by Veljkovic (Veljkovic et al, 2012).

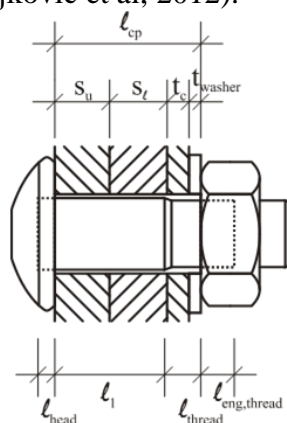


Figure 5.5 – Dimensions of friction connection

Table 5.14 – Dimensions of friction connection

Detail	Connection 1 [mm]	Connection 2 [mm]
Shell thickness upper tower shell s_u	20	15
Shell thickness lower tower shell s_l	21	16
Thickness of cover plate t_c	8	
Diameter of bolt whole d_0	33	
Nominal diameter of bolt shank d	30	
Minor diameter of bolt thread d_3	25.7	
Outside diameter of the plane head bearing surface of the bolt d_w	50	
Thickness of washer t_{washer}	4	
Substitutional extension length of bolt head l_{head}	7.5	
Length of bolt shank l_{shank}	37.1	32.3
Free length of unengaged loaded thread l_{thread}	15.9	10.8
Length of engaged loaded part of thread $l_{eng.thread}$	15	
Substitutional extension length of nut l_{nut}	12	

The number of required bolts, bolt-rows and all the needed design verifications are calculated within the next chapter.

5.5.2 ULS

The friction connections were designed using the *Excel-Tool* by HISTWIN. All design verifications were performed acc. to chapter 3.3.2.2 using the formulas presented in chapter 4.3.1. The results for different slip factors for the contact surface in the friction joint 1 and 2 are presented in Table 5.15 and 5.16. The connections were optimized for the extreme loads given in Table 5.1. The starting point was ensuring the minimum distance between bolt's rows acc. to Eurocode (EC 3-1-8): $p_2 = 2.4 \cdot d_0 = 2.4 \times 33 = 79.2$ mm.

Table 5.15 – Ultimate resistance of friction connection 1 with different contact surface

	Connection 1			
	Zinc coating		Weathering steel	
Slip factor μ	0.45		0.79	
Number of bolt rows n_r	130		123	
Number of bolts per row n_s	5		3	
Number of bolts in connection	650		369	
Diameter of tower D [mm]	3917			
Shell thickness lower and upper shell	21	20	21	20
Width of shell segment c [mm]	94	94	100	100
Net width of shell segment $c_{net} = c - d_0$ [mm]	61	61	67	67
Cross section reduction due holes and cuts c_{net} / c	0.649	0.649	0.670	0.670
Max slip resistance at ULS [N/mm ²]	205.09	215.34	203.06	213.21
Max allowable stress in gross cross section [N/mm ²]	298.51	298.51	308.20	308.20
Ultimate resistance of connection $\sigma_{ult,Rd}$ [N/mm ²]	205.09		203.06	

Table 5.16 – Ultimate resistance of friction connection 2 with different contact surface

	Connection 2			
	Zinc coating		Weathering steel	
Slip factor μ	0.45		0.79	
Number of bolt rows n_r	127		73	
Number of bolts per row n_s	3		3	
Number of bolts in connection	381		219	
Diameter of tower D [mm]	3448			
Shell thickness lower and upper shell	16	15	16	15
Width of shell segment c [mm]	85	85	148	148
Net width of shell segment $c_{net} = c - d_0$ [mm]	52	52	115	115
Cross section reduction due holes and cuts c_{net} / c	0.612	0.612	0.777	0.777
Max slip resistance at ULS [N/mm ²]	178.61	190.51	180.08	192.09
Max allowable stress in gross cross section [N/mm ²]	281.41	281.41	357.43	357.43
Ultimate resistance of connection $\sigma_{ult,Rd}$ [N/mm ²]	178.61		180.08	

Table 5.17 – Design verification of friction connection 1 and 2

	Resulting maximum tensile stresses in tower shell $\sigma_{ult,Ed}$ [N/mm ²]	Design verification $\sigma_{ult,Ed} / \sigma_{ult,Rd}$	
		Zinc coating	Weathering steel
Connection 1	200.2	0.98	0.99
Connection 2	177.4	0.99	0.99

5.5.3 Fatigue

The fatigue design of the friction connections was performed acc. to chapter 3.2.2.1 using the formulas presented in chapter 4.3.2. For friction connection fatigue design verification a programme was created with *MS Excel*. This chapter only present the results obtained with it. The complete *Excel* sheet is presented in Appendix C.

For fatigue design verification of the friction connections, the load variation range in the preloaded bolts, $\Delta F_{p,C}$, has to be checked. It depends on the shell stresses and on the bolt and connection geometry. The elastic resilience of the bolted connection was determined acc. to VDI Guideline (VDI, 2003). As the relation between fatigue loads and the response of bolts in friction connections (stress variation ranges) is linear, damage equivalent load (DEL) method can be applied. All needed parameters are presented in Table 5.18.

Table 5.18 – Resulting pre-load variation range in bolts; all input parameters are in Table 5.14

Description	Equation / Parameter	Connection 1	Connection 2
Mean shell thickness	s_{mean}	20.5 mm	15.5 mm
Maximum stress in “mean shell”	$\max \Delta \sigma_{z,mean} = \frac{c_{mean}}{c_{mean} - d_0} \cdot \sigma_{ult,Ed}$	308.6 N/mm ²	290.0 N/mm ²
elastic resilience of bolt head	$\delta_{head} = \frac{\ell_{head}}{E_{bolt} \cdot A_{nom}}$	5.053 E-08	5.053 E-08
elastic resilience of shank	$\delta_{shank} = \frac{\ell_i}{E_{bolt} \cdot A_i}$	2.499 E-07	2.176 E-07
elastic resilience of unengaged loaded part of thread	$\delta_{free\ thread} = \frac{\ell_{thread}}{E_{bolt} \cdot A_{d_3}}$	1.459 E-07	9.909 E-08
elastic resilience of engaged bolt thread	$\delta_{eng.\ thread} = \frac{\ell_{eng.\ thread}}{E_{bolt} \cdot A_{d_3}}$	1.376 E-07	1.376 E-07
elastic resilience of nut	$\delta_{nut} = \frac{\ell_{nut}}{E_{nut} \cdot A_{nom}}$	8.084 E-08	8.084 E-08
elastic resilience of the preloaded bolt	$\delta_{bolt} = \delta_{head} + \delta_{shank} + \delta_{free\ thread} + \delta_{eng.\ thread} + \delta_{nut}$	6.648 E-07	5.857 E-07
elastic resilience of clamping package	$\delta_{cp} = \frac{2 \cdot \ln \left[\frac{(d_w + d_0) \cdot (d_w + \ell_{cp} \cdot \tan \varphi - d_0)}{(d_w - d_0) \cdot (d_w + \ell_{cp} \cdot \tan \varphi + d_0)} \right]}{E_{cp} \cdot \pi \cdot d_0 \cdot \tan \varphi}$	1.246 E-07	1.103 E-07
total resilience of the joint	$\delta_{joint} = \delta_{bolt} + \delta_{cp}$	7.894 E-07	6.960 E-07
Maximum resulting pre-load variation range in bolts	$\max \Delta F_{p,C} = \beta \cdot \frac{v \cdot \max \Delta \sigma_{z,mean} \cdot s_{mean}}{\delta_{joint} \cdot E_{shell}}$	-14.31 kN	-11.53 kN

Pre-load variation range in bolts for the DEL in net shell cross section	$\Delta F_{p,C,DEL} = \beta \cdot \frac{\nu \cdot \Delta \sigma_{z,DEL,net} \cdot S_{mean}}{\delta_{joint} \cdot E_{shell}}$	-0.85 kN	-0.68 kN
--	--	----------	----------

The DEL were given for each load component for different Wöhler slopes. As mentioned before, the state of art is to use a single Wöhler slope of $m=4$. Therefore, the fatigue stress of the pre-loaded bolts at $N_{ref} = 2 \times 10^8$ cycles was calculated with a Wöhler curve with constant slope $m=4$. For the pre-loaded bolts detail category 50 were used and for the shell detail category 90, acc. to (EC 3-1-9).

Characteristic fatigue resistance associated with a reference number of cycles ($N_{ref} = 2 \times 10^8$):

$$\Delta \sigma_{bolt,R} = 50 \cdot \left(\frac{2 \times 10^6}{2 \times 10^8} \right)^{\frac{1}{4}} = 15.81 \text{ N/mm}^2$$

$$\Delta \sigma_{shell,R} = 90 \cdot \left(\frac{2 \times 10^6}{2 \times 10^8} \right)^{\frac{1}{4}} = 28.46 \text{ N/mm}^2$$

Damage equivalent tensile stresses in bolts and in gross cross-section (connection 1 and 2):

$$\Delta \sigma_{bolt,1,DEL} = \frac{F_{p,C,DEL}}{A_s} = \frac{850}{561} = 1.51 \text{ N/mm}^2$$

$$\Delta \sigma_{bolt,2,DEL} = \frac{F_{p,C,DEL}}{A_s} = \frac{680}{561} = 1.22 \text{ N/mm}^2$$

$$\Delta \sigma_{shell,1,DEL} = 18.3 \text{ N/mm}^2$$

$$\Delta \sigma_{shell,2,DEL} = 17.2 \text{ N/mm}^2$$

The final fatigue design verification then reads:

$$\frac{\gamma_{Ff} \Delta \sigma_{DEL}}{\Delta \sigma_R / \gamma_{Mf}} \leq 1.0 \quad \text{with} \begin{cases} \gamma_{Ff} = 1.0 \\ \gamma_{Mf} = 1.15 \end{cases}$$

Table 5.19 – Design verification of friction connection 1 and 2

		Design verification	
Connection 1	Bolts	0.1	Verified
	Shell	0.6	Verified
Connection 2	Bolts	0.1	Verified
	Shell	0.5	Verified

5.6 Comparison

In chapter 3.3, the higher fatigue resistance, simple design and reduction cost have been named as the major arguments for the replacement of flange connections by friction connection with open slotted holes. In this chapter a comparison of the two connection solutions is presented.

5.6.1 Resistance

5.6.1.1 Ultimate resistance

The used flange connections have enough resistance, but in order to improve it, thicker flanges, more and bigger bolts would be needed, which are limited for a given geometry. Thus the margin for improvement is limited when compared to friction connections.

The static resistance of friction connections is attained by choosing appropriate faying surfaces and defining the amount of bolts. For a given surface type, the static resistance of the friction connection is set by the number of bolts. The number of bolts row is limited by a minimum spacing but it is possible to increase the number of bolts per row. The tower resistance to static loads can thus be resumed to material strength which may be improved by using higher steel grades, in order to achieve the desired resistance.

5.6.1.2 Fatigue resistance

Fatigue strength of flange connections depends on the amount of bolts and their size, which is limited for a given geometry. Although fatigue failure of bolted ring flange connections is controlled by failure of the bolts, the resistance of the bolts exclusively is not enough to establish the resistance of the connection, the solicitations depend on the geometry and pretension. Fatigue design is laborious due to the intrinsic nonlinearity.

The fatigue strength of friction connections depends on the gross cross-section. It can be improved by increasing shell thickness, while the fatigue strength of the flange connection is limited by bolt and flange size limits. Since is possible to independently adjust both resistances (ultimate and fatigue resistance) in friction connection, optimization is possible.

5.6.2 Material

The material costs for flange and friction connections is presented below. Constructions (fabrication and installation) aspects are only compared qualitatively. Furthermore, as the material costs were provided by *REpower* in December 2007 (Veljkovic et al, 2012), (Husson, 2008), the prices of Tension Control Bolts (TCB) used for friction connections are dated from August 2007 (Veljkovic et al, 2012), (Husson, 2008).

Table 5.20 – Material costs of flange connection 1

Component	Unit price [€]	Amount	Total Price [€]
Flange ($d_a=3917\text{mm}$)	6762.00	2	13524
Bolt (M42x245 10.9)	20.32	124	2520
		Total:	16044

Table 5.21 – Material costs of flange connection 2

Component	Unit price [€]	Amount	Total Price [€]
Flange ($d_a=3448\text{mm}$)	4395.00	2	8790
Bolt (M36x205 10.9)	11.40	116	1322
		Total:	10112

Table 5.22 and Table 5.23 present the material costs for both friction connections with ethyl silicate zinc rich paint.

Table 5.22 – Material costs for friction connection 1 with ethyl silicate zinc rich paint and optimum dimensions

Component	Unit price [€]	Amount	Total Price [€]
Bolt (M30x110 S10T)	5.45	650	3543
		Total:	3543

Table 5.23 – Material costs for friction connection 2 with ethyl silicate zinc rich paint and optimum dimensions

Component	Unit price [€]	Amount	Total Price [€]
Bolt (M30x110 S10T)	5.45	369	2011
		Total:	2011

The total material costs for two flange connections is about 26156 €, while the costs for the friction connection is 5554€, accounting on prices from 2008 (Veljkovic et al, 2012), (Husson, 2008). This supports what has been previously determined by HISTWIN about the reduction costs around 80%. Furthermore, using weathering steel would decrease the total amount of required bolts by 40%.

Fabrication and installation costs were not included on this estimation. The machining and drilling operations on flanges demand around five hours (Husson, 2008). Flanges must be welded and if tolerances are not fulfilled, additional machining will be needed. In contrast, friction connections only require cutting holes in the steel plates. That could be executed by lasers before rolling or, the slotted holes could even be produced by steel producers, which reduces de fabrication time (Veljkovic et al, 2012). Furthermore, to avoid distortion, the slots can be cut as closed and opened afterwards by cutting the tubes manually (Husson, 2008). Therefore, it is reasonable to say that in serial production fabrication costs of friction connections would be lower comparing to flange connections.

Moreover, despite friction connections require much more bolts, they are smaller and the tightening tools are said to be easier to handle. The tightening procedure of TCB has also some advantages (see chapter 3.4.3) considering speed of tightening which is two times faster than conventional bolts. In addition, only one operator is needed on one side of the structure, with a special electric wrench.

6 CONCLUSION AND RECOMMENDATIONS

In this thesis, the higher fatigue resistance, simple design and reduction cost have been named as the major arguments for the replacement of ring flange connections by friction connection with long open slotted holes. Based on the presented design example of the flange and friction connections it is possible to say that the implementation of a new type of friction connection in wind towers may be beneficial from the point of view of the overall material consumption, allowing for improved fatigue resistance. The currently used flange connections are seen as limiting factor for usage of higher strength steels because of its low fatigue resistance (detail category between 36* and 71). The use of friction connection allows the fatigue detail to change to higher value, probably closer to the one for the bare material. Thus, the design limit for tubular steel towers shifts from the fatigue resistance of the connection to the stability resistance of the tower shell, which justify the use of thinner plates offering the opportunity to use higher strength steel, resulting in a decrease of dead weight of the structure. Therefore it is important to understand the behaviour of friction connections when exposed to cyclic loading.

As friction connections with slotted holes have simple resistance models, the design process of wind towers is simplified. Particularly, as the relation between fatigue loads and the response of bolts in friction connections is linear, Damage Equivalent Loads (DEL) can be used for fatigue calculations. The static resistance at the Ultimate Limit State (ULS) is controlled by the friction coefficient of the surface and the number of bolts, whereas the fatigue strength is controlled by the shell thickness. Therefore, as the static and fatigue resistances depend on different parameters, they can be adjusted independently, leading to a simplified design optimization. Nevertheless, one important parameter to study and quantify is the loss of pretension force in the bolts during the tower life time, since the ULS resistance depends directly on this parameter.

The advantages of friction connections are highlighted in diverse documents (Veljkovic et al, 2012), (Heistermann et al, 2009), (Husson, 2008) by estimating the potential cost savings when comparing to ring flange connections. It was estimated that material cost savings of approximately 80% could be achieved, which contributes to direct savings of about 20,000€ for a typical 80m-high tower. As fabrication and installation costs were not included on that estimation they could be object of further work on this domain.

Despite all mentioned advantages, this solution needs further experimental studies on fatigue behaviour of real prototypes in order to enhance the design and ensure its safety.

REFERENCES

- Alcoa Fastening Systems (2015). “BobTail – The next generation HuckBolt”. Alcoa Fastening Systems & Rings, United States of America
- APREN: Associação Portuguesa de Energias Renováveis: www.apren.pt
- August Friedberg GmbH: www.august-friedberg.de
- Bickford, J. H. (1995). “An introduction to the design and behaviour of bolted joints” (3rd edition). Marcel Dekker, New York
- Bickford, J. H. (1998). “Handbook of Bolts and Bolted Joints”. Marcel Dekker, New York
- Bolt science: <http://www.boltscience.com>
- Cosgrove, T. C. (2004). “Tension Control Bolts, Grade S10T in Friction Grip Connections”. The Steel Construction Institute. Ascot, England
- DIBt, (2005). "Richtlinie für Windenergieanlagen - Einwirkungen und Standsicherheitsnachweise für Turm und Gründung". Deutsches Institut für Bautechnik
- Eccles, B. (2011a). “Self-loosening of threaded fasteners”. www.boltscience.com, Issue 2, pp. 22, 23
- Eccles, B. (2011b). “Why nuts and bolts can self-loosen”, www.boltscience.com
- EN 1990: 2010, “Eurocode – Basis of structural design”, European Committee for Standardization, 2010
- EN 1993-1-8: 2010, “Eurocode 3 – Design of steel structures – Part 1-8: Design of joints”, European Committee for Standardization, 2010
- EN 1993-1-9: 2010, “Eurocode 3 – Design of steel structures – Part 1-9: Fatigue”, European Committee for Standardization, 2010
- Encyclopedia of Alternative Energy: www.daviddarling.info/encyclopedia/H/AE_horizontal-axis_wind_turbine.html
- EWEA: The European Wind Energy Association. (February 2016). “Wind in power – 2015 European statistics” @ <http://www.ewea.org/>

-
- Fric, N., Budevac, D., Markovic, Z., Dobric, J., Isakovic, J. (2014). “Huck bobtail fastening system – new solution for high-strength lockbolts”, *Journal of Applied Engineering Science*, Paper 12, pp. 23-28
- Germanischer Lloyd, (2010). “Rules and Guidelines, Industrial Services: Guideline for the Certification of Wind Turbines”. Renewables Certification, Hamburg
- Grampian Fasteners – <https://www.grampianfasteners.com/manufacturers/nordlock>
- Groover, M. P. (2010). “Fundamentals of Modern Manufacturing: Materials, Processes, and Systems” (4th edition). Wiley, New Jersey
- GWEC: Global Wind Energy Council. (2015) “Global Wind Report – annual market update – 2015” @ <http://www.gwec.net/>
- Hau, E. (2006). “Wind turbines - Fundamentals, Technologies, Application, Economics” (2nd edition). Springer, Berlin.
- Heistermann, C., Husson, W., Veljkovic, M. (2009). “Flange connection vs. friction connection in towers for wind turbines”. Proc. of Nordic steel and construction conference (NSCC 2009), pp. 296 – 303, Malmö
- Heistermann C. (2011). “Behaviour of Pretensioned Bolts in Friction Connections”. Licentiate Thesis, Luleå University of Technology, Luleå
- Heistermann, C. (2014). “Resistance of Friction Connections with Open Slotted Holes in Towers for Wind Turbines”. Doctoral Thesis, Luleå University of Technology, Luleå
- Husson, W. (2008). “Friction Connections with Slotted Holes for Wind Towers”. Licentiate Thesis, Luleå University of Technology, Luleå
- IEA: International Energy Agency: <https://www.iea.org/>
- Nord-Lock Group – Bolt Securing System, Technical Information - <http://www.nord-lock.com/nord-lock/wedge-locking>
- Pavlovic, M., Heistermann, C., Veljkovic, M., Pak, D., Feldmann, M., Rebelo, C., Simões, L.S. (2015). “Friction connection vs. ring flange connection in steel towers for wind converters”. *Engineering Structures* 98, pp. 151-162
- Sørensen, J. D., Sørensen, J. N. (2011), “Wind Energy Systems: Optimising Design and Construction for Safe and Reliable Operation”. Woodhead Publishing, Cambridge
- UK TCB Brochure@ <http://www.tcbolts.com>. Tension Control Bolts Limited, England
-

Veljkovic, M. and Husson, W. (2009). “High-strength wind turbine steel towers”. Elforsk rapport: 09:11

Veljkovic, M., Feldmann, M., Naumes, J., Pak, D., Rebelo, C. and Simões da Silva, L. (2010). “Friction connection in tubular towers for a wind turbine”. *Stahlbau*, 79: pp. 660-668, Berlin

Veljkovic, M., Heistermann, C., Husson, W., Limam, M., Feldmann, M., Naumes, J. et al. (2012). “High-strength tower in steel for wind turbines (HISTWIN)”. Grant agreement n° RFSR-CT-2006-00031, RFCS Publications, European Commission, Brussels.

Veljkovic, M., Heistermann, C., Pavlovic, M., Feldmann, M., Pak, D., Richter, C., Rebelo, C., Pinto, P., Matos, R., Baniotopoulos, C., Gkantou, M., Dehan, V., Haremza, C., Nusse, G., (2015). “High-strength steel tower for wind turbines – (HISTWIN_Plus)”. Grant agreement n° RFS2-CT-2014-00023, RFCS Publications, European Commission, Brussels.

Verein Deutscher Ingenieure, (2003). “VDI Guideline 2230: – Part 1: Systematic calculation of high duty bolted joints – Joints with one cylindrical bolt”. *VDI-Handbuch Konstruktion*. Beuth Verlag GmbH, Berlin.

APPENDIX

Appendix A – Static resistance at ULS – Flange connections

Flange connection 1 (H = 21770 mm)

Input data					
symbol	value	unit	explanation	comment	
Internal forces					
Design load case:		Maximum design stress in shell:			
F _x =	-886	[kN]		$\sigma_{ult.Ed} = \frac{M_r}{W_i} - \frac{F_z}{A_i}$	
F _y =	27	[kN]			
F _z =	-2443	[kN]		W _i = 254,8E+6 [mm ³]	
F _r =	886	[kN]		A _i = 260,0E+3 [mm ²]	
M _x =	1129	[kNm]		σ _{ult.Ed} = 200,2 [N/mm ²]	
M _y =	-48617	[kNm]			
M _z =	-1368	[kNm]			
M _r =	48631	[kNm]			
Material data and geometry:					
Cross-section values:					
S	355		type of steel		
t	20	[mm]	material thickness		
d _{outer}	3917	[mm]	outer diameter		
t	21	[mm]	material thickness (below)		
d _{outer(lower)}	3962	[mm]	lower shell outer diameter		
Flange connection:					
	10,9	[-]	grade of the bolts		
	42	[mm]	bolt diameter		
d _{bolt}	45	[mm]			
A _s	1121	[mm ²]			
f _{ub}	1000	[N/mm ²]			
a	90,5	[mm]	distance between flange edge and axis of bolt		
b	74,5	[mm]	distance between flange axis of bolt and shell (b= d-s/2)		
c	95	[mm]	shell stripe width		
d	84,5	[mm]			
t _f	90	[mm]			
s	20	[mm]			
Y _{M0}	1,1				
Y _{M2}	1,25				
Calculation					

symbol	value	unit	explanation	comment
Design resistances of the single components				
Design tensile resistance of bolts				
$F_{t,Rd}$	807,1	[kN]	$F_{t,Rd} = \frac{0,9 \cdot f_{ub} \cdot A_s}{\gamma_{M2}}$	
Design plastic bending resistance of shell				
$M_{pl,Rd,sh}$	306,6	[kNcm]	$M_{pl,Rd,sh} = \frac{W_{pl,sh} \cdot f_{y,sh}}{\gamma_{M0}} = \frac{c \cdot s^2 \cdot f_{y,sh}}{4 \cdot \gamma_{M0}}$	
Design plastic resistance of shell				
$N_{pl,Rd,sh}$	613,2	[kN]	$N_{pl,Rd,sh} = \frac{A_{sh} \cdot f_{y,sh}}{\gamma_{M0}} = \frac{c \cdot s \cdot f_{y,sh}}{\gamma_{M0}}$	
Design plastic bending resistance of shell considering $M-N$ -interaction				
$M_{N,pl,Rd,sh}$	-	[kN]	$M_{N,pl,Rd,sh} = \left[1 - \left(\frac{Z_{ult}}{N_{pl,Rd,sh}} \right)^2 \right] \cdot M_{pl,Rd,sh}$	
Design plastic bending resistance of net cross-section of flange				
$M_{pl,Rd,fl,net}$	3267,6	[kN]	$M_{pl,Rd,fl,net} = \frac{W_{pl,net,fl} \cdot f_{y,fl}}{\gamma_{M0}} = \frac{(c - d_0) \cdot t_{fl}^2 \cdot f_{y,fl}}{4 \cdot \gamma_{M0}}$	
Verification				

Verification				
symbol	value	unit	explanation	comment
Ultimate resistance if the flange acc. to the plastic hinge theory				
$Min \{Z_{ult,1}; Z_{ult,2}; Z_{ult,3}\}$				
Yielding (failure) of the bolt				
	$Z_{ult,1} = F_{t,Rd}$			
	Zult,1= 807,1	[kN]		
Yielding (failure) of the bolt and at the same time plastic hinge in shell				
	$Z_{ult,2} = \frac{F_{t,Rd} \cdot a + M_{N,pl,Rd,sh}(Z_{ult,2})}{a + b} = -\frac{N_{pl,Rd,sh}^2 \cdot (a + b)}{2 \cdot M_{pl,Rd,sh}} + N_{pl,Rd,sh} \cdot \sqrt{1 + \frac{N_{pl,Rd,sh}^2 \cdot (a + b)^2 + 4 \cdot F_{t,Rd} \cdot a \cdot M_{pl,Rd,sh}}{4 \cdot M_{pl,Rd,sh}^2}}$			
	Zult,2= 451,2	[kN]		
Plastic hinge in shell and flange (failure of the connection)				
	$Z_{ult,3} = \frac{M_{N,pl,Rd,sh}(Z_{ult,3}) + M_{pl,Rd,fl,net}}{b} = -\frac{N_{pl,Rd,sh}^2 \cdot b}{2 \cdot M_{pl,Rd,sh}} + \sqrt{\frac{N_{pl,Rd,sh}^4 \cdot b^2}{4 \cdot M_{pl,Rd,sh}^2} + \frac{M_{pl,Rd,fl,net} + M_{pl,Rd,sh}}{M_{pl,Rd,sh}} \cdot N_{pl,Rd,sh}^2}$			
	Zult,3= 456,9	[kN]		
Failure mode *	Ultimate tensile force in segment shell		Ultimate tensile stress in tower shell	
*acc. To plastic hinge theory from Petersen	Zult,Rd [kN]		σult,Rd [N/mm²]	
2 = Yielding of bolt in combination with a plastic hinge in shell	451,2		237,5	
Resulting max. tensile stresses in tower shell (σult,Rd [N/mm²])				
Design verification				
σult,Ed / σult,Rd		Verified		
200,2		0,8		
Input				

Flange connection 2 (H = 48390 mm)

Input data				
symbol	value	unit	explanation	comment
Internal forces				
Design load case:		Maximum design stress in shell:		
F _x =	-864	[kN]		$\sigma_{ult,Ed} = \frac{M_r}{W_i} - \frac{F_z}{A_i}$
F _y =	7	[kN]		
F _z =	-1846	[kN]		W _i =
F _r =	864	[kN]		A _i =
M _x =	1635	[kNm]		σ _{ult,Ed} =
M _y =	-25168	[kNm]		177,4
M _z =	-1363	[kNm]		[N/mm ²]
M _r =	25221	[kNm]		
Material data and geometry:				
Cross-section values:				
S	355		type of steel	
t	15	[mm]	material thickness	
d _{outer}	3448	[mm]	outer diameter	
t	16	[mm]	material thickness (below)	
d _{outer(lower)}	3492	[mm]	lower shell outer diameter	
Flange connection:				
	10,9	[-]	grade of the bolts	
d _{bolt}	36	[mm]	bolt diameter	
d ₀	39	[mm]		
A _s	817	[mm ²]		
f _{ub}	1000	[N/mm ²]		
a	58	[mm]	distance between flange edge and axis of bolt	
b	54,5	[mm]	distance between flange axis of bolt and shell (b= d-s/2)	
c	90	[mm]	shell stripe width	
d	62	[mm]		
t _f	75	[mm]		
s	15	[mm]		
Y _{M0}	1,1			
Y _{M2}	1,25			
<div style="background-color: #cccccc; padding: 5px; display: inline-block;">Calculation</div>				

symbol	value	unit	explanation	comment
Design resistances of the single components				
Design tensile resistance of bolts				
$F_{t,Rd}$	588,2	[kN]	$F_{t,Rd} = \frac{0,9 \cdot f_{ub} \cdot A_s}{\gamma_{M2}}$	
Design plastic bending resistance of shell				
$M_{pl,Rd,sh}$	163,4	[kNcm]	$M_{pl,Rd,sh} = \frac{W_{pl,sh} \cdot f_{y,sh}}{\gamma_{M0}} = \frac{c \cdot s^2 \cdot f_{y,sh}}{4 \cdot \gamma_{M0}}$	
Design plastic resistance of shell				
$N_{pl,Rd,sh}$	435,7	[kN]	$N_{pl,Rd,sh} = \frac{A_{sh} \cdot f_{y,sh}}{\gamma_{M0}} = \frac{c \cdot s \cdot f_{y,sh}}{\gamma_{M0}}$	
Design plastic bending resistance of shell considering $M-N$ -interaction				
$M_{N,pl,Rd,sh}$	-	[kN]	$M_{N,pl,Rd,sh} = \left[1 - \left(\frac{Z_{ult}}{N_{pl,Rd,sh}} \right)^2 \right] \cdot M_{pl,Rd,sh}$	
Design plastic bending resistance of net cross-section of flange				
$M_{pl,Rd,fl,net}$	2314,6	[kN]	$M_{pl,Rd,fl,net} = \frac{W_{pl,net,fl} \cdot f_{y,fl}}{\gamma_{M0}} = \frac{(c - d_0) \cdot t_{fl}^2 \cdot f_{y,fl}}{4 \cdot \gamma_{M0}}$	
Verification				

Verification				
symbol	value	unit	explanation	comment
Ultimate resistance if the flange acc. to the plastic hinge theory				
$Min \{Z_{ult,1}; Z_{ult,2}; Z_{ult,3}\}$				
Yielding (failure) of the bolt				
	$Z_{ult,1} = F_{t,Rd}$			
	Zult,1=	588,2	[kN]	
Yielding (failure) of the bolt and at the same time plastic hinge in shell				
	$Z_{ult,2} = \frac{F_{t,Rd} \cdot a + M_{N,pl,Rd,sh}(Z_{ult,2})}{a + b} = -\frac{N_{pl,Rd,sh}^2 \cdot (a + b)}{2 \cdot M_{pl,Rd,sh}} + N_{pl,Rd,sh} \cdot \sqrt{1 + \frac{N_{pl,Rd,sh}^2 \cdot (a + b)^2 + 4 \cdot F_{t,Rd} \cdot a \cdot M_{pl,Rd,sh}}{4 \cdot M_{pl,Rd,sh}^2}}$			
	Zult,2=	310,4	[kN]	
Plastic hinge in shell and flange (failure of the connection)				
	$Z_{ult,3} = \frac{M_{N,pl,Rd,sh}(Z_{ult,3}) + M_{pl,Rd,fl,net}}{b} = -\frac{N_{pl,Rd,sh}^2 \cdot b}{2 \cdot M_{pl,Rd,sh}} + \sqrt{\frac{N_{pl,Rd,sh}^4 \cdot b^2}{4 \cdot M_{pl,Rd,sh}^2} + \frac{M_{pl,Rd,fl,net} + M_{pl,Rd,sh}}{M_{pl,Rd,sh}} \cdot N_{pl,Rd,sh}^2}$			
	Zult,3=	426,0	[kN]	
Failure mode *	Ultimate tensile force in segment shell		Ultimate tensile stress in tower shell	
*acc. To plastic hinge theory from Petersen	Zult,Rd [kN]		σult,Rd [N/mm²]	
2 = Yielding of bolt in combination with a plastic hinge in shell	310,4		229,9	
Resulting max. tensile stresses in tower shell (σult,Rd [N/mm²])				
Design verification				
σult,Ed / σult,Rd				
177,4		0,8		Verified
Input				

Appendix B – Fatigue resistance – Flange connections

Flange connection 1 (H = 21770 mm)

Input data				
symbol	value	unit	explanation	comment
Material data and geometry:				
Cross-section values:				
S	355		type of steel	
t	20	[mm]	material thickness	
d _{outer}	3917	[mm]	outer diameter	
t	21	[mm]	material thickness (below)	
d _{outer(lower)}	3962	[mm]	lower shell outer diameter	
Flange connection:				
	10,9	[-]	grade of the bolts	
f _{ub}	1000	[N/mm ²]		
E _{bolt}	210	[GPa]	Young's-modulus of bolt material	
E _{fl}	210	[GPa]	Young's-modulus of flange material	
d _{bolt}	42	[mm]	nominal bolt diameter	
d _o	45	[mm]	diameter of bolt hole	
d _{washer}	78	[mm]		
A _s	1121	[mm ²]	tensile stress area of bolt	
A _{nom}	1385	[mm ²]	nominal cross section of bolt	
F _{p,C}	713,4	[kN]	characteristic preload force in bolt	
F _{t,Rd}	807	[kN]	design tensile resistance of the bolt	
Flange geometry:				
a	90,5	[mm]	distance between flange edge and axis of bolt	
b	74,5	[mm]	distance between flange axis of bolt and shell (b= d-s/2)	
c	95	[mm]	shell stripe width	
d	84,5	[mm]		
t _f	90	[mm]		
s	20	[mm]		
Y _{M0}	1,1			<div style="text-align: center;"> <input type="button" value="Calculation"/> </div>
Y _{M2}	1,25			

symbol	value	unit	explanation	comment
Elastic structural behaviour of L-flange connections				
Bolt stiffness				
$C_S =$	1615833	[N/mm]	$C_S = \frac{1}{\int_0^{t_s} \frac{1}{E_S A_S(x)} dx} \approx \frac{E_{bolt} \cdot A_{nom}}{2 \cdot t_{fl}}$	
Clam solid stiffness				
$C_D =$	6589098	[N/mm]	$C_D = \frac{1}{2 \cdot \int_0^{t_s} \frac{1}{E_D A_D(x)} dx} \approx \frac{E_{fl} \cdot \pi}{4 \cdot 2 \cdot t_{fl}} \cdot \left[\left(d_{washer} + \frac{2 \cdot t_{fl}}{10} \right)^2 - d_0^2 \right]$	
Curve parameters				
$p =$	0,197		$p = \frac{C_S}{C_S + C_D}$	
$q =$	0,803		$q = \frac{C_D}{C_S + C_D}$	
$\lambda^* =$	2,176		$\lambda^* = \frac{0.7 \cdot a + b}{0.7 \cdot a}$	
$Z_I =$	230,2	[kN]	$Z_I = \frac{a - 0.5 \cdot b}{a + b} \cdot F_{p,C}$	
$Z_{II} =$	408,2	[kN]	$Z_{II} = \frac{1}{\lambda^* \cdot q} \cdot F_{p,C}$	
Bolt-load function				

Verification

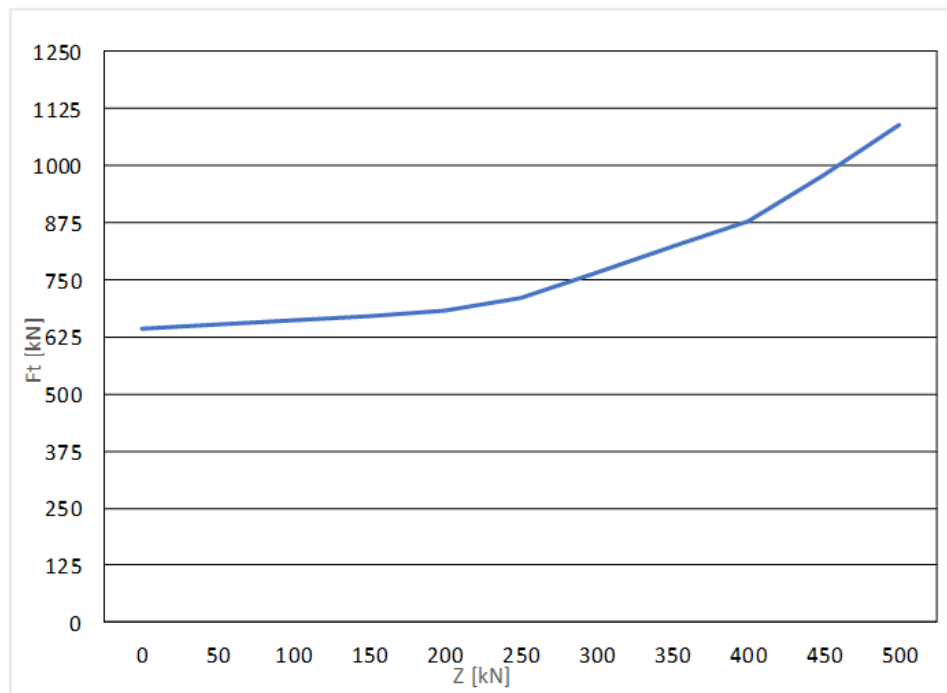
symbol	value	unit	explanation	comment
--------	-------	------	-------------	---------

Bolt-load function acc. to Schmidt/Neuper

The final bolt-load is given by:

$$\begin{aligned}
 Z \leq Z_I &\quad \rightarrow \quad F_{t,I} = F_{p,C} + p \cdot Z \\
 Z_I < Z \leq Z_{II} &\quad \rightarrow \quad F_{t,II} = F_{p,C} + p \cdot Z_I + \left[\lambda^* \cdot Z_{II} - (F_{p,C} + p \cdot Z_I) \right] \cdot \frac{Z - Z_I}{Z_{II} - Z_I} \\
 Z > Z_{II} &\quad \rightarrow \quad F_{t,III} = \lambda^* \cdot Z
 \end{aligned}$$

Note: A re-adjustment of the pre-load $F_{p,C}$ of all bolts within 6-month is assumed. Thus, acc. to DIBt-Guideline, 90% of the nominal pre-load can be taken into account.



Input

Verification

symbol	value	unit	explanation	comment
--------	-------	------	-------------	---------

Bolt-load function acc. to Schmidt/Neuper

Z [kN]	F _{t,Ed} [kN]
0	642,0
50	651,9
100	661,7
150	671,6
200	681,4
250	709,7
300	766,1
350	-
400	-
450	-
500	-

Note: Only loads which produce stresses below the bolt yield strength will be considered.

F_{t,Rd}= 807 [kN] design tensile resistance of the bolt

Resulting axial stress variation ranges $\Delta\sigma_N$ in bolts in function of load ranges $\Delta Z = Z_{max} - Z_{min}$

A_s= 1121 [mm²] tensile stress area of bolt

$\Delta\sigma_N$ to Z _{max} [kN]	from Z _{min} [kN]										
	0	50	100	150	200	250	300	350	400	450	500
0											
50	8,8										
100	17,6	8,8									
150	26,4	17,6	8,8								
200	35,1	26,4	17,6	8,8							
250	60,4	51,6	42,8	34,0	25,2						
300	110,7	101,9	93,1	84,4	75,6	50,3					
350	-	-	-	-	-	-	-				
400	-	-	-	-	-	-	-	-			
450	-	-	-	-	-	-	-	-	-		
500	-	-	-	-	-	-	-	-	-	-	

Wöhler curve

Verification

symbol	value	unit	explanation	comment
--------	-------	------	-------------	---------

Wöhler curve

Note 1: As the calculation method used to determine the bolt force functions does not consider the influence of bending moment on the bolt, the Wöhler curve for bolts in tension given in EN1993-1-9 has to be reduced to detail category **36***.

Note 2: Additionally, the reduction factor, k_s , is used when the bolts have nominal diameters d larger than 30 mm.

$k_s = 0,919 \quad k_s = (30/d)^{0,25}$

$\Delta\sigma_C = 40$

Properties of the considered Wöhler curve 36*

Bolt	k_s	$\Delta\sigma_C$ with $N_c=2 \cdot 10^6$	$\Delta\sigma_D$ with $N_c=10^7$
M42	0,919	36,8	21,1

Single damages can be derived by: $D_i = \frac{n_{E,i}}{N_{R,i}}$

with:

$$N_{R,i} = \begin{cases} N_C \cdot \left(\frac{\Delta\sigma_C / \gamma_{Mf}}{\gamma_{Ff} \cdot \Delta\sigma_N} \right)^3 & \text{if } \gamma_{Ff} \cdot \Delta\sigma_N \geq \Delta\sigma_D / \gamma_{Mf} \\ N_D \cdot \left(\frac{\Delta\sigma_D / \gamma_{Mf}}{\gamma_{Ff} \cdot \Delta\sigma_N} \right)^5 & \text{if } \Delta\sigma_N < \Delta\sigma_D / \gamma_{Mf} \end{cases} \quad \text{with } \gamma_{Mf} = 1.15 \text{ and } \gamma_{Ff} = 1.0$$

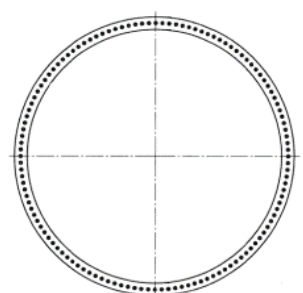
Rainflow matrix for damages caused by one cycle per load variation range ΔZ

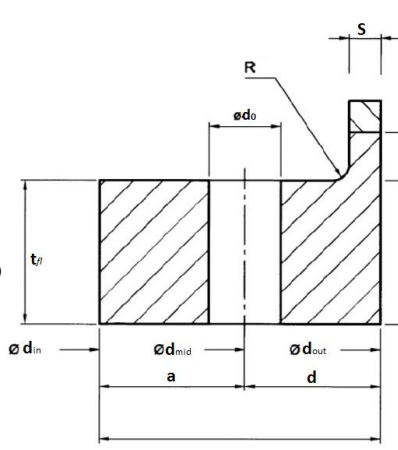
Di [cycle ⁻¹]	from Zmin [kN]											
	to Zmax [kN]	0	50	100	150	200	250	300	350	400	450	500
0												
50	2,5E-09											
100	8,0E-08	2,5E-09										
150	2,8E-07	8,0E-08	2,5E-09									
200	6,6E-07	2,8E-07	8,0E-08	2,5E-09								
250	3,4E-06	2,1E-06	1,2E-06	6,0E-07	2,5E-07							
300	2,1E-05	1,6E-05	1,2E-05	9,2E-06	6,6E-06	2,0E-06						
350	#####	#####	#####	#####	#####	#####	#####					
400	#####	#####	#####	#####	#####	#####	#####	#####				
450	#####	#####	#####	#####	#####	#####	#####	#####	#####			
500	#####	#####	#####	#####	#####	#####	#####	#####	#####	#####		

Rainflow Matrix

Flange connection 2 (H = 48390 mm)

Input data				
symbol	value	unit	explanation	comment
Material data and geometry:				
Cross-section values:				
S	355		type of steel	
t	15	[mm]	material thickness	
d _{outer}	3448	[mm]	outer diameter	
t	16	[mm]	material thickness (below)	
d _{outer(lower)}	3492	[mm]	lower shell outer diameter	
Flange connection:				
f _{ub}	10,9	[-]	grade of the bolts	
f _{ub}	1000	[N/mm ²]		
E _{bolt}	210	[GPa]	Young's-modulus of bolt material	
E _{fl}	210	[GPa]	Young's-modulus of flange material	
d _{bolt}	36	[mm]	nominal bolt diameter	
d ₀	39	[mm]	diameter of bolt hole	
d _{washer}	66	[mm]		
A _s	817	[mm ²]	tensile stress area of bolt	
A _{nom}	1018	[mm ²]	nominal cross section of bolt	
F _{p,C}	519,9	[kN]	characteristic preload force in bolt	
F _{t,Rd}	588	[kN]	design tensile resistance of the bolt	
Flange geometry:				
a	58	[mm]	distance between flange edge and axis of bolt	
b	54,5	[mm]	distance between flange axis of bolt and shell (b= d-s/2)	
c	90	[mm]	shell stripe width	
d	62	[mm]		
t _f	75	[mm]		
s	15	[mm]		
Y _{M0}	1,1			
Y _{M2}	1,25			
<div style="border: 1px solid black; display: inline-block; padding: 5px 20px; background-color: #F0F0F0;">Calculation</div>				





symbol	value	unit	explanation	comment
Elastic structural behaviour of L-flange connections				
Bolt stiffness				
C_S	1425200	[N/mm]	$C_S = \frac{1}{\int_0^{t_s} \frac{1}{E_S A_S(x)} dx} \approx \frac{E_{bolt} \cdot A_{nom}}{2 \cdot t_{fl}}$	
Clam solid stiffness				
C_D	5541769	[N/mm]	$C_D = \frac{1}{2 \cdot \int_0^{t_s} \frac{1}{E_D A_D(x)} dx} \approx \frac{E_{fl} \cdot \pi}{4 \cdot 2 \cdot t_{fl}} \cdot \left[\left(d_{washer} + \frac{2 \cdot t_{fl}}{10} \right)^2 - d_0^2 \right]$	
Curve parameters				
p	0,205		$p = \frac{C_S}{C_S + C_D}$	
q	0,795		$q = \frac{C_D}{C_S + C_D}$	
λ^*	2,342		$\lambda^* = \frac{0.7 \cdot a + b}{0.7 \cdot a}$	
Z_I	142,1	[kN]	$Z_I = \frac{a - 0.5 \cdot b}{a + b} \cdot F_{p,C}$	
Z_{II}	279,0	[kN]	$Z_{II} = \frac{1}{\lambda^* \cdot q} \cdot F_{p,C}$	
Bolt-load function				

Verification

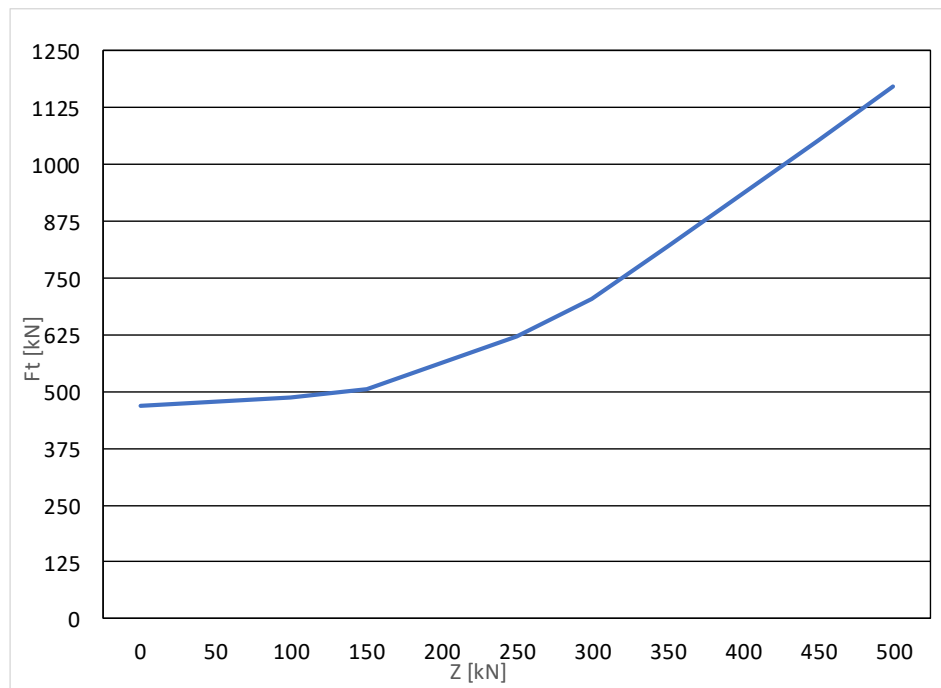
symbol	value	unit	explanation	comment
--------	-------	------	-------------	---------

Bolt-load function acc. to Schmidt/Neuper

The final bolt-load is given by:

$$\begin{aligned}
 Z \leq Z_I &\quad \rightarrow \quad F_{t,I} = F_{p,C} + p \cdot Z \\
 Z_I < Z \leq Z_{II} &\quad \rightarrow \quad F_{t,II} = F_{p,C} + p \cdot Z_I + \left[\lambda^* \cdot Z_{II} - (F_{p,C} + p \cdot Z_I) \right] \cdot \frac{Z - Z_I}{Z_{II} - Z_I} \\
 Z > Z_{II} &\quad \rightarrow \quad F_{t,III} = \lambda^* \cdot Z
 \end{aligned}$$

Note: A re-adjustment of the pre-load $F_{p,C}$ of all bolts within 6-month is assumed. Thus, acc. to DIBt-Guideline, 90% of the nominal pre-load can be taken into account.



Input

Verification																																																																																																																																																																
symbol	value	unit	explanation	comment																																																																																																																																																												
Bolt-load function acc. to Schmidt/Neuper																																																																																																																																																																
<table border="1" style="margin-left: auto; margin-right: auto; border-collapse: collapse; text-align: center;"> <thead> <tr style="background-color: #D9E1F2;"> <th>Z [kN]</th> <th>Ft,Ed [kN]</th> </tr> </thead> <tbody> <tr><td>0</td><td>467,9</td></tr> <tr><td>50</td><td>478,1</td></tr> <tr><td>100</td><td>488,4</td></tr> <tr><td>150</td><td>506,0</td></tr> <tr><td>200</td><td>563,2</td></tr> <tr><td>250</td><td>-</td></tr> <tr><td>300</td><td>-</td></tr> <tr><td>350</td><td>-</td></tr> <tr><td>400</td><td>-</td></tr> <tr><td>450</td><td>-</td></tr> <tr><td>500</td><td>-</td></tr> </tbody> </table>					Z [kN]	Ft,Ed [kN]	0	467,9	50	478,1	100	488,4	150	506,0	200	563,2	250	-	300	-	350	-	400	-	450	-	500	-																																																																																																																																				
Z [kN]	Ft,Ed [kN]																																																																																																																																																															
0	467,9																																																																																																																																																															
50	478,1																																																																																																																																																															
100	488,4																																																																																																																																																															
150	506,0																																																																																																																																																															
200	563,2																																																																																																																																																															
250	-																																																																																																																																																															
300	-																																																																																																																																																															
350	-																																																																																																																																																															
400	-																																																																																																																																																															
450	-																																																																																																																																																															
500	-																																																																																																																																																															
<p>Note: Only loads which produce stresses below the bolt yield strength will be considered.</p>																																																																																																																																																																
<p>Ft,Rd= 588 [kN] design tensile resistance of the bolt</p>																																																																																																																																																																
<p>Resulting axial stress variation ranges $\Delta\sigma_N$ in bolts in function of load ranges $\Delta Z = Z_{max} - Z_{min}$</p>																																																																																																																																																																
<p>As= 817 [mm²] tensile stress area of bolt</p>																																																																																																																																																																
<table border="1" style="width: 100%; border-collapse: collapse; text-align: center;"> <thead> <tr> <th style="padding: 5px;">$\Delta\sigma_N$</th> <th colspan="11" style="padding: 5px;">from Zmin [kN]</th> </tr> <tr style="border-bottom: 1px solid black;"> <th style="padding: 5px;">to Zmax [kN]</th> <th style="padding: 5px;">0</th> <th style="padding: 5px;">50</th> <th style="padding: 5px;">100</th> <th style="padding: 5px;">150</th> <th style="padding: 5px;">200</th> <th style="padding: 5px;">250</th> <th style="padding: 5px;">300</th> <th style="padding: 5px;">350</th> <th style="padding: 5px;">400</th> <th style="padding: 5px;">450</th> <th style="padding: 5px;">500</th> </tr> </thead> <tbody> <tr><td style="padding: 5px;">0</td><td style="padding: 5px;"></td><td style="padding: 5px;"></td><td style="padding: 5px;"></td><td style="padding: 5px;"></td><td style="padding: 5px;"></td><td style="padding: 5px;"></td><td style="padding: 5px;"></td><td style="padding: 5px;"></td><td style="padding: 5px;"></td><td style="padding: 5px;"></td><td style="padding: 5px;"></td></tr> <tr><td style="padding: 5px;">50</td><td style="padding: 5px;">12,5</td><td style="padding: 5px;"></td><td style="padding: 5px;"></td><td style="padding: 5px;"></td><td style="padding: 5px;"></td><td style="padding: 5px;"></td><td style="padding: 5px;"></td><td style="padding: 5px;"></td><td style="padding: 5px;"></td><td style="padding: 5px;"></td><td style="padding: 5px;"></td></tr> <tr><td style="padding: 5px;">100</td><td style="padding: 5px;">25,0</td><td style="padding: 5px;">12,5</td><td style="padding: 5px;"></td><td style="padding: 5px;"></td><td style="padding: 5px;"></td><td style="padding: 5px;"></td><td style="padding: 5px;"></td><td style="padding: 5px;"></td><td style="padding: 5px;"></td><td style="padding: 5px;"></td><td style="padding: 5px;"></td></tr> <tr><td style="padding: 5px;">150</td><td style="padding: 5px;">46,6</td><td style="padding: 5px;">34,1</td><td style="padding: 5px;">21,6</td><td style="padding: 5px;"></td><td style="padding: 5px;"></td><td style="padding: 5px;"></td><td style="padding: 5px;"></td><td style="padding: 5px;"></td><td style="padding: 5px;"></td><td style="padding: 5px;"></td><td style="padding: 5px;"></td></tr> <tr><td style="padding: 5px;">200</td><td style="padding: 5px;">116,6</td><td style="padding: 5px;">104,1</td><td style="padding: 5px;">91,6</td><td style="padding: 5px;">70,0</td><td style="padding: 5px;"></td><td style="padding: 5px;"></td><td style="padding: 5px;"></td><td style="padding: 5px;"></td><td style="padding: 5px;"></td><td style="padding: 5px;"></td><td style="padding: 5px;"></td></tr> <tr><td style="padding: 5px;">250</td><td style="padding: 5px;">-</td><td style="padding: 5px;">-</td><td style="padding: 5px;">-</td><td style="padding: 5px;">-</td><td style="padding: 5px;">-</td><td style="padding: 5px;"></td><td style="padding: 5px;"></td><td style="padding: 5px;"></td><td style="padding: 5px;"></td><td style="padding: 5px;"></td><td style="padding: 5px;"></td></tr> <tr><td style="padding: 5px;">300</td><td style="padding: 5px;">-</td><td style="padding: 5px;">-</td><td style="padding: 5px;">-</td><td style="padding: 5px;">-</td><td style="padding: 5px;">-</td><td style="padding: 5px;">-</td><td style="padding: 5px;"></td><td style="padding: 5px;"></td><td style="padding: 5px;"></td><td style="padding: 5px;"></td><td style="padding: 5px;"></td></tr> <tr><td style="padding: 5px;">350</td><td style="padding: 5px;">-</td><td style="padding: 5px;">-</td><td style="padding: 5px;">-</td><td style="padding: 5px;">-</td><td style="padding: 5px;">-</td><td style="padding: 5px;">-</td><td style="padding: 5px;">-</td><td style="padding: 5px;"></td><td style="padding: 5px;"></td><td style="padding: 5px;"></td><td style="padding: 5px;"></td></tr> <tr><td style="padding: 5px;">400</td><td style="padding: 5px;">-</td><td style="padding: 5px;">-</td><td style="padding: 5px;">-</td><td style="padding: 5px;">-</td><td style="padding: 5px;">-</td><td style="padding: 5px;">-</td><td style="padding: 5px;">-</td><td style="padding: 5px;">-</td><td style="padding: 5px;"></td><td style="padding: 5px;"></td><td style="padding: 5px;"></td></tr> <tr><td style="padding: 5px;">450</td><td style="padding: 5px;">-</td><td style="padding: 5px;">-</td><td style="padding: 5px;">-</td><td style="padding: 5px;">-</td><td style="padding: 5px;">-</td><td style="padding: 5px;">-</td><td style="padding: 5px;">-</td><td style="padding: 5px;">-</td><td style="padding: 5px;">-</td><td style="padding: 5px;"></td><td style="padding: 5px;"></td></tr> <tr><td style="padding: 5px;">500</td><td style="padding: 5px;">-</td><td style="padding: 5px;">-</td><td style="padding: 5px;">-</td><td style="padding: 5px;">-</td><td style="padding: 5px;">-</td><td style="padding: 5px;">-</td><td style="padding: 5px;">-</td><td style="padding: 5px;">-</td><td style="padding: 5px;">-</td><td style="padding: 5px;">-</td><td style="padding: 5px;"></td></tr> </tbody> </table>					$\Delta\sigma_N$	from Zmin [kN]											to Zmax [kN]	0	50	100	150	200	250	300	350	400	450	500	0												50	12,5											100	25,0	12,5										150	46,6	34,1	21,6									200	116,6	104,1	91,6	70,0								250	-	-	-	-	-							300	-	-	-	-	-	-						350	-	-	-	-	-	-	-					400	-	-	-	-	-	-	-	-				450	-	-	-	-	-	-	-	-	-			500	-	-	-	-	-	-	-	-	-	-	
$\Delta\sigma_N$	from Zmin [kN]																																																																																																																																																															
to Zmax [kN]	0	50	100	150	200	250	300	350	400	450	500																																																																																																																																																					
0																																																																																																																																																																
50	12,5																																																																																																																																																															
100	25,0	12,5																																																																																																																																																														
150	46,6	34,1	21,6																																																																																																																																																													
200	116,6	104,1	91,6	70,0																																																																																																																																																												
250	-	-	-	-	-																																																																																																																																																											
300	-	-	-	-	-	-																																																																																																																																																										
350	-	-	-	-	-	-	-																																																																																																																																																									
400	-	-	-	-	-	-	-	-																																																																																																																																																								
450	-	-	-	-	-	-	-	-	-																																																																																																																																																							
500	-	-	-	-	-	-	-	-	-	-																																																																																																																																																						
<div style="border: 1px solid gray; background-color: #D9E1F2; padding: 5px; display: inline-block;">Wöhler curve</div>																																																																																																																																																																

Verification

symbol	value	unit	explanation	comment
--------	-------	------	-------------	---------

Wöhler curve

Note 1: As the calculation method used to determine the bolt force functions does not consider the influence of bending moment on the bolt, the Wöhler curve for bolts in tension given in EN1993-1-9 has to be reduced to detail category **36***.

Note 2: Additionally, the reduction factor, k_s , is used when the bolts have nominal diameters d larger than 30 mm.

$k_s = 0,955 \quad k_s = (30/d)^{0,25}$

$\Delta\sigma_C = 40$

Properties of the considered Wöhler curve 36*

Bolt	k_s	$\Delta\sigma_C$ with $N_c=2.10^6$	$\Delta\sigma_D$ with $N_c=10^7$
M36	0,955	38,2	22,0

Single damages can be derived by: $D_i = \frac{n_{E,i}}{N_{R,i}}$

with:

$$N_{R,i} = \left\{ \begin{array}{l} N_C \cdot \left(\frac{\Delta\sigma_C / \gamma_{Mf}}{\gamma_{Ef} \cdot \Delta\sigma_N} \right)^3 \quad \text{if } \gamma_{Ef} \cdot \Delta\sigma_N \geq \Delta\sigma_D / \gamma_{Mf} \\ N_D \cdot \left(\frac{\Delta\sigma_D / \gamma_{Mf}}{\gamma_{Ef} \cdot \Delta\sigma_N} \right)^5 \quad \text{if } \Delta\sigma_N < \Delta\sigma_D / \gamma_{Mf} \end{array} \right\} \quad \text{with } \gamma_{Mf} = 1.15 \text{ and } \gamma_{Ef} = 1.0$$

Rainflow matrix for damages caused by one cycle per load variation range ΔZ

Di [cycle ⁻¹]	from Zmin [kN]										
to Zmax [kN]	0	50	100	150	200	250	300	350	400	450	500
0											
50	1,2E-08										
100	2,1E-07	1,2E-08									
150	1,4E-06	5,4E-07	1,4E-07								
200	2,2E-05	1,5E-05	1,0E-05	4,7E-06							
250	#####	#####	#####	#####	#####						
300	#####	#####	#####	#####	#####	#####					
350	#####	#####	#####	#####	#####	#####	#####				
400	#####	#####	#####	#####	#####	#####	#####	#####			
450	#####	#####	#####	#####	#####	#####	#####	#####	#####		
500	#####	#####	#####	#####	#####	#####	#####	#####	#####	#####	

Rainflow Matrix

Appendix C – Fatigue resistance – Friction connections

Friction connection 1 (H = 21770 mm)

Input data				
symbol	value	unit	explanation	comment
Internal forces				
Design load case:		Maximum design stress in shell:		
Fx=	-886	[kN]		$\sigma_{ult,Ed} = \frac{M_r}{W_i} - \frac{F_z}{A_i}$
Fy=	27	[kN]		
Fz=	-2443	[kN]		
Fr=	886	[kN]		Wi= 254,8E+6 [mm ³]
Mx=	1129	[kNm]		Ai= 260,0E+3 [mm ²]
My=	-48617	[kNm]		
Mz=	-1368	[kNm]		σ _{ult,Ed} = 200,2 [N/mm ²]
Mr=	48631	[kNm]		
Material data and geometry:				
Cross-section values:				
S	460		type of steel	
t	20	[mm]	material thickness	
douter	3917	[mm]	outer diameter	
t	21	[mm]	material thickness (below)	
douter(lower)	3962	[mm]	lower shell outer diameter	
Friction connection:				
dbolt	10,9	[-]	grade of the bolts	d0= 33 [mm] diameter of bolt hole
As	30	[mm]	bolt diameter	dw= 50 [mm]
fub	561	[N/mm ²]		d3= 25,7 [mm] minor diameter of bolt thread
ns	1000	[N/mm ²]		Anom= 707 [mm ²]
nr	5			Ai= 707 [mm ²]
ntotal	130			Ad3= 519 [mm ²]
tc	650		thickness of cover plate	cnet= 61 mm
twasher	8	[mm]	thickness of washer	c= 94 mm
Ebolt	210000	[Mpa]		
Enut	210000	[Mpa]		
Eshell	210000	[Mpa]		
Ecp	210000	[Mpa]		
lhead	7,5	[mm]	Substitutional extension length of bolt head	
li	32,3	[mm]	Length of bolt shank	
lhthread	10,8	[mm]	Free length of unengaged loaded thread	
leng.thread	15	[mm]	Length of engaged loaded part of thread	
lnut	12	[mm]	Substitutional extension length of nut	
lcp	43,1	[mm]		
Damage Equivalent Loads				

Input data				
symbol	value	unit	explanation	comment
Internal forces				
Damage equivalent loads:				
$\Delta F_x =$	96	[kN]	$\Delta \sigma_{N,DEL} = \gamma_M \cdot \frac{M_y}{W}$	
$\Delta F_y =$	67	[kN]		
$\Delta F_z =$	29	[kN]		
$\Delta M_x =$	3342	[kNm]		
$\Delta M_y =$	4243	[kNm]		
$\Delta M_z =$	1229	[kNm]		
$\Delta \sigma_{z,DEL} =$			18,3	[N/mm ²]
<div style="border: 1px solid #ccc; display: inline-block; padding: 5px 20px; background-color: #f0f0f0;">Calculation</div>				

Fatigue Design

Maximum stress in "mean shell"

$$\Delta\sigma_{z,mean} = 308,6 \text{ [N/mm}^2\text{]}$$

$$c_{mean} = 94,0 \text{ mm}$$

$$\max \Delta\sigma_{z,mean} = \frac{c_{mean}}{c_{mean} - d_0} \cdot \sigma_{ult,Ed}$$

Elastic resilience of bolt thread

$$\delta_{head} = 5,053E-08 \quad \delta_{head} = \frac{\ell_{head}}{E_{bolt} \cdot A_{nom}}$$

Elastic resilience of shank

$$\delta_{shank} = 2,176E-07 \quad \delta_{shank} = \frac{\ell_i}{E_{bolt} \cdot A_i}$$

Elastic resilience of unengaged loaded part of the thread

$$\delta_{free\ thread} = 9,909E-08 \quad \delta_{free\ thread} = \frac{\ell_{thread}}{E_{bolt} \cdot A_{d_3}}$$

Elastic resilience of engaged bolt thread

$$\delta_{eng\ thread} = 1,376E-07 \quad \delta_{eng\ thread} = \frac{\ell_{eng.thread}}{E_{bolt} \cdot A_{d_3}}$$

Elastic resilience of nut

$$\delta_{nut} = 8,084E-08 \quad \delta_{nut} = \frac{\ell_{nut}}{E_{nut} \cdot A_{nom}}$$

Elastic resilience of the preloaded bolt

$$\delta_{bolt} = 5,857E-07$$

$$\delta_{bolt} = \delta_{head} + \delta_{shank} + \delta_{free\ thread} + \delta_{eng.thread} + \delta_{nut}$$

Elastic resilience of the preloaded bolt

$$\delta_{cp} = 1,1E-07 \quad \delta_{cp} = \frac{2 \cdot \ln \left[\frac{(d_w + d_0) \cdot (d_w + \ell_{cp} \cdot \tan\phi - d_0)}{(d_w - d_0) \cdot (d_w + \ell_{cp} \cdot \tan\phi + d_0)} \right]}{E_{cp} \cdot \pi \cdot d_0 \cdot \tan\phi}$$

$$\tan\phi = 0,473815$$

ϕ - angle of deformation cone taken as $\phi=35^\circ$

Total resilience of the joint

$$\delta_{joint} = 6,960E-07 \quad \delta_{joint} = \delta_{bolt} + \delta_{cp}$$

Maximum resulting pre-load variation range in bolts

$$\Delta F_{p,C} = 16,23 \text{ [kN]} \quad \max \Delta F_{p,C} = \beta \cdot \frac{v \cdot \max \Delta\sigma_{z,mean} \cdot s_{mean}}{\delta_{joint} \cdot E_{shell}}$$

$s_{mean} = 20,5 \text{ mm}$
mean shell thickness of both tower cross sections

Pre-load variation range in bolts for the DEL in net shell cross section

$$\Delta F_{p,C,DEL} = 0,96 \text{ [kN]} \quad \Delta F_{p,C,DEL} = \beta \cdot \frac{v \cdot \Delta\sigma_{z,DEL,net} \cdot s_{mean}}{\delta_{joint} \cdot E_{shell}}$$

$$\beta = 1,25$$

$$v = 0,3$$

$$\Delta\sigma_{z,DEL,net} = 18,32$$

Verification

Verification				
symbol	value	unit	explanation	comment
Characteristic fatigue resistance				
Nref=	2,0E+08			$\Delta\sigma_{E,ref} = \left(\sum_i \frac{n_i \Delta\sigma_i^m}{N_{ref}} \right)^{\frac{1}{m}}$
m=	4			
ni=	2,0E+06			
$\Delta\sigma_i$ =	50,0		bolts detail category	$\Delta\sigma_{bolt,R}$ = 15,81 [N/mm ²]
ni=	2,0E+06			
$\Delta\sigma_i$ =	90,0		shell detail category	$\Delta\sigma_{shell,R}$ = 28,46 [N/mm ²]
DEL				
$\Delta\sigma_{bolt,DEL}$ =	1,72	[N/mm ²]	$\Delta\sigma_{bolt,DEL} = \frac{F_{p,C,DEL}}{A_s}$	
$\Delta\sigma_{shell,DEL}$ =	18,32	[N/mm ²]		
Fatigue Design Verification				
YFf=	1,0			<div style="border: 2px solid black; padding: 5px; width: fit-content; margin: auto;"> $\frac{\gamma_{Ff} \cdot \Delta\sigma_{DEL}}{\Delta\sigma_R / \gamma_{Mf}} \leq 1$ </div>
YMf=	1,15			
	Design verification			
Bolts			0,1	Verified
Shell			0,6	Verified
	Input			

Friction connection 2 (H = 48390 mm)

Input data				
symbol	value	unit	explanation	comment
Internal forces				
Design load case:		Maximum design stress in shell:		
Fx=	-864	[kN]		$\sigma_{ult.Ed} = \frac{M_r}{W_i} - \frac{F_z}{A_i}$
Fy=	7	[kN]		
Fz=	-1846	[kN]		Wi= 151,1E+6 [mm ³]
Fr=	864	[kN]		Ai= 174,7E+3 [mm ²]
Mx=	1635	[kNm]		$\sigma_{ult.Ed} = 177,4 \text{ [N/mm}^2\text{]}$
My=	-25168	[kNm]		
Mz=	-1363	[kNm]		
Mr=	25221	[kNm]		
Material data and geometry:				
Cross-section values:				
S	460		type of steel	
t	15	[mm]	material thickness	
douter	3448	[mm]	outer diameter	
t	16	[mm]	material thickness (below)	
douter(lower)	3492	[mm]	lower shell outer diameter	
Friction connection:				
	10,9	[-]	grade of the bolts	d0= 33 [mm] diameter of bolt hole
dbolt	30	[mm]	bolt diameter	dw= 50 [mm]
As	561	[mm ²]		d3= 25,7 [mm] minor diameter of bolt thread
fub	1000	[N/mm ²]		Anom= 707 [mm ²]
				Ai= 707 [mm ²]
ns	3			Ad3= 519 [mm ²]
nr	127			cnet= 52 mm
ntotal	381			c= 85 mm
tc	8	[mm]	thickness of cover plate	
twasher	4	[mm]	thickness of washer	
Ebolt	210000	[Mpa]		
Enut	210000	[Mpa]		
Eshell	210000	[Mpa]		
Ecp	210000	[Mpa]		
lhead	7,5	[mm]	Substitutional extension length of bolt head	
li	32,3	[mm]	Length of bolt shank	
lthread	10,8	[mm]	Free length of unengaged loaded thread	
leng.thread	15	[mm]	Length of engaged loaded part of thread	
lnut	12	[mm]	Substitutional extension length of nut	
lcp	43,1	[mm]		
Damage Equivalent Loads				

Input data				
symbol	value	unit	explanation	comment
Internal forces				
Damage equivalent loads:				
$\Delta F_x =$	81	[kN]		
$\Delta F_y =$	61	[kN]		
$\Delta F_z =$	29	[kN]		
$\Delta M_x =$	1707	[kNm]		
$\Delta M_y =$	2359	[kNm]		
$\Delta M_z =$	1229	[kNm]		
			$\Delta \sigma_{N,DEL} = \gamma_M \cdot \frac{M_y}{W}$	
			$\Delta \sigma_{z,DEL} =$	17,2 [N/mm ²]
<div style="border: 1px solid #ccc; display: inline-block; padding: 5px 20px; background-color: #f0f0f0;"> Calculation </div>				

Fatigue Design

Maximum stress in "mean shell"

$$\Delta\sigma_{z,mean} = \frac{290,0}{85,0} \text{ [N/mm}^2\text{]}$$

$$\max \Delta\sigma_{z,mean} = \frac{c_{mean}}{c_{mean} - d_0} \cdot \sigma_{ult,Ed}$$

Elastic resilience of bolt thread

$$\delta_{head} = 5,053E-08 \quad \delta_{head} = \frac{\ell_{head}}{E_{bolt} \cdot A_{nom}}$$

Elastic resilience of shank

$$\delta_{shank} = 2,176E-07 \quad \delta_{shank} = \frac{\ell_i}{E_{bolt} \cdot A_i}$$

Elastic resilience of unengaged loaded part of the thread

$$\delta_{free\ thread} = 9,909E-08 \quad \delta_{freethread} = \frac{\ell_{thread}}{E_{bolt} \cdot A_{d_3}}$$

Elastic resilience of engaged bolt thread

$$\delta_{eng\ thread} = 1,376E-07 \quad \delta_{eng.thread} = \frac{\ell_{eng.thread}}{E_{bolt} \cdot A_{d_3}}$$

Elastic resilience of nut

$$\delta_{nut} = 8,084E-08 \quad \delta_{nut} = \frac{\ell_{nut}}{E_{nut} \cdot A_{nom}}$$

Elastic resilience of the preloaded bolt

$$\delta_{bolt} = 5,857E-07$$

$$\delta_{bolt} = \delta_{head} + \delta_{shank} + \delta_{freethread} + \delta_{eng.thread} + \delta_{nut}$$

Elastic resilience of the preloaded bolt

$$\delta_{cp} = 1,1E-07 \quad \delta_{cp} = \frac{2 \cdot \ln \left[\frac{(d_w + d_0) \cdot (d_w + \ell_{cp} \cdot \tan\phi - d_0)}{(d_w - d_0) \cdot (d_w + \ell_{cp} \cdot \tan\phi + d_0)} \right]}{E_{cp} \cdot \pi \cdot d_0 \cdot \tan\phi}$$

$$\tan\phi = 0,473815$$

ϕ - angle of deformation cone taken as $\phi=35^\circ$

Total resilience of the joint

$$\delta_{joint} = 6,960E-07 \quad \delta_{joint} = \delta_{bolt} + \delta_{cp}$$

Maximum resulting pre-load variation range in bolts

$$\Delta F_{p,C} = 11,53 \text{ [kN]} \quad \max \Delta F_{p,C} = \beta \cdot \frac{v \cdot \max \Delta\sigma_{z,mean} \cdot s_{mean}}{\delta_{joint} \cdot E_{shell}}$$

$s_{mean} = 15,5$ mm
mean shell thickness of both tower cross sections

Pre-load variation range in bolts for the DEL in net shell cross section

$$\Delta F_{p,C,DEL} = 0,68 \text{ [kN]} \quad \Delta F_{p,C,DEL} = \beta \cdot \frac{v \cdot \Delta\sigma_{z,DEL,net} \cdot s_{mean}}{\delta_{joint} \cdot E_{shell}}$$

$$\beta = 1,25$$

$$v = 0,3$$

$$\Delta\sigma_{z,DEL,net} = 17,17$$

Verification

Verification				
symbol	value	unit	explanation	comment
Characteristic fatigue resistance				
Nref=	2,0E+08			
m=	4			
$\Delta\sigma_{E,ref} = \left(\sum_i \frac{n_i \Delta\sigma_i^m}{N_{ref}} \right)^{\frac{1}{m}}$				
ni=	2,0E+06			
$\Delta\sigma_i$ =	50,0		bolts detail category	$\Delta\sigma_{bolt,R}$ =
				15,81 [N/mm ²]
ni=	2,0E+06			
$\Delta\sigma_i$ =	90,0		shell detail category	$\Delta\sigma_{shell,R}$ =
				28,46 [N/mm ²]
DEL				
$\Delta\sigma_{bolt,DEL}$ =	1,22		$\Delta\sigma_{bolt,DEL} = \frac{F_{p,C,DEL}}{A_s}$	
$\Delta\sigma_{shell,DEL}$ =	17,17			
Fatigue Design Verification				
YFf=	1,0			
YMf=	1,15			
<div style="border: 2px solid black; padding: 5px; display: inline-block;"> $\frac{\gamma_{Ff} \cdot \Delta\sigma_{DEL}}{\Delta\sigma_R / \gamma_{Mf}} \leq 1$ </div>				
Design verification				
Bolts	0,1			Verified
Shell	0,5			Verified
<div style="border: 1px solid black; padding: 5px; display: inline-block; background-color: #F5F5F5;">Input</div>				

Appendix D – Design tools already developed

Front page of the Web based app (Veljkovic et al, 2015)

Design load case

N_k Axial Force	[kN]	1809.63
$V_{x,k}$ Shear force in x-direction	[kN]	656.3
$V_{y,k}$ Shear force in y-direction	[kN]	20
$M_{res,k}$ Resulting bending moment	[kN]	3207.7
$M_{T,k}$ Torsional moment	[kN]	1013.3

Selected WEA

output _{rated} Turbine power rating	[MW]	2
$r_{hub,k}$	[m]	40

Steel

E Elastic modulus	0	[N/mm ²]
ν Poisson's ratio	0.0	[]
f_y Yield point	0	[N/mm ²]
f_u Tensile strength	0	[N/mm ²]

Bolted Connection

Δd Hole tolerance	0	[mm]
b_s Slot hole width	0	[mm]
d_w Diameter of transferring load	0.0	[mm]
f_{ub} Bolt strength	0	[N/mm ²]
f_y Yield strength	0	[N/mm ²]
A_s Stress area	0	[mm ²]

Screenshots of the iOS based app (Veljkovic et al, 2015)

Wind Tower Connections

Histwin Friction Connection

Flange Connection

Design load case

N_k Axial Force	[kN]	1809,63
$V_{x,k}$ Shear force in x-direction	[kN]	656,3
$V_{y,k}$ Shear force in y-direction	[kN]	